Algorithmic Outline of Unsteady Aerodynamics (AERODYN) Modules

Project WE-201103

FINAL REPORT

September 2, 2011

PREPARED FOR:

Alliance For Sustainable Energy, LLC
Management and Operating Contractor for the National Renewable Energy Laboratory ("NREL")

Subcontract No. AFT-1-11326-01
Under
Prime Contract No. DE-AC36-08GO28308

Contract Technical Monitor: Patrick Moriarty
Contract Administrator: Heidi Oliver

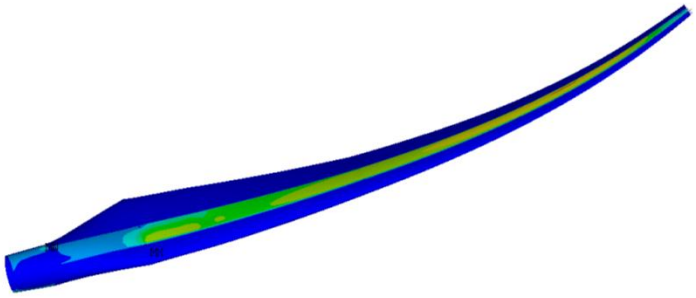

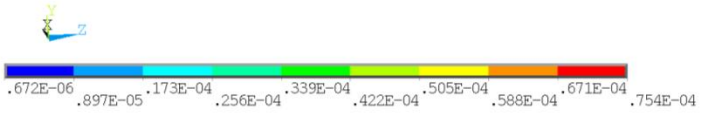

PREPARED BY:
Rick Damiani, Ph.D., P.E.
rdamiani@RRDEngineering.com
Tel: +1-970-581-8091

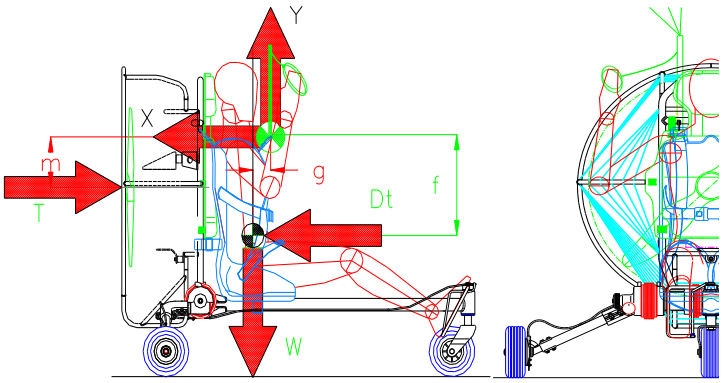

RRD ENGINEERING

670 Cody St.
Lakewood, Colorado 80215, USA

DISCLAIMER

This Report is intended for initial distribution to the National Renewable Energy Laboratory (NREL).

The information contained in this report is provided to NREL in good faith, but with no warranties of any kind, expressed or implied, including but not limited to merchantability and/or fitness for a particular purpose. Any damages whatsoever, be they special, consequential, incidental, indirect or otherwise arising from the use of any information provided in the present report are disclaimed. In no event shall the author of the present report or RRD Engineering be liable for any loss, claim, liability, injury or damages suffered by any corporation or any person for (but not limited to) negligence, breach of contract, loss of revenue, loss of business profits, business interruption, or loss of information.

This report is submitted in satisfaction of all the deliverables that are required under Subcontract No. AFT 1-11326-01 issued on 6/28/2011 to RRD Engineering by Alliance For Sustainable Energy, LLC, Management and Operating Contractor for NREL.

EXECUTIVE SUMMARY

A critical review of the current status of the AeroDyn software was performed. The theory behind each of the current aerodynamics algorithms was critically assessed, documented, and included in this report.

Additionally, the input/output parameters for each recently developed AeroDyn module were thoroughly reviewed and documented, including the general workflow of the various subroutines and their interconnection.

A thorough examination of the necessary reference frames was conducted, and a series of new graphs is proposed to illustrate the relationships between forces, coefficients, and velocity components, also bringing to an agreement rotorcraft nomenclature and conventions with the respective wind-turbine ones.

This report contains all the required formulas to at least cover the theoretical models included to date in AeroDyn.

Refinements and extensions of the currently implemented theory were also investigated. Among the newly proposed models are: a new tip-loss model to adopt in the BEMT (Blade Element Momentum Theory); alternative extensions of the BEMT to other wake states, including possible measures to mitigate observed instabilities in the iterative solution; coning angle treatment; GDW (Generalized Dynamic Wake) improved tip-loss model; GDW vortex-ring state transition and alleviation of instabilities at low wind speeds; GDW wake curvature effects due to finite yaw rate.

Five main issues were noted with the current implementation of AeroDyn, besides a few minor points. The first one relates to the handling of the body velocities in the calculation of the induction factors; currently, only the tangential induction accounts for the total (body + wind) velocity, whereas the body kinematic contribution is added a-posteriori in the calculation of the axial induction. Secondly, the LBM (unsteady aerodynamics, Leishman-Beddoes Model) module should be incorporated within the iteration process in the BEMT. The last three issues relate to the GDW implementation. The time-integration of the GDW states is prone to numerical errors in its current non-dimensional formulation if the RPM changes from time-step to time-step. Two alternatives were proposed to eliminate that problem, including the possibility of implementing a fully dimensional version of the governing equations. Furthermore, it is recommended that a new sign convention be adopted (more in line with the original literature and rotorcraft model). Finally, a new treatment of induced velocity and induction factors is suggested, which also requires an overhaul of the apparent-mass matrix formulation.

Other minor points were discussed, including some potential typos in the currently utilized formulas.

This document shows the recommended algorithm organization and major input/output of subroutines, as well as suggested flowcharts describing how they should communicate with each other.

TABLE OF CONTENTS

LIST OF SYMBOLS

a	Axial induction factor
$\overline{a}$	Axial induction factor spatially averaged throughout the rotor plane
a'	Tangential induction factor
a_s	Speed of sound
a_{skw}	Corrected value of a (for yaw/tilt angles)
a_{up}	Upper bound for a in the transitional function in Maniaci's (2011) method
AOA	Angle of attack [deg or rad]
AOI	Angle of Incidence (AOA-$AOA\|_{0\text{-lift}}$)
AR	Blade aspect ratio ($b^2/S=b/c$ for rectangular blade)
$A_{1..5}$	LBM model constants
A_∞	Upwind surface of a control volume (inlet)
A_E	Downwind surface of a control volume (outlet)
$[A_n^m]$	$= [L_{ln}^{mm}]\|_{X_w=0}$, matrix used in the vortex-ring correction to $[M]$ in the GDWT
b	Index for blade
$b_{1..5}$	LBM model constants
BE	Blade element
BL	Boundary Layer
BEM	Blade Element Model
BEMT	Blade Element Momentum Theory
BL	Boundary Layer
c	Airfoil chord
CFD	Computational Fluid Dynamics
CH	$\frac{U^2 C_{th}}{U_\infty^2}\sigma_r$, similar to a BE thrust coefficient
CH_{CS}	CH following Shen et al.'s (2005) method
C_c	Chordwise force coefficient (2D)
C_c^{pot}	Chordwise force coefficient in potential (attached) flow conditions (LBM)
C_d	Drag coefficient (2D) (airfoil)
C_{d3D}	Airfoil drag coefficient modified for rotational augmentation effects

C_{dt} Tower (sectional) 2D drag coefficient

C_{d0} Airfoil 0-lift drag coefficient

C_l Airfoil lift coefficient

C_{l3D} Airfoil lift coefficient modified for rotational augmentation effects

$C_{l\alpha}$ Slope of airfoil lift coefficient vs. AOA curve

C_m Moment coefficient about the ¼-chord (2D)

C_{mq} Slope of the C_m vs. q (pitching rate) static curve

$C_{mq}(s, M)$ Moment-coefficient-response to a unit step in q (unsteady slope of the C_m vs. q curve)

C_{m_q} Moment coefficient about the ¼-chord, response to a step change in pitching rate

C_{m0} Moment coefficient about the ¼-chord (2D) at 0-lift

$C_{m\alpha}$ Slope of the C_m vs. α static curve

$C_{m\alpha}(s, M)$ Moment-coefficient response to a unit step in α (AOA) (unsteady slope of the C_m vs. α curve)

C_{m_α} Moment coefficient about the ¼-chord, response to a step change in AOA

$C_{m_{\alpha,q}}$ Moment coefficient about the ¼-chord, response to a step change in AOA and pitching rate

C_n^m Constants in the pressure Legendre/Fourier expansion in the GDWT multiplying cosine terms

C_m^v Contribution from the LE vortex to the moment coefficient about the ¼-chord (LBM)

C_n Normal (to chord) force coefficient (2D)

C_{nq} Slope of the C_n vs. q (pitching rate) static curve

$C_{nq}(s, M)$ Normal-force coefficient-response to a unit step in q (unsteady slope of the C_n vs. q curve)

$C_{n\alpha}$ Slope of the C_n vs. α static curve

$C_{n\alpha}(s, M)$ Normal-force coefficient-response to a unit step in α (unsteady slope of the C_n vs. α curve)

C_{n1} Critical condition for C_n' signifying LE separation and vortex advection (LBM)

C_{n2} As C_{n1}, but for negative AOAs

C_{n_g} Normal (to chord) force coefficient response to a step change in gust speed w_g

C_{n_q} Normal (to chord) force coefficient response to a step change in pitching rate

C_{n_α} Normal (to chord) force coefficient response to a step change in AOA

$C_{n_{\alpha,q}}$ Normal (to chord) force coefficient response to a step change in AOA and pitching rate

C_n^{pot} Normal (to chord) force coefficient in potential (attached) flow conditions (LBM)

C_n^v Normal (to chord) force coefficient due to LE vorticity (LBM)

C_n'	Normal (to chord) force coefficient accounting for delays at the LE pressure and BL separation (LBM)
C_{th}	Airfoil aerodynamic force component normal to plane of rotation
C_{ths}	C_{th} following Shen et al.'s (2005) correction model for tip-loss
C_{tq}	Airfoil aerodynamic force component along plane of rotation
C_{tqs}	C_{tq} following Shen et al.'s (2005) correction model for tip-loss
C_{Th}	Rotor thrust coefficient
$C_{th_{b,e}}$	Airfoil aerodynamic force component normal to plane of rotation for BE e and blade b (GDWT)
C_V	Increment in vortex lift (LBM)
d	Horizontal distance of blade element from tower centerline in tower shadow treatment
div	Divergence operator
D	Rotor diameter [m], also drag force [N]
D_f	Deficiency function associated with f'', accounting for lag in TE separation development (LBM)
D_p	Deficiency function associated with C_n', accounting for lag in LE pressure response and BL separation (LBM)
D_{α_f}	Deficiency function associated with α_f' (LBM)
D_n^m	Constants in the pressure Legendre/Fourier expansion in the GDWT multiplying sine terms
e	Index for BE
f	Separation point distance from airfoil LE as fraction of chord length
f_c	Separation point distance from airfoil LE as fraction of chord length calculated for reconstructing C_c (LBM)
$\underline{f_g}$	Generic body force per unit mass
f_{tr}	Transitioning function in Maniaci's (2011) method
$f_{VR}(\sigma_{VR})$	Function participating in the vortex-ring correction in GDWT
f'	f under unsteady conditions (LBM)
f''	f' lagged
f_c'	f_c under unsteady conditions (LBM)
f_c''	f_c' lagged
F	Product of tip and hub loss function
F_g	Body force potential function

F_H	Hub loss function
F_R	Generic response function to a disturbance
F_T	Tip loss function
F_{TP}	Tip loss function following Peters (2011) (GDWT)
F_{TS}	Tip loss function following Shen et al. (2005)
F_{TX}	Tip loss function following Xu and Sankar (2002)
FFb	Blade Reference Frame
FF_{HR}	Rotorcraft inflow reference system
FFn	Nacelle Reference Frame
FFs	Shaft Reference Frame
FF0	Earth (Inertial) Reference Frame
g	Gravitational acceleration
g_s	Constant in Shen et al's (2005) tip loss model
g_1, g_2	Constants in the deficiency functions for gust responses
$g_{VR}(\rho_{VR})$	Function participating in the vortex-ring correction in GDWT
G_1, G_2	Constants in the deficiency functions for gust responses
GDW	see GDWT
GDWT	Generalized Dynamic Wake Theory
HAWT	Horizontal Axis Wind Turbine(s)
H_l^k	Function of indices *k* and *l* used in GDWT
$\hat{\imath}$	x-axis unit vector; (in the context of the current reference frame)
I/O	Input/Output
$[I]$	Identity matrix
j	$\sqrt{-1}$; also iteration step counter
$\hat{\jmath}$	y-axis unit vector; (in the context of the current reference frame)
k	Generic index of harmonics in GDWT (similar to m)
$k_{1..3}$	Constants in the LBM model (pitching moment model in TE separated conditions)
k_α	Factor in the T_α time-constant of attached flow (LBM)
k_q	Factor in the T_q time-constant of attached flow (LBM)

$\hat{k}$ z-axis unit vector; (in the context of the current reference frame)

K Generic constant or tunable parameter

K_{Cd} Factor in the calculation of the axial induction factor via Maniaci's (2011) method

K_{Cl} Factor in the calculation of the axial induction factor via Maniaci's (2011) method

K_{nc}, K_{ns} Factors in the Fourier expansion in Pitt and Peters's (1981) model

$\underline{K_o}$ Angular momentum of an air parcel w.r.t. the point O in the current reference frame

K_q Time-derivative of q in the calculation of C_{nq}^{nc} in LBM attached/potential flow

K_q' Deficiency function in the calculation of C_{nq}^{nc} in LBM attached/potential flow

K_q'' Deficiency function in the calculation of C_{mq}^{nc} in LBM attached/potential flow

K_q''' Deficiency function in the calculation of C_{mq}^{c} in LBM attached/potential flow

K_{Re} Factor in the formulation of X_{Weq}(GDWT)

K_α Time-derivative of AOA in the calculation of C_n^{nc} in LBM attached/potential flow

K_α' Deficiency function in the calculation of C_n^{nc} in LBM attached/potential flow

l Generic index of radial modes (GDWT) (similar to n)

L Lift force [N]

$L_{b,e}$ Lift force for the e-th element of the b-th blade (GDWT)

LB Leishman-Beddoes dynamic stall model

LE Leading edge of an airfoil

$[L]$ L-operator in GDWT

$[L^c]$,$[L^s]$ Matrices in GDWT (partitions of $[L]$), functions of the wake-skew parameter and $[V^c]$,$[V^s]$, for cosine and sine terms respectively

$[\tilde{L}^c]$,$[\tilde{L}^s]$ Matrices in GDWT functions of the wake-skew parameter, for cosine and sine terms respectively

$[L_{ln}^{km}]^c[L_{ln}^{km}]^s$ As $[\tilde{L}^c]$,$[\tilde{L}^s]$

m Harmonic number (GDWT), index of harmonic

m_{max} Max harmonic number (GDWT)

$\dot{m}$ Mass flow rate

M Mach number

$[M]$ Apparent-mass matrix (GDWT)

$[M^c]$,$[M^s]$ Partitions of $[M]$ in GDWT for cosine and sine terms respectively

$\underline{M_o}$	Moment resultant calculated w.r.t. the point O in the current reference frame
MT	Momentum Theory
n	Radial expansion mode number (GDWT), index of radial mode
$\underline{n}$	Normal (to surface) unit vector
N_b	Number of blades
NREL	National Renewable Energy Laboratory
NWTC	National Wind Technology Center (NREL)
p	Static pressure
p_∞	Freestream static pressure
$P_n^m(\upsilon)$	Legendre function of the first kind, m harmonic index, n radial mode index (GDWT)
$\hat{P}_n^m(\upsilon)$	Modified $P_n^m(\upsilon)$ (GDWT)
q	Pitching rate (non-dimensional)
$Q_n^m(\upsilon)$	Legendre function of the second kind, m harmonic index, n radial mode index (GDWT)
r	Radial distance of blade element
$\underline{r}$	Generic position vector
$\hat{r}(\upsilon)$	Non-dimensional r (see GDWT) coordinate on rotor-disc surface in ellipsoidal reference frame
$\hat{r}_e$	$\hat{r}$ for e-th blade element
R	Rotor radius (blade length)
RHS	Right-hand-side
RPM	Rotational speed in rounds per minute
R_H	Hub radius
Re	Reynolds number =ρ*U*c/ν
s	Distance traveled by airfoil in semi-chords (LBM indicial treatment)
S	Boundary surface of a control volume
S_{lat}	Lateral surface of a control volume
S_1, S_2	Constants in the LBM TE separation flow treatment
SS	Steady-State
t	Time variable; also t-th time step in LBM
$\hat{t}$	Non-dimensional t

TE	Trailing edge of an airfoil
TSR	Tip-speed ratio (see also λ)
T_h	Thrust force
T_f	Time-constant associated with TE separation f'' (LBM)
T_p	Time-constant associated with pressure response at the LE and C_n' (LBM)
T_q	$= 0.75 k_q T_I$ (LBM) (LBM)
$T_{m,q}$	Time-constant in the attached/potential flow treatment (LBM)
T_{sh}	Time constant related to Strohual's non-dimensional frequency of LE vortex-shedding (LBM)
T_α	$= 0.75 k_\alpha T_I$ (LBM)
T_I	$= c/a_s$, (LBM)
T_V	Time constant associated with the increment and decay of the vorticity at the LE (LBM)
T_{Vl}	Non-dimensional time constant associated with the full vortex advection from LE to TE (LBM)
T_q'	Time-constant for attached flow treatment (LBM)
T_α'	Time-constant for attached flow treatment (LBM)
$T_{m,q}'$	Time-constant for attached flow treatment (LBM)
$T_{m,\alpha}'$	Time-constant for attached flow treatment (LBM)
$TwrC$	Tower constant (usually 0.1) in the Bak et al. (2001) model for tower dam effects
u	Component along x (current reference frame) of the air velocity
$\underline{u}$	Induced velocity (GDWT)
$u_{i=1..3}$	Components (current reference frame) of the induced velocity (GDWT)
u_w	Tower-dam velocity deficit along x (local wind velocity reference frame, not necessarily FF0)
u_{wk}	Tower wake (normalized, horizontal) velocity deficit, (in Powles's (1983) model for tower shadow)
$\underline{U}$	Resultant body-relative air-velocity (induction included) at the local blade element
U	magnitude of $\underline{U}$
U_H	Inflow air velocity component along the rotor disc in FF_{HR} reference system (GDW)
U_∞	Freestream wind velocity component normal to rotor plane (along X_{FF0} direction)
$\underline{U}_\infty$	Freestream wind velocity
$\underline{U}_{\infty h}$	Freestream wind horizontal velocity
$\underline{U_E}$	Wind velocity at the outlet of a control volume

v Magnitude of $\underline{v}$

v_w Tower-damvelocity deficit along y (local wind velocity reference frame, not necessarily FF0)

$\underline{v}$ Air parcel velocity vector

$v_{i=1..3}$ Generic air velocity component

v_θ Tangential air velocity component

Vol Control Volume

VNTotal Component normal to the local plane of rotation, of the total relative air-velocity (no induction)

VSTotal Component tangent to the local blade shear-center axis (deflected) and to the local plane of rotation, of the total relative air-velocity (no induction)

VTTotal Component tangent to the local plane of rotation and circle, of the total relative air-velocity (no induction)

V_H Inflow air velocity component normal to the rotor disc in FF_{HR} reference system (GDWT)

$V_{i=1..3}$ Inflow air velocity components in FF_{HR} reference system (GDWT) with $\Psi_0 = 0$

$V_{id=1..3}$ Lagged $V_{i=1..3}$ (GDWT)

V_M Mass-flow parameter (GDWT)

V_T Relative air-velocity component along the tangent to the local rotational circle (tangential velocity), including body rigid and elastic motions

V_{TOT} Magnitude of $\underline{V_{TOT}}$

$\underline{V_{TOT}}$ Total (resultant) velocity (accounting for induction) at the rotor disc, (spatial mean)

$[V^c]$,$[V^s]$, Matrices functions of V_{TOT} and V_M (GDWT), for cosine and sine terms respectively

V_n^m Elements of $[V^c]$,$[V^s]$ for (m-th harmonic,n-th radial mode)

w Component along z (current reference frame) of the wind velocity

w_g Wind gust speed perpendicular to local $\underline{U}$

$\hat{x}_{AC}$ Distance from LE of the aerodynamic center as fraction of chord

$\hat{x}_{cp}$ Normalized (by the chord) distance of the center of pressure from the LE

$\bar{\bar{x}}_{cp}$ Constant (=0.2 for most airfoils) in the calculation of the center of pressure location under the presence of LE vortex (LBM)

$\hat{x}_{cp}^v$ Normalized (by the chord) distance of the center of pressure from the ¼-chord location due to the presence of the LE vortex (LBM)

$X_\sharp$, or x x-axis, or coordinate along that axis, of the current "FF" reference frame

X_W Wake skew parameter (=tan($\frac{\chi}{2}$))

X_{Wd} Lagged X_W

X_{Weq} Modified X_W to account for wake curvature (GDWT)

$X1, X2$ Deficiency functions (LBM)

$Y_\#$, or y y-axis, or coordinate along that axis, of the current "FF" reference frame

Y_1, Y_2 Factors in the Shen et al.'s (2005) tip-loss model

$Z_\#$, or z z-axis, or coordinate along that axis, of the current "FF" reference frame

Z_1, Z_2 Deficiency functions for the response to gusts

GREEK

α Angle of Attack (see also AOA)

α_f Effective AOA for lags associated with BL evolution (LBM)

α_m Modified AOA to account for large (>π/2) angles (LBM)

α_D Angle of Attack of relative air velocity (no induction) w.r.t. the rotor plane

α_E Effective AOI at ¾-chord (LBM)

α_0, α_{0L} Angle of attack at 0-lift (AOL)

α_1 Threshold value for the AOA used in the LBM TE flow separation treatment

α_f' Lagged α_f (LBM)

$\alpha_l^k(\hat{t})$ States of the GDWT relative to cosine terms of the Fourier expansion

β_M Prandtl-Glauert compressibility factor, $\sqrt{1-M^2}$

$\beta_l^k(\hat{t})$ States of the GDWT relative to sine terms of the Fourier expansion

ξ Free-stream coordinate and axis (pointing upwind), refer to FF_{HR} and GDW

$\hat{\underline{\xi}}$ Unit vector associated with ξ, refer to FF_{HR} and GDW

δ Tilt angle

∂ Angle between the in-plane velocity component and the vertical

δ_{ij} Kronecker delta

$\Delta\#$ Variation (Delta) of quantity #

Δp_{rot} Pressure drop due to rotation of the wake

Δ_{VR} Function to account for vortex-ring in GDWT

ε Generic disturbance (see LBM and Duhamel Integral)

η Coordinate in the ellipsoidal reference frame; $\eta = 0$ corresponds to the rotor disc

η_e Recovery factor in the LBM TE separated flow treatment

$\varphi_l^k(\hat{r})$ Radial shape function (GDW)

ϕ Generic response function to a step variation of an independent variable (see LBM and Duhamel Integral)

ϕ_α^c Circulatory normal-force indicial response to a step variation in AOA

ϕ_α^{nc} Non-circulatory normal-force indicial response to a step variation in AOA

$\phi_{m,\alpha}^{nc}$ Non-circulatory moment indicial response to a step variation in AOA

ϕ_q^c Circulatory normal-force indicial response to a step variation in q

ϕ_q^{nc} Non-circulatory normal-force indicial response to a step variation in in q

$\phi_{m,q}^c$ Circulatory moment indicial response to a step variation in q

$\phi_{m,q}^{nc}$ Non-circulatory moment indicial response to a step variation in q

ϕ_W Non-dimensional pressure distribution (see GDW)

ϕ_{WD} Non-dimensional pressure difference distribution at the rotor disc (see GDW)

ϕ_W^A Non-dimensional pressure distribution (see GDW), acceleration part

ϕ_W^V Non-dimensional pressure distribution (see GDW), advection part

Φ Inflow angle: angle between relative air velocity and plane of rotation

γ Yaw angle

Γ_{ln}^{km} Partitions in the formulation of the $[\tilde{L}^c]$,$[\tilde{L}^s]$ matrices (GDWT)

κ Generic constant or tunable parameter (e.g., =2.2 in GDWT $[M]$ modification factor; ≃0.01-0.02 in Maniaci's formulation)

κ_a, κ_b, κ_c Empirical constants in Du and Selig's (1998) method for rotational augmentation effects

κ_{Cl}, κ_{Cd} Correction functions for C_l and C_d for rotational augmentation effects

κ_{cw} Wake curvature (GDWT)

κ_s Wake curvature term due to pitch of rotor (GDWT) (rotorcraft aerodynamics only)

λ Tip-speed ratio (TSR)

λ_f Normalized (or not), spatially-averaged, relative air-velocity normal to the rotor plane in FF$_{HR}$ (GDWT)

λ_{fd} Lagged λ_f (GDWT)

λ_m Normalized (or not), spatially-averaged induction velocity normal to the rotor plane in FF$_{HR}$ (GDWT)

λ_r	Local speed ratio
λ_w	Defined as -λ_f
μ	Advance ratio (GDWT), (normalized or not) spatially-averaged component of relative air-velocity along the rotor disc
μ_d	Lagged μ (GDWT)
μ_a	Air dynamic viscosity
υ	Coordinate in the ellipsoidal reference frame; $\hat{r}(\upsilon) = \sqrt{1-\upsilon^2}$ is the radial coordinate
υ_a	Kinematic viscosity [m²/s]
υ_0	$= \sqrt{\left\lvert\frac{\tau_1^{0c}}{\sqrt{3}}\right\rvert}$ (GDWT) participating in vortex-ring correction
Ψ	Azimuth angle
Ψ_{HR}	Azimuth angle in FF$_{HR}$ reference frame
Ψ_0	$= \Psi - \Psi_{HR}$
θ	Aerodynamic twist angle or pitch angle
Θ	Coning angle
ϑ	Azimuth coordinate
ρ	Air density
ρ_{VR}	$= \left\lvert\frac{\lambda_f+\lambda_m}{\upsilon_0}\right\rvert$ (GDWT) participating in vortex-ring correction
ρ_n^m	Factor in the calculation of $\hat{P}_n^m$ used in GDWT
σ	Solidity, $N_b\, c$ / (πD)
σ_r	Local Solidity, $N_b\, c$ / ($2\pi r$)
σ_s, σ_t	Generic integrand coordinates (see LBM treatment and Duhamel Integral)
σ_{VR}	$= \left\lvert\frac{\mu}{\upsilon_0}\right\rvert$ (GDWT) participating in vortex-ring correction
$[\underline{\tau}]$, τ_{ij}	Viscous stress tensor, generic (i-th,j-th) component (i,j=1..3)
$\underline{\tau_n}$	Viscous stress vector associated to surface normal $\underline{n}$
τ_V	Non-dimensional time tracking the LE vortex motion over the airfoil (LBM)
τ_n^{mc}	Pressure coefficients in the GDWT treatment related to cosine terms
τ_n^{ms}	Pressure coefficients in the GDWT treatment related to sine terms
χ	Wake skew angle, angle between $V_{TOT}$and the Z$_{FFHR}$ axis
χ_0	Nominal wake skew angle, angle between air-velocity vector (no induction) and the Z$_{FFHR}$ axis

Ω Rotational speed [rad/s] (=2*p*RPM/60)

SUBSCRIPTS

b Blade

C critical value

D Actuator Disc (conditions at the rotor)

E Outlet (exit conditions)

R Blade tip radius, (tip conditions)

t *t-th* time step (see LBM)

T Blade tip, (tip conditions, e.g.: u_{3T} Component normal to the rotor plane of the induced velocity, at blade tip (GDWT))

∞ Inlet (free stream conditions)

SUPERSCRIPTS

C circulatory

NC non-circulatory

$\widehat{\#}$ non-dimensional (normalized) quantity #

$\breve{\#}$ non-dimensional time derivative of the quantity #

LIST OF FIGURES

LIST OF TABLES

1. PROJECT INTRODUCTION

The objective of the present study was to critically review the theory and implementation of AeroDyn, a computer program capable of assessing aerodynamic loads on Horizontal Axis Wind Turbines (HAWTs).

The AeroDyn code is open-source and written in Fortran 90, and can be found (in its version 13.00.00 31 Mar 2010, at the time of this writing) at http://wind.nrel.gov/designcodes/simulators/aerodyn/; basic references can be found in Laino and Hansen (2002); and Moriarty and Hansen (2005).

The code is composed of several modules (See Appendix A-M) that interface with one another and with externally driving routines. Each module captures a particular aspect of the aerodynamic physics.

Currently, AeroDyn is not meant to be a stand-alone program. It interfaces with aero-elastic and structural codes (such as YawDyn, FAST, SymDyn, [http://wind.nrel.gov/designcodes/], and MSC ADAMS®), which add turbine inertia, stiffness, and electrical characteristics.

The ultimate goal of AeroDyn is to assemble the state-of-the-art mathematical and physical models to accurately represent aerodynamic loads on the turbine blades, also accounting for the effect of the support tower. Additionally, AeroDyn loads can be spanwise integrated leading to total aerodynamic torque and power. The models are required to be simple enough so to be implemented in a computer code to give quick answers to the designer and rapid outputs to the interfacing structural routines. AeroDyn is not intended, to this end, to be either a high-end fidelity or a CFD code for instance.

The code has been recently certified by Germanischer Lloyd WindEnergie for the "calculation of onshore wind turbine loads for design and certification" (http://wind.nrel.gov/designcodes/papers/GL_Certific.pdf).

The current version of AeroDyn, however, is outdated and needs to be rewritten to ensure its accuracy and maintainability in the future.

The study documented in this report performed the first step in that direction, i.e. a thorough review of the theory behind each of the current aerodynamics algorithms and of the way they should be connected in AeroDyn.

This document provides the main theoretical basis, validity assumptions, and equations needed to re-write the code. A comprehensive analysis of the state-of-the-art, physical models was conducted, and suggestions toward the extension of some of the models are included in this report.

Future efforts at NREL/NWTC will be dedicated to produce a simple driver for the routine, that will help with the future development, validation, and debugging. Additionally, AeroDyn should become the main routine of reference for aerodynamic loading and performance of HAWTs, and as such it should encompass and trump WT_Perf [http://wind.nrel.gov/designcodes/simulators/wtperf].

This report is divided into three main parts.

The first part illustrates the physical theory behind the BEMT (Blade Element Momentum Theory and its extension modules) and the GDWT (Generalized Dynamic Wake Theory). Section 2 illustrates the main

reference frames and coordinate system conventions used in AeroDyn. Sections 3-11 summarize the theory and the equations behind the BEMT and its extensions to account for tower effects, off-axis flow, limited number of blades (tip-losses), and braked windmill state. Section 12 discusses the unsteady aerodynamics model (including dynamic stall). Section 13 provides the equations needed for the implementation of the GDW. In this part, several comments on the current implementation are offered throughout the text, emphasizing some inconsistencies with the literature-recommended procedures and theory.

The second part of the report describes the suggested algorithm organization of AeroDyn and of its main modules.

The third part consists of the Appendices. Appendix A shows the high-level flowcharts for all of the current AeroDyn modules, presenting how the various routines are currently interconnected. Appendix B through M provide detailed information of each current subroutine and function, with the exception of the externally invoked ***NWTC_Library*** and its subcomponents, which form a package of numerical recipes and I/O file-operation routines. Those Appendices show all the input and output variables for all the subroutines and functions, and list in detail all of the steps taken in the code, and therefore can be seen as a detailed commentary to the code.

In this report, the following font convention is used:

- an italicized, bold, and underscored keyword indicates the name of a function or routine (e.g., ***AD_GetInput***)
- an italicized and bold keyword indicates a FORTRAN module name (e.g., ***AeroSubs***)
- a bold keyword indicates a FORTRAN derived type (e.g., **AllAeroMarkers**)
- an italicized keyword denotes a FORTRAN variable (e.g., *CLA*)
- the letter case is kept as in the FORTRAN code
- yellow highlights are minor bugs or points of the code that should be revised/corrected/improved

Concluding remarks are given in Section 17.

PART I: THEORY REVIEW

2. REFERENCE FRAME SYSTEMS

Here are summarized the main reference frames of interest to AeroDyn.

The first reference frame (FF0) is the inertial system fixed at the earth surface: the x-axis (X_{FF0}) is directed along the main (nominal) wind direction and lies on the Earth's surface; the z-axis (Z_{FF0}) points upward and is aligned with the tower axis; the y-axis (Y_{FF0}) follows the right-hand-rule convention (see Figure 1).

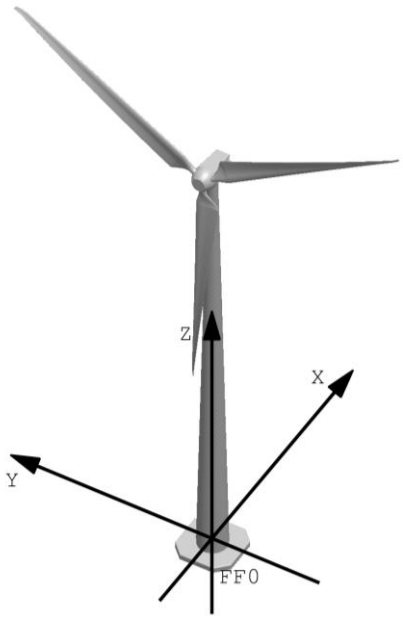

Figure 1. FF0 reference frame: x-axis aligned with the wind (south in general), z-axis upward, y-axis follows right-hand rule.

A reference frame (FFb) associated with the blade is given in Figure 2, where the z-axis (Z_{FFb}) is aligned with the pitch axis and points towards the blade tip, the y-axis points towards the TE (Y_{FFb}), and the x-axis (X_{FFb}) follows the right-hand-rule.

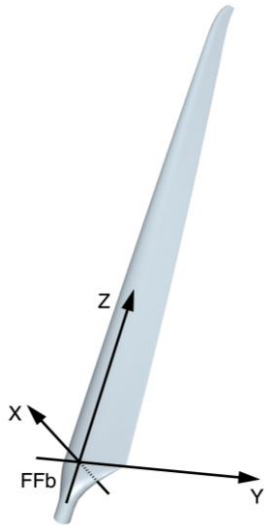

Figure 2. Blade fixed reference frame FFb. Note y-axis towards the TE of the blade, and z-axis towards the blade tip, x-axis follows the right-hand rule.

In Figure 3, the local pitch angle (θ), inflow angle (Φ), and angle of attack (AOA) are shown together with the FFb reference frame for the generic blade element (BE).

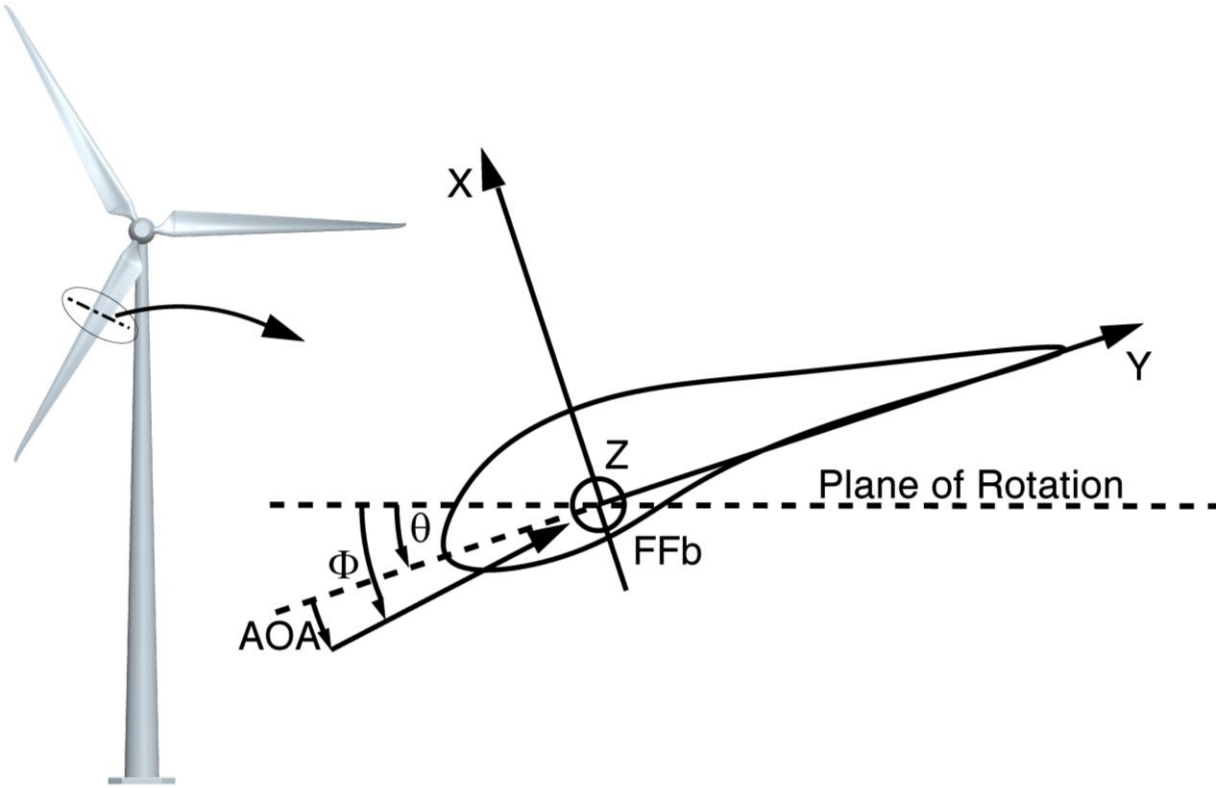

Figure 3. Definition of local pitch θ, inflow angle Φ, and angle of attack (AOA) at the blade element level.

In Figure 4, the reference frame fixed with the nacelle (FFn), and the yaw angle (γ) definition (positive as shown) are displayed. The x-axis is directed downwind; the z-axis is aligned with the tower axis and directed upward; the y-axis follows the right-hand-rule.

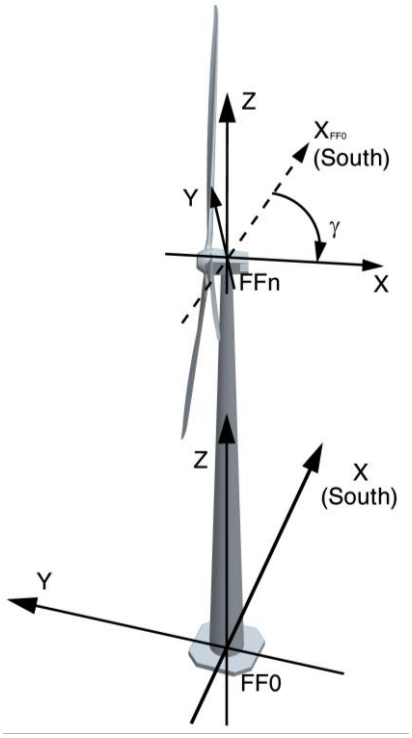

Figure 4. Nacelle reference frame (FFn) and definition of yaw angle.

In Figure 5, tilt (δ) and coning angle (Θ) definitions are shown (negative as displayed) together with FFs, i.e. the shaft reference frame, where the x-axis is aligned with the rotational shaft and directed downwind, the y axis points to the left when looking from the tower downwind, and the z-axis follows the right-hand-rule.

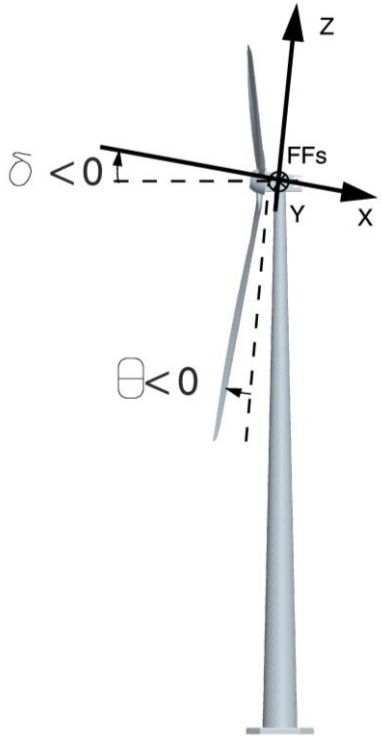

Figure 5. Definition of Tilt and Coning angles. The shaft reference frame FFs is also shown.

The rotorcraft inflow reference frame (see Figure 6) has the z-axis directed opposite to X_{FFS}, and the x-axis and y-axis lie on the plane of the rotor, with the x-axis corresponding nominally to the 12 o'clock position. The azimuth angle Ψ_{HR} is measured from the negative X_{FFHR} axis and clockwise as shown in the Figure. The angle χ_0 is the angle formed by the incoming flow with Z_{FFHR}, measured in the plane (X_{FFHR},Z_{FFHR}), on which $\underline{U}_\infty$ is supposed to lie (i.e. with no further wind directional error). If a further directional error exists, the X_{FFHR} axis is rotated by (Ψ_0) to bring the plane (X_{FFHR},Z_{FFHR}) to contain $\underline{U}_\infty$, while still pointing upward; therefore Figure 6 can still be referred to as the general FF_{HR} system, and Ψ_{HR} would be equal to Ψ (standard clockwise azimuth from 6 o'clock) less some bias (Ψ_0).

The axis coordinate ξ is aligned with $\underline{U}_\infty$ but pointing upstream. In the GDW treatment (see Section 13), the FF_{HR} is the main reference system, and more nomenclature is added such as the non-dimensional advance ratio μ and normal flow velocity λ_f(see Figure 6). An angle χ (wake skew angle) is also defined analogously to χ_0, but considering the resultant velocity (i.e. induction included).

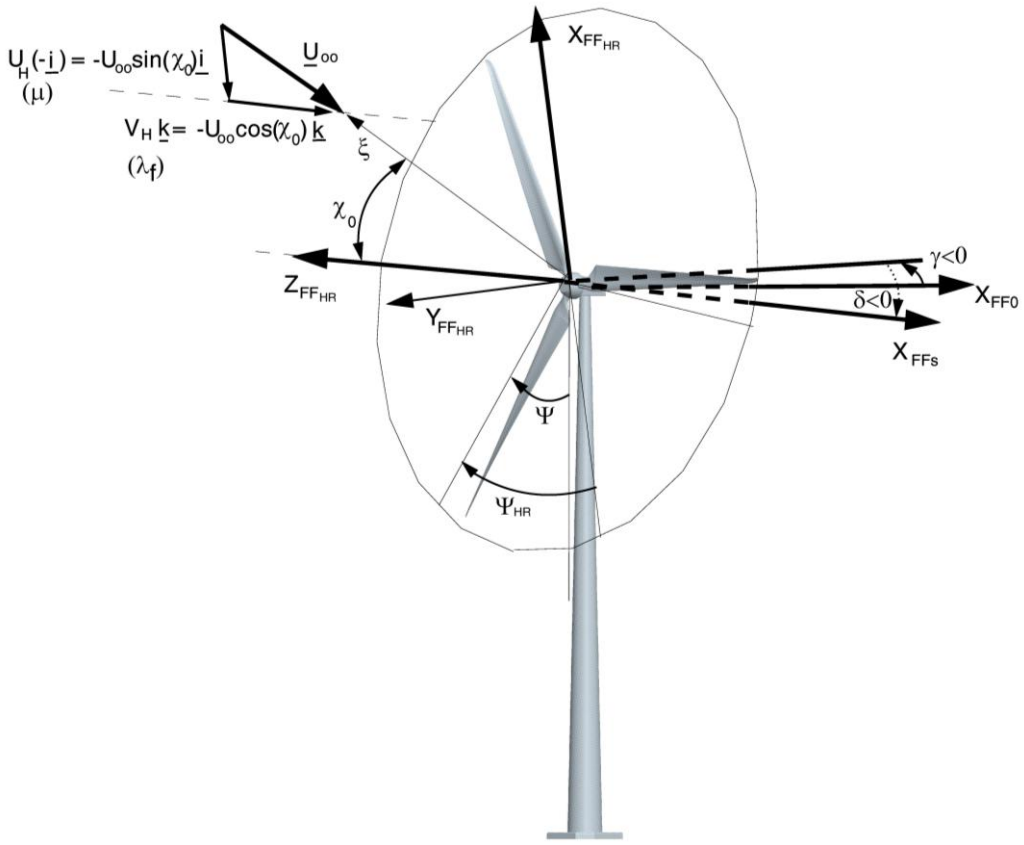

Figure 6. Rotorcraft-derived reference system (FF_{HR}) and notation (see text for more details).

3. MOMENTUM THEORY

The Momentum Theory (MT) is based on momentum balance equations along and about the X_{FF0} axis, derived considering the so-called disk-actuator theory (Manwell et al. (2002)).

A control volume (*Vol*) surrounding the rotor disk and bounded by the surface *S* is envisioned as in Figure 7. The surface *S* is composed of the streamtube (S_{lat}) and two surfaces perpendicular to X_{FF0}, one upwind (A_∞) and one downwind (A_E) of the rotor, where the static pressure is the undisturbed freestream and recovered freestream-pressure (p_∞), respectively. By definition, the wind velocity is tangent to the local streamline on S_{lat}, and its magnitude is the freestream wind speed (U_∞).

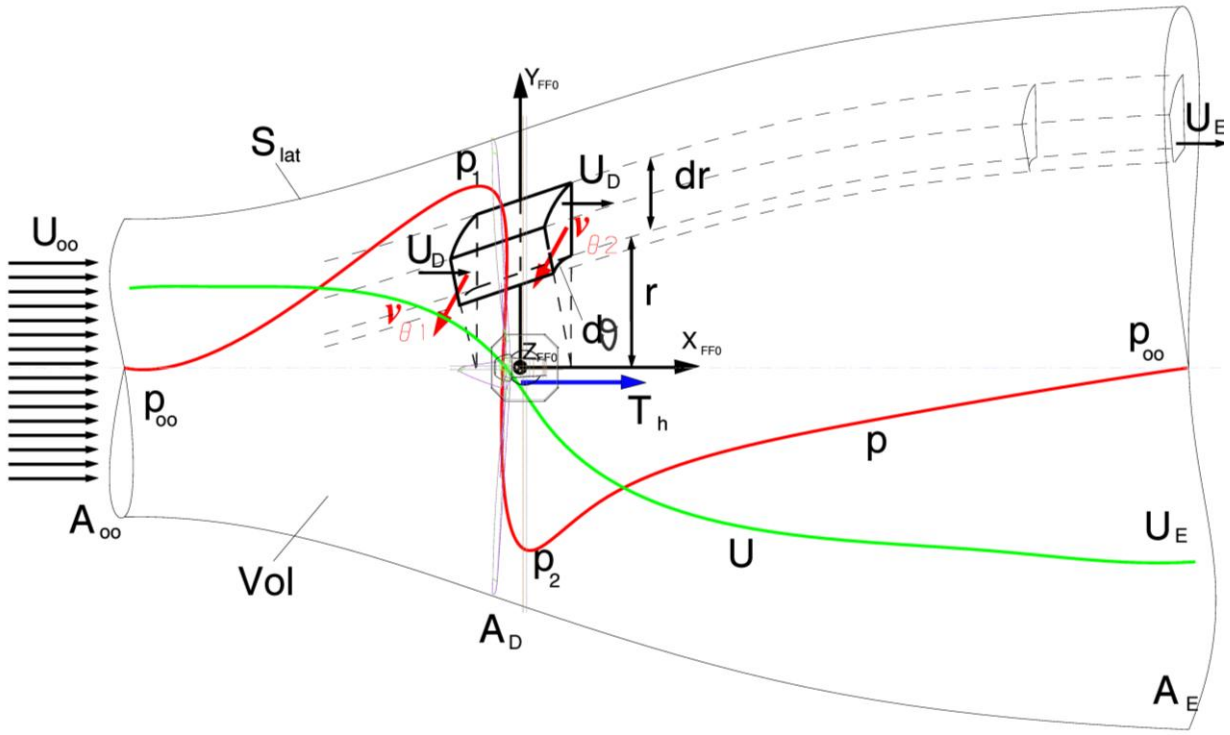

Figure 7. Control Volume (StreamTube) used in Momentum Theory. The pressure and air velocity trends are also shown.

3.1 AXIAL MOMENTUM BALANCE

The mass, momentum, and energy budget equations can then be written for the control volume as follows.

The first equation is the axial momentum budget and can be written as:

$$\frac{d}{dt}\int_{Vol}\rho\, dVol = \int_{Vol}\left[\frac{d\rho}{dt} + \rho\, div(\underline{v})\right] dVol = \int_{Vol}\left[\frac{\partial\rho}{\partial t} + div(\rho\underline{v})\right] dVol = 0 \quad (1)$$

Under the assumption of Steady-State (SS) conditions, Eq. (1) can be rewritten for the Gauss-Green theorem as:

$$\int_{Vol} \left[div(\rho \underline{v}) \right] dVol = \int_{Slat} \rho \underline{v} \cdot \underline{n}\, dS = -\rho_\infty U_\infty A_\infty + \rho_E U_E A_E = 0 \tag{2}$$

where the subscripted U indicates the generic wind speed along the main X_{FF0} axis, and the subscripts indicate either freestream conditions (∞) or outlet (E) conditions.

The second equality in Eq. (2) is justified since S_{lat} is a streamtube by definition. Note that the mass flow rate can be expressed as:

$$\dot{m} = \rho_E U_E A_E = \rho_D U_D A_D \tag{3}$$

where the subscript D indicates conditions at the actuator disc. Symbols are defined in Figure 7 and in the 'List of Symbols' section at the beginning of the report.

The momentum budget can be written as in Eq. (4) :

$$\frac{d}{dt} \int_{Vol} \rho\, \underline{v}\, dVol = \int_{Vol} \rho\, \underline{f_g}\, dVol - \int_S p\, \underline{n}\, dS + \int_S \underline{\tau_n}\, dS - T_h \hat{\imath} = 0 \tag{4}$$

where T_h is the thrust on the rotor disk. Given the assumptions on the control volume, the integral of the pressures on S_{lat} cancels out with that on A_E and A_∞.

Furthermore, by limiting Eq. (4) to the X_{FF0} axis, i.e. applying the scalar product between Eq. (4) and unit vector $\hat{\imath}$, one obtains:

$$\frac{d}{dt} \int_{Vol} \rho\, \underline{v} \cdot \hat{\imath}\, dVol = \int_{Vol} \left[\frac{\partial \rho u}{\partial t} + \mathrm{div}(\rho u \underline{v}) \right] dVol = -T_h + \int_S \underline{\tau_n} \cdot \hat{\imath}\, dS \tag{5}$$

where the last equality is true for the assumptions of no body-forces along $\hat{\imath}$ ($\underline{f_g} \cdot \hat{\imath} = 0$), and for the assumed streamtube properties. Assuming again SS conditions, and invoking the Gauss-Green theorem, Eq. (5) rewrites:

$$\int_{Vol} \mathrm{div}(\rho u \underline{v})\, dVol = -\rho_\infty U_\infty^2 A_\infty + \rho_E U_E^2 A_E = -T_h + \int_S \underline{\tau_n} \cdot \hat{\imath}\, dS \tag{6}$$

The stress vector is:

$$\underline{\tau_n} = [\underline{\tau}]\underline{n} \tag{7}$$

where the individual components of the stress tensor $[\underline{\tau}]$ can be written as:

$$\tau_{ij} = -\frac{2}{3}\mu\, div(\underline{v})\delta_{ij} + \mu(v_{i,j} + v_{j,i}) \tag{8}$$

with i and j=1..3 (the three components in the current reference frame).

In the foregoing treatment, the comma in subscript denotes a derivative.

The inlet and outlet surfaces can be thought far enough from the actuator disk that the velocity gradients become negligible. If, additionally, the streamtube is such that the shear layer is very thin at the boundary S_{lat}, then the last integral in Eq. (6) can be ignored. Analogously, setting the fluid viscosity to nil (ideal fluid) would attain the same result.

Under those conditions, the Thrust Equation from momentum theory can be written as in Eq. (9):

$$-\rho_\infty U_\infty^2 A_\infty + \rho_E U_E^2 A_E = -T_h = \dot{m}(U_E - U_\infty) \tag{9}$$

The energy budget can be derived by dot-product of Eq. (4) and the air velocity $\underline{v}$:

$$\frac{d}{dt}\int_{Vol} \rho\, \underline{v}\, dVol \cdot \underline{v} = \int_{Vol} \rho\, \underline{f_g} \cdot \underline{v}\, dVol - \int_S p\, \underline{n} \cdot \underline{v}\, dS + \int_S \underline{\tau_n} \cdot \underline{v}\, dS - T_h \hat{\imath} \cdot \underline{v} \tag{10}$$

Proceeding analogously to what was done previously, Eq. (10) can be simplified as in Eq. (11):

$$\int_{Vol} \frac{d}{dt}\left(\frac{\rho v^2}{2}\right) + \rho\, v^2 \mathrm{div}(\underline{v})\, dVol = \int_{Vol} -\rho\, \vec{\nabla} F_g \cdot \underline{v}\, dVol - \int_{Vol} \mathrm{div}(p\, \underline{v})\, dS + \int_{Vol} \mathrm{div}(\underline{\tau_i}) v_i\, dS - T_h U_D \tag{11}$$

The first integral on the RHS of Eq. (11) has been cast in terms of a potential function F_g (say $=gz$). The third integral can be considered negligible under the same assumptions declared above (small gradients) or assuming inviscid flow.

A further assumption is now introduced to simplify Eq. (11): the flow is assumed incompressible.

This assumption, in the case of SS conditions, amounts to:

$$\mathrm{div}(\underline{v}) = 0 \tag{12}$$

Eq. (11) is then rearranged as follows:

$$\int_{Vol} \underline{v} \cdot \vec{\nabla}\frac{\rho v^2}{2}\, dVol = \int_{Vol} -\rho\, \vec{\nabla} F_g \cdot \underline{v}\, dVol - \int_{Vol} \underline{v} \cdot \vec{\nabla} p\, dS - T_h U_D \tag{13}$$

or equivalently:

$$\int_{Vol} \underline{v} \cdot \vec{\nabla}\left[\frac{\rho v^2}{2} + p + \rho F_g\right] dVol = -T_h U_D \tag{14}$$

Now dividing the original control volume into two sub-volumes (Vol_1 and Vol_2) connected at the actuator disk, one could re-write the energy budget in each one to obtain:

$$\int_{Vol_{1\text{ or }2}} \underline{v} \cdot \vec{\nabla}\left[\frac{\rho v^2}{2} + p + \rho F_g\right] dVol = 0 = \int_{S_{1\text{ or }2}} \left[\frac{\rho v^2}{2} + p + \rho F_g\right] \underline{v} \cdot \underline{n}\, dS \tag{15}$$

where the second equality made use of the incompressibility assumption and the Gauss-Green theorem.

It can be easily shown that carrying out the integral in Eq. (15) for the two sub-volume surfaces yields:

$$\begin{aligned} \frac{\rho U_\infty^2}{2} + p_\infty + \rho g z_\infty &= \frac{\rho U_D^2}{2} + p_{D1} + \rho g z_{D1} \\ \frac{\rho U_D^2}{2} + p_{D2} + \rho g z_{D1} &= \frac{\rho U_E^2}{2} + p_\infty + \rho g z_E \end{aligned} \tag{16}$$

where it was assumed that F_g=gz is the body force potential, and the numbers in the subscripts denote the upwind (1) or downwind (2) actuator-disc conditions. The contribution to potential energy ($\rho g z$) is small and thus may be ignored even if small variations in height were to be considered.

The thrust on the actuator disk can then be expressed as:

$$T_h = (p_{D1} - p_{D2}) A_D = \frac{\rho (U_\infty^2 - U_E^2)}{2} A_D \tag{17}$$

where the second equality made use of the results of Eq. (16).

Finally, equating Eq.s (17) and (9) one obtains:

$$\frac{\rho (U_\infty + U_E)}{2} A_D = \dot{m} = \rho\, U_D A_D \tag{18}$$

Eq. (18) expresses the result that the air speed at the disk is the average between the free stream wind speed and the outlet wind speed.

The following expressions for the air velocity at the disk and at the control-volume outlet can be obtained by introducing the induction factor a:

$$\begin{aligned} U_D &= (1-a) U_\infty \text{ (definition)} \\ U_E &= (1-2a) U_\infty \end{aligned} \tag{19}$$

The thrust at the actuator disk can be re-expressed as:

$$T_h = \dot{m}\,(U_\infty - U_E) = \rho\, 2a\,(1-a) U_\infty^2 A_D \tag{20}$$

The thrust coefficient (C_{Th}) becomes:

$$C_{Th} = \frac{T_h}{\frac{\rho}{2} U_\infty^2 A_D} = 4\,a\,(1-a) \tag{21}$$

Eq. (21) represents one of the two main results of the Momentum Theory.

3.2 ANGULAR MOMENTUM BALANCE

If the rotation in the wake were to be considered, the angular momentum of an air parcel could be calculated with respect to a fixed point, i.e. the hub center or the center of the actuator disk. In this way, one could expect to obtain an expression for the rotor torque.

The angular momentum can be written, with symbols still as in Figure 7, as:

$$\underline{K_o} = \int_{Vol} \underline{r} \times \rho \underline{v}\, dVol \tag{22}$$

Therefore Newton's second law can be written as:

$$\underline{M_o} = \dot{\underline{K}}_o = \frac{d}{dt} \int_{Vol} \underline{r} \times \rho \underline{v}\, dVol \tag{23}$$

Following what was done in Section 3.1, Eq. (23) can be expanded as in Eq. (24):

$$\begin{aligned} \underline{M_o} = \dot{\underline{K}}_o &= \int_{Vol} \frac{d}{dt}\left(\underline{r} \times \rho \underline{v}\right) + \underline{r} \times \rho \underline{v}\, \mathrm{div}\left(\underline{v}\right) dVol = \\ &= \int_{Vol} \frac{\partial}{\partial t}\left(\underline{r} \times \rho \underline{v}\right) + \underline{v} \cdot \vec{\nabla}\left[\underline{r} \times \rho \underline{v}\right] + \underline{r} \times \rho \underline{v}\, \mathrm{div}\left(\underline{v}\right) dVol \end{aligned} \tag{24}$$

Finally one may write:

$$\underline{M_o} = \dot{\underline{K}}_o = \frac{\partial \underline{K_o}}{\partial t} + \int_{Vol} \underline{v} \cdot \vec{\nabla}\left[\underline{r} \times \rho \underline{v}\right] + \left(\underline{r} \times \rho \underline{v}\right) \mathrm{div}\left(\underline{v}\right) dVol = \frac{\partial \underline{K_o}}{\partial t} + \int_{S} \underline{r} \times \rho \underline{v}\left(\underline{v} \cdot \underline{n}\right) dS \tag{25}$$

where the last equality made use of the usual Gauss-Green's theorem applied to the tensor field $\left(\underline{r} \times \rho \underline{v}\right) \underline{v}$ (see also Shey (1973)).

Assuming again SS conditions as in Section 3.1, the elemental angular momentum rate of change is equal to the elemental torque exerted on the parcel as in Eq. (26):

$$\underline{dM_o} \cdot \hat{\imath} = dM_{ox} = \left(\underline{r} \times \rho \underline{v}\right) \cdot \hat{\imath}\, \left(\underline{v} \cdot \underline{n}\right) dS = -\rho \underline{v} \cdot \left(\underline{r} \times \hat{\imath}\right)\left(\underline{v} \cdot \underline{n}\right) dS \tag{26}$$

If $\underline{r}$ is limited to the actuator disk plane which is perpendicular to X_{FF0}, then Eq.(26) is re-written as:

$$dM_{ox} = \rho v_\theta r\, \left(\underline{v} \cdot \underline{n}\right) dS \tag{27}$$

where v_θ is the tangential air-velocity. Considering again the flow as incompressible, and either the assumption of no radial flow or that of axial-symmetric flow, and carrying out the integration of Eq. (27) to an elemental volume located across the rotor plane as in Figure 7, yields:

$$dM_{ox} = \rho \Delta v_\theta r\, U_D\, r d\vartheta dr = d\dot{m}\, r \Delta v_\theta \tag{28}$$

In fact, under those assumptions, the only term left is Δv_θ, i.e. the variation of the tangential air velocity along the X_{FF0} axis.

The free stream is by definition uniform, thus non-rotating (i.e., $v_{\theta 1} = 0$). The extraction of energy by the rotating rotor will cause the flow to acquire a tangential, or rotational, component in its wake that is opposite in direction to the rotor rotational velocity and double in magnitude. Introducing the tangential induction factor a', the near wake tangential velocity, $v_{\theta 2}$, can be written as:

$$v_{\theta 2} = \Delta v_\theta = 2\Omega r a' \tag{29}$$

Therefore the torque in Eq. (28) can be simplified as:

$$dM_{ox} = \rho \Delta v_\theta r \, U_D \, r d\vartheta dr = \rho r d\vartheta dr \, (1-a) U_\infty \, r^2 2\Omega a' \tag{30}$$

Integrating Eq. (30) across the rotor (actuator) disk would yield an expression for the overall torque exerted on the air parcel by the rotor, which is opposite to that gained by the rotor itself.

This is the second main result of the MT theory.

The increase in kinetic energy due to the rotation imparted to the freestream into the wake corresponds to a drop in pressure that can be assumed equal to:

$$\Delta p_{\text{rot}} = \frac{\rho}{2} (2\Omega r a')^2 \tag{31}$$

This pressure drop is radially balanced (in the wake downstream of the rotor) by the centrifugal force. However, this effect may be included in the overall axial balance derived in Section 3.1 (see Section 5).

3.3 Expression for Extractable Power

The axial momentum balance was derived with attention to the whole control volume, and therefore produced an expression for the thrust that applies to the entire actuator disk.

One could extend those results by assuming an individual element of the rotor area, dS, just as it was done for the angular momentum balance:

$$\frac{\rho}{2} (U_\infty^2 - U_E^2) dA_D = \rho \, U_\infty^2 (1-a) 2a \, r d\vartheta dr = dT_h \tag{32}$$

where results from Eq. (17) and (19) are used to obtain the first equality.

The extractable power can be expressed in terms of torque times the rotor rotational speed or, equivalently, as the thrust times the local flow velocity:

$$dP = \, dM_{ox} \, \Omega = dT_h U_D \tag{33}$$

By substituting Eq.s (30) and (32) into Eq. (33), one obtains a relationship between the axial and tangential induction factor:

$$\frac{a(1-a)}{a'} = \left(\frac{\Omega r}{U_\infty}\right)^2 = \lambda_r^2 \tag{34}$$

Where λ_r is the local speed ratio.

3.4 MT Conclusions

The main equations of the Momentum Theory have been derived from first principles. While the derivation may not be necessary given the established equations in the industry common practice, the review of the basic equations underlying the physics of the Momentum Theory allows for a critical identification of its assumptions. Furthermore, the current AeroDyn's Theory manual (Moriarty and Hansen (2004)) omits the various steps to get to the BEMT equations, which are here shown in detail.

The Momentum Theory assumptions are:

1. Steady-State (time invariance)
2. Incompressible Flow
3. Small velocity gradients along the control volume boundaries (or inviscid flow)
4. Either axial-symmetric flow, or no radial flow

Note that the condition of inviscid flow is not absolutely necessary as long as the shear layer around the assumed control volume is of limited proportions. The more loaded is the rotor, the larger and more complex the control volume; therefore, for large induction factors, where vortex ring or braked windmill states are encountered (see Section 7), the theory loses applicability.

The outcome of the MT is a set of relationships that allow calculating the thrust, torque, and power exerted by the flow on the turbine rotor as a function of two parameters: the induction factors a and a'.

Determining the values of the induction factors is a task for the BEMT (Blade Element Momentum Theory) (see Section 5).

Note that the air velocities in the equations presented so far are to be intended as body relative; the body motions due to structural deflections should thus be included in both U_∞ and $v_{\theta 2}$, and the calculation of the induction factors should proceed accordingly. In AeroDyn, the tangential velocity does not include a correction for body motions, and that should be corrected (see also later discussions and Section 5.2).

4. BLADE ELEMENT MODEL

In the Blade Element Model (BEM), a blade segment and its local airfoil aerodynamics are considered. Consequently, the basic 2D characteristics of the airfoil are assumed valid. In other words, one assumption of the method is that the individual blade elements are radially independent.

Following Figure 8, the elemental thrust (thrust on rotor due to the actions on the generic blade element) can be written as:

$$dL\ \cos\Phi + dD\ \sin\Phi = dT_h \tag{35}$$

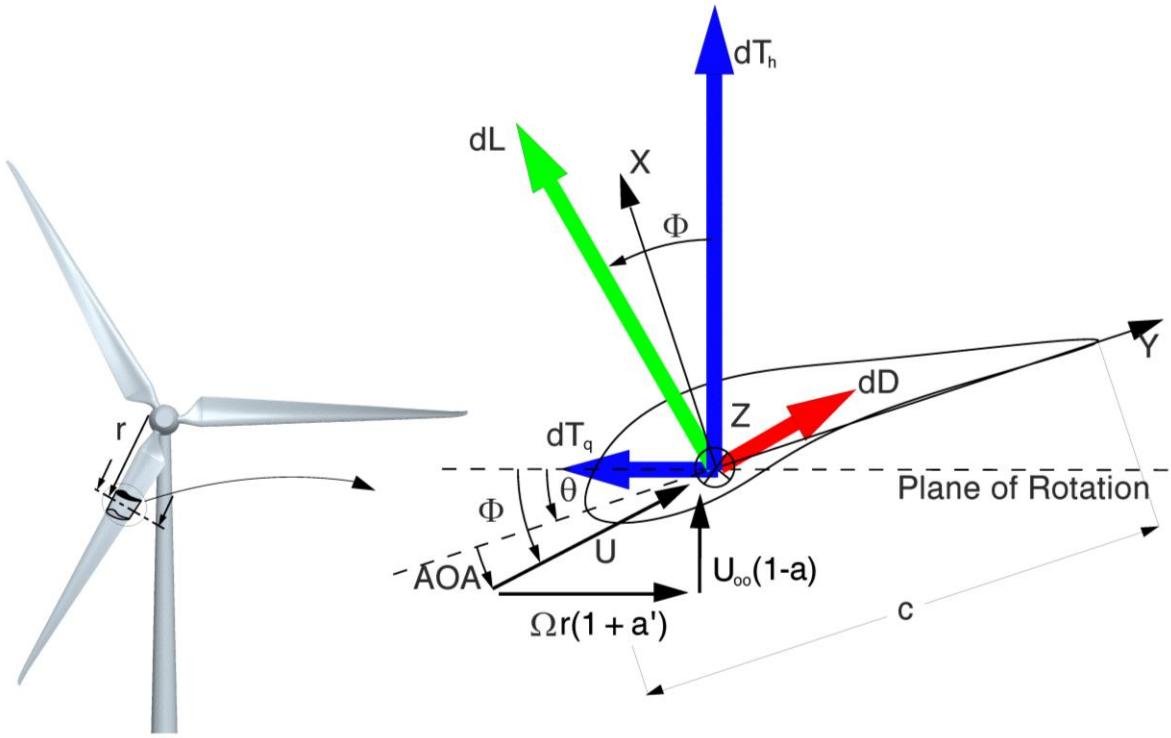

Figure 8. Basic BEMT reference frame and definitions of velocities and forces at the blade element level.

Analogously, one could write the elemental torque (torque on rotor due to the actions on the generic blade element):

$$(dL\ \sin\Phi - dD\ \cos\Phi)r = dM_{ox} \tag{36}$$

The expressions for lift and drag are the common 2D functions of the local chord (c), and lift and drag coefficients, (C_l and C_d, respectively):

$$\begin{aligned} dL &= \frac{\rho}{2} U^2 C_l\ c\ dr \\ dD &= \frac{\rho}{2} U^2 C_d\ c\ dr \end{aligned} \tag{37}$$

where U is the local air velocity relative to the airfoil, whose components are the axial and tangential air velocities introduced in the previous sections, and whose magnitude can be derived from Eq. (38):

$$U^2 = U_\infty^2(1-a)^2 + (1+a')^2\,(\Omega r)^2 = \frac{U_\infty^2(1-a)^2}{(\sin\Phi)^2} = \frac{(1+a')^2\,(\Omega r)^2}{(\cos\Phi)^2} = \frac{(1+a')\Omega r(1-a)U_\infty}{\cos\Phi\ \sin\Phi} \tag{38}$$

It is convenient to define the following thrust and tangential coefficients (see Figure 8):

$$\begin{aligned} C_{th} &= C_l\ \cos\Phi + C_d\ \sin\Phi \\ C_{tq} &= C_l\ \sin\Phi - C_d\cos\Phi \end{aligned} \tag{39}$$

The first one contributes to rotor thrust, and the second to rotor torque.

4.1 BEM CONCLUSIONS

The main equations of the BEM have been derived from simple aerodynamics definitions. The main assumption is the applicability of 2D airfoil characteristics. This limitation can be extended if appropriate aerodynamic coefficients are used for the airfoil stations along the blade. For instance, a modification for rotational effects (Coriolis and centrifugal effects on the boundary layer development) could be introduced. Other effects could be due to the presence of a coning angle, which would in turn result in an effective airfoil (obtained via a cross-section lying on the rotation plane) slightly different from that obtained via a cross-section normal to the pitch axis. The largest effect is by far the downwash due to the tip vortex, and that can be accounted for in the combination of the BEM with MT theories (see also Section 6).

5. BLADE ELEMENT MOMENTUM THEORY

The Blade Element Momentum Theory (BEMT) combines results from BEM and MT, i.e. results from Section 3 and 4.

Equating the two expressions for the thrust on an element (Eq.s (35) and (32)) and making use of Eq.s (39) yields:

$$\frac{\rho}{2}U^2(C_l\ \cos\Phi + C_d\ \sin\Phi)c\ dr\ = \rho\ U_\infty^2(1-a)2a\ r\frac{2\pi}{N_b}dr = dT_h \tag{40}$$

Note that the elemental control volume for the MT side has here been defined with an azimuth aperture of $\frac{2\pi}{N_b}$, which is equal to the sector of influence of 1 blade.

By inserting Eq. (38) (second equality) for U in the above equation and rearranging, one gets to the expression for the induction factor a:

$$a\ = \frac{1}{1+\frac{4(\sin\Phi)^2}{\sigma_r C_{th}}} \tag{41}$$

Eq. (41) consists of an implicit expression for a, since the RHS is also a function of the induction factor: the inflow angle Φ, the AOA, and the thrust coefficient C_{th} all depend on a. The RHS in Eq. (41) can be calculated from the previous step value of a in an iterative fashion.

AeroDyn, in the routine ***AXIND*** (module ***Aerosubs***, see Appendix C), defines:

$$CH\ = \frac{U^2 C_{th}}{U_\infty^2}\sigma_r \tag{42}$$

and then calculates the solution (a) from the following quadratic equation:

$$\frac{CH}{4} - a(1-a)F = 0 \tag{43}$$

which is equivalent to Eq. (40) rearranged, and where the tip and hub loss are included in the factor F (see Section 6).

The AeroDyn solution to Eq. (43) is expressed as:

$$a = \frac{1}{2}\left(1-\sqrt{1-\frac{CH}{F}}\right) \tag{44}$$

The other solution of the quadratic equation, which would sum the radical to one, is not considered valid as it would tend to give an excessive value for a.

Turning the attention to the moment-of-momentum equations, by equating the expressions in Eq. (30) and (36), one can write:

$$\frac{\rho}{2}U^2(C_l\ \sin\Phi - C_d\ \cos\Phi)r\ c\ dr = \rho r\frac{2\pi}{N_b}dr\ (1-a)U_\infty\ r^2 2\Omega a' = dM_{ox} \tag{45}$$

Carrying out similar steps to the momentum equation above, and using the last equality of (38), Eq. (45) can be rewritten as:

$$a' = \frac{1}{\frac{4\sin\Phi\cos\Phi}{\sigma_r C_{tq}} - 1} \tag{46}$$

Analogously to *a*, *a'* can be calculated iteratively, and the RHS of Eq. (46) can be calculated from the previous iteration value of *a* and *a'*.

AeroDyn, in the routine ***AXIND*** (module ***Aerosubs***, see Appendix C), calculates:

$$a' = \frac{\sigma_r C_{tq}(1+a')}{4F\sin\Phi\cos\Phi} \tag{47}$$

where the *a'* on the RHS is the previous iteration step value for the induction factor, and where the tip and hub loss are included in the factor *F*. Eq. (47) is simply Eq. (45) where no other manipulations are carried out to solve for *a'*. Additionally, if the drag component has to be excluded from the tangential induction factor calculation (*EquilDT* =.FALSE. (***Switch***), see Appendix C and Appendix D), a different formulation is used:

$$a' = \frac{1}{2}\sqrt{\left(1 + \frac{4\,Fa\,(1-a)U_\infty^2}{V_T^2}\right)} - 1 \tag{48}$$

where V_T denotes the tangential component of the velocity including rigid and elastic body motions.

Eq. (48) is Harman's (1994) method applied in the code PROPX, and it is based on the following assumption: $\tan(\Phi) = \frac{a'V_T}{aU_\infty} = \frac{(1-a)U_\infty}{(1+a')V_T}$. While the second equality is satisfied by the foregoing treatment (see for example Eq. (38)), the first equality implies that the induction vector is normal to the resultant (local) relative air-velocity $\underline{U}$. That is the so-called Goldstein's (1929) hypothesis, which has been shown to be applicable at least to some ideal cases. However, there seems to be an inconsistency in the treatment of the body-motion velocities: they participate a-posteriori in the calculation of the induction factors in the case of axial flow (normal to the plane of rotation), and a-priori in the case of tangential flow (in-plane velocities) (see also the discussion on this topic in Section 5.2).

Eq. (46) should in any case be preferred to Eq.s (47)-(48) however, as it clearly separates the new and old values of a', and therefore it should lead to faster convergence.

Aerodyn's ***AXIND*** also carries out several checks to prevent a division by zero in Eq. (47) when Φ = 0° or 90°. Indeed, instability problems have been reported in the solution of Eq. (47), and it is likely that Eq. (46) may also be afflicted by the same problem. A discussion on this subject is offered in Section 5.1.

If the extra pressure drop due to wake rotation is included in the momentum balance, then Eq. (40) can be rewritten as:

$$\frac{\rho}{2}U^2 C_{th} c\, dr = \rho\left[U_\infty^2(1-a)2a + \frac{1}{2}(2\Omega r a')^2\right] r\frac{2\pi}{N_b}dr = dT_h \tag{49}$$

By expanding Eq. (45), carrying out some algebraic operations and rearranging, one may write:

$$\sigma_r C_{tq}\, U^2 = 2r\,(1-a)U_\infty\, 2\Omega a'$$

or

$$a' = \frac{\sigma_r C_{tq}}{4\lambda_r(\sin\Phi)^2}\,(1-a) \tag{50}$$

Substituting this value for a' into Eq. (49), again making use of the expression in Eq. (38) for U^2, yields:

$$\frac{1}{4}\frac{U_\infty^2\,(1-a)^2}{(\sin\Phi)^2}C_{th}\,\sigma_r = \left[U_\infty^2(1-a)a + (\Omega r)^2\left(\frac{\sigma_r C_{tq}}{4\lambda_r(\sin\Phi)^2}\,(1-a)\right)^2\right] \tag{51}$$

Carrying out some algebra leads to the following expression for the axial induction factor a:

$$\frac{a}{(1-a)} = \frac{\sigma_r}{4(\sin\Phi)^2}\left[C_{th} - \frac{\sigma_r\, C_{tq}^2}{4(\sin\Phi)^2}\right] \tag{52}$$

Solving for a:

$$a = \frac{K}{K+1}$$

with (53)

$$K = \frac{\sigma_r}{4(\sin\Phi)^2}\left[C_{th} - \frac{\sigma_r\, C_{tq}^2}{4(\sin\Phi)^2}\right]$$

Eq. (46) and Eq. (53) can be iteratively solved to find a and a'. Alternatively, Eq. (41) and Eq. (46) can be used, neglecting the wake-rotation induced pressure-drop.

5.1 Instability Considerations in the Numerical Solution of the Induction Factors

Maniaci (2011) discusses instability issues related to solving the equations for the axial induction factor.

While the author is referring to the WT_Perf code [http://wind.nrel.gov/designcodes/simulators/wtperf/], similar considerations apply to AeroDyn, and in fact, the two codes should be merged at one point. AeroDyn is the code that should render aerodynamic performance and loading conditions on a wind turbine, and WT_perf should be made into a driver for AeroDyn to calculate just that, assuming no contributions from structural deflections in case.

The instability issues occur at an axial induction factor near 1, or near the vortex-ring state (Hansen, (2003)), though the actual solutions lie in the windmill state (see also Section 7).

Furthermore, the algorithm does not convergence due to the BEM portion of the model, and in particular within the calculation of a', i.e. the tangential and not the axial induction factor. The latter can then be

calculated from a' as for instance in Eq. (50). As it can be seen from Eq. (46) and (39), in fact, the expression for a' has a singularity near Φ =0, which tends to occur when a approaches 1. The solution to the convergence problem devised by Maniaci (2011) is to eliminate the contribution of C_d to C_{tq} with a smooth transition function centered about the axial induction factor value of 1. Eq. (46) (accounting for tip and hub losses, see also Section 6) can be re-written as:

$$a' = \frac{\frac{\sigma_r C_{tq}}{4F \sin\Phi \cos\Phi}}{1 - \frac{\sigma_r C_{tq}}{4F \sin\Phi \cos\Phi}} = \frac{K}{1-K} \tag{54}$$

The factor K is then separated in a part dependent on C_l (K_{Cl}), and one dependent on C_d (K_{Cd}), with the latter containing a function, f_{tr}, varying smoothly from 0 to 1 (0 being the value for a=1):

$$K = K_{Cl} - f_{tr}(\lambda_r, \sigma_r C_{tq}) K_{Cd} \tag{55}$$

with

$$K_{Cl} = \frac{\sigma_r C_l}{4F \cos\Phi} \qquad K_{Cd} = \frac{\sigma_r C_d}{4F \sin\Phi}$$

The transition region is given by a symmetrical sinusoidal function, with trough at a=1, and with an upper bound given by the following expression based on best-fit analysis of experimental data:

$$a_{up} = \left(1.0718 * \left|\sigma_r C_{tq}\right| - 0.003\right)|\lambda_r| + (1+\kappa) \tag{56}$$

where κ is an offset that best fits the experimental data (≃0.01-0.02).

The procedure seems to be quite effective at eliminating convergence issues, though the penalty is that some contribution to the load calculation due to drag (minor except at higher AOAs) is neglected and the computational time to arrive at convergence is increased.

5.2 REMARKS ON AIR VELOCITY COMPONENTS USAGE IN AERODYN

The air velocities ($\underline{U}_\infty$ and thus $\underline{U}$) in the foregoing treatment are to be considered as body relative; i.e., rigid-body motions and motions due to structural deflections need to be accounted for in a vector sum with the wind velocity to give a total velocity.

The best way to proceed is to calculate from the total velocity (prior to induction) a *VNTotal*, component normal to the local plane of rotation, and a *VTTotal*, component along the local plane of rotation and tangent to the local rotation circle. The third component *VSTotal* (tangent to both the local, deflected blade shear-center axis, and the local rotation plane) would have secondary effects on the boundary layer development, but may be important for stall delay and rotational augmentation issues.

AeroDyn (in ***AD_CalculateLoads*** (***Aerodyn***), see Appendix B and Appendix N) calculates the following velocity components: *VTTotal*, i.e. the tangential velocity (in-plane) as a vector sum of the body motion and wind velocity; *VNWind*, i.e. wind velocity component normal to the plane of the rotor; and *VNElement*, i.e. in-plane component of the body motion velocity.

It additionally calculates the square of the wind velocity component normal to the rotor plane (*VelNormalToRotor2*), which should be equivalent to $VNWind^2$.

In ***AXIND*** (***AeroSubs***, see Appendix C), the induction factors' calculations are performed by considering the induction a acting only on the wind velocity component normal to the plane of rotation; the body motion is added a-posteriori to find the resultant relative air-velocity. On the other hand, a' multiplies both the body motion and the wind velocity components in the plane of rotation (a-priori fashion).

A similar treatment takes place in ***VINDINF*** (***AeroSubs***, see Appendix C).

That should be revised. It seems reasonable to assume that *VNWind* should be replaced by a *VNTotal*, i.e. the analog of *VTTotal* for the component normal to the rotation plane.

6. TIP AND HUB (ROOT) LOSSES

The MT assumes an infinite number of blades for the actuator disc model to be valid. The finite number of blades will cause the flow to depart from the approximation of the basic BEMT.

The so-called Extended BEMT (EBEMT See Maniaci (2011)) includes corrections for the finite number of blades and for the tip-loss, as well as other corrections for turbine states other than 'windmill' (see Section 8).

The first model that attempted to account for tip-losses was proposed by Glauert (1963). That model is based on the fact that the ratio between the averaged induced velocity and the induced velocity at the generic blade element tends to zero at the tip according to an expression developed by Prandtl (1927). Several other corrections to the BEMT have been proposed in the literature (see a brief review in Shen (2009) and Shen et al. (2005)).

The original Prandtl's correction was formulated as follows:

$$F_T = \frac{2}{\pi}\cos^{-1}\left[\exp\left(-\frac{N_b\left(1-\frac{r}{R}\right)}{\frac{2r}{R}\sin\Phi}\right)\right] \tag{57}$$

where r and R are the local blade element and blade-tip distances from the root respectively, measured along the blade axis.

F_T is the tip-loss factor and multiplies the forces as derived from the MT.

Analogously, a hub-loss factor could be devised as:

$$F_H = \frac{2}{\pi}\cos^{-1}\left[\exp\left(-\frac{N_b\left(\frac{r}{R_H}-1\right)}{\frac{2r}{R_H}\sin\Phi}\right)\right] \tag{58}$$

The root loss physics has not been fully validated, and it has been shown that the model does not always provide accurate results (Peters (2011)).

The overall hub and tip loss factor is then:

$$F = F_H F_L \tag{59}$$

F can be used in the equations derived in Section 3 and 5, and it is simply demonstrated that Eq.s (41) and (46) (or alternatively Eq. (53)) rewrite as in the following:

$$a = \frac{1}{1+\frac{4F(\sin\Phi)^2}{\sigma_r C_{th}}} \tag{60}$$

$$a' = \frac{1}{\frac{4F \sin\Phi \cos\Phi}{\sigma_r C_{tq}} - 1} \tag{61}$$

Or alternatively (accounting for extra pressure drop due to wake rotation):

$$a = \frac{K}{K+1}$$

with (62)

$$K = \frac{\sigma_r}{4F(\sin\Phi)^2}\left[C_{th} - \frac{\sigma_r\, C_{tq}^2}{4F(\sin\Phi)^2}\right]$$

Shen et al. (2005) argue that existing tip-loss corrections are inconsistent and fail to predict the correct physical behavior in the proximity of the blade tip. The authors define two new corrected coefficients C_{ths} and C_{tqs} to account for three-dimensional effects at the tip:

$$C_{ths} = F_{TS} C_{th}$$

and (63)

$$C_{tqs} = F_{TS} C_{tq}$$

They also introduce a new tip-loss model including additional aerodynamic effects at the tips:

$$F_{TS} = \frac{2}{\pi}\cos^{-1}\left[exp\left(-g_S \frac{N_b(R-r)}{2r\sin\Phi}\right)\right] \tag{64}$$

where

$$g_S = exp(-0.125\,(N_b\lambda - 21)) + 0.1$$

This model has been at least partially validated against experimental rotor data from NREL, against the Swedish WG 500 rotor, and against CFD data (See Shen (2009)), and it showed good agreement.

Shen et al.'s (2005) model may be preferred to the Xu and Sankar's (2002) model currently implemented in AeroDyn, since that was based on CFD results alone. Additionally, Shen et al's (2005) model extends the applicability of the BEMT to the turbulent wake state, see Section 7, and it should only be applied following that treatment for the BEMT.

For completeness, Xu and Sankar's (2002) model is shown below:

$$F_{TX} = \begin{cases} -\dfrac{(F_T^{0.85} + 0.5)}{2}, 0.7 \le r/R \le 1 \\ 1 - \dfrac{r}{R}\left(\dfrac{1 - F_{T(0.7)}}{0.7}\right), r/R \le 0.7 \end{cases} \tag{65}$$

where $F_{T(0.7)} = F_T(\frac{r}{R} = 0.7)$.

In AeroDyn, the routine ***GetTipLoss*** (***AeroSubs***) shows some inconsistencies that need to be corrected in order for this last model to be properly implemented (See Appendix C).

7. EXTENSION OF THE BEMT TO OTHER TURBINE STATES

The BEMT theory has been developed on the basis that both the MT and BEM are applicable. For the MT to be applicable, the induction factors cannot exceed certain values (say a<0.3-0.5). At higher values of a, in fact, the wake velocity would be directed upwind as shown in Figure 9, for the turbulent wake (or windmill-brake) state and vortex-ring state.

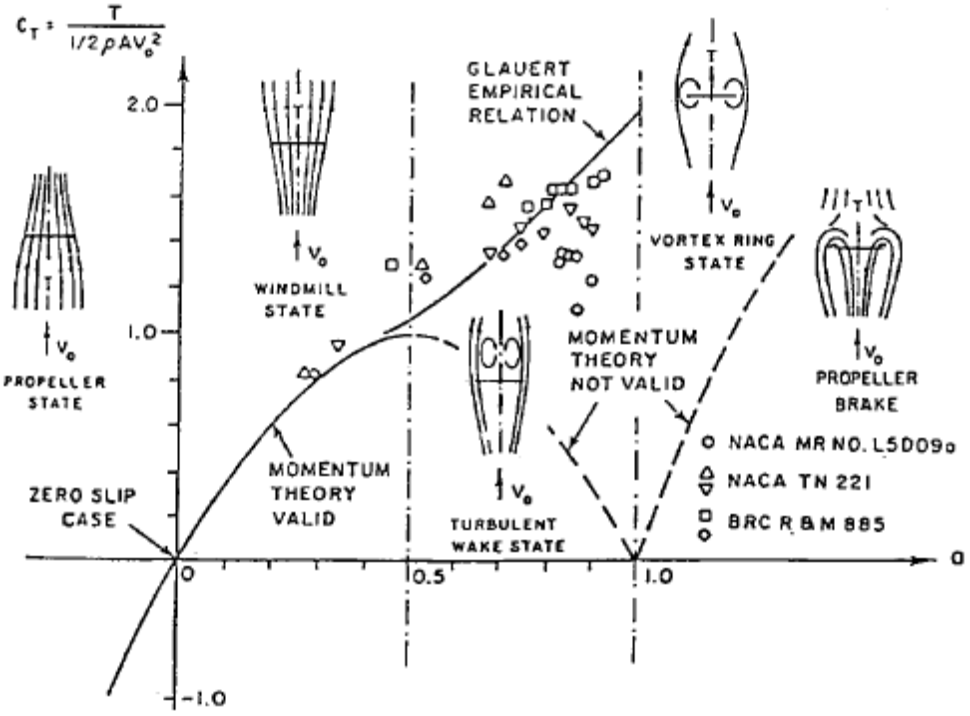

Figure 9. Turbine Wake States (From Eggleston and Stoddard (1987)).

Various corrections have been proposed (see Buhl (2005)) to extend the range of operability of the BEMT model. AeroDyn currently utilizes the following expression for the thrust coefficient in the turbulent wake state (for ***CH/F*>0.96**):

$$a = 0.1432 + \sqrt{-0.55106 + .6427 * CH/F} \tag{66}$$

Note that this is not what is presented in the AeroDyn's Theory Manual (Moriarty and Hansen (2004)) (i.e., Buhl's (2005) formula), but rather a variation of the original Glauert's relationship (Eggleston and Stoddard (1987)) following Hibbs and Radkey (1981).

Buhl's (2005) model for the axial induction factor can be written as follows:

$$a = \begin{cases} \dfrac{1-\sqrt{1-CH}}{2F}, CH \le 0.96F \\ \dfrac{18F - 20 - 3\sqrt{CH(50-36F)+12F(3F-4)}}{36F-50}, CH > 0.96F \end{cases} \tag{67}$$

The tangential induction factor can be derived from Eq. (54) or Eq. (61).

Pratumnopharat and Leung (2011) analyze six different models for the turbulent-wake state and compare them to the measured data from an experimental campaign conducted at the NWTC/NREL. The authors conclude that Shen et al's (2005) model gives the highest correlation to the measured data. Buhl's (2005) model gives a slightly lower correlation coefficient to the measured data, but it actually gives a closer match in terms of calculated annual energy production.

Shen et al. (2005) carry out a slightly different treatment for the BEMT, starting with a rearrangement of Eq. (40) as in Eq. (68):

$$\frac{\rho}{2}U^2 C_{ths} c\, dr = \frac{\rho}{2}(U_\infty^2 - U_E^2) r \frac{2\pi}{N_b} dr = \rho \frac{(U_\infty + U_E)}{2}(U_\infty - U_E) r \frac{2\pi}{N_b} dr$$
$$= \rho U_D (U_\infty - U_E) r \frac{2\pi}{N_b} dr = dT_h \tag{68}$$

The correction is then applied to the induced velocity on the MT side of Eq. (68) for both U_D and U_E terms, to give:

$$\frac{\rho}{2}\frac{U_\infty^2 (1-a)^2}{(\sin\Phi)^2} C_{ths} c\, dr = \rho U_\infty^2 (1 - aF) 2aF\, r \frac{2\pi}{N_b} dr = dT_h \tag{69}$$

Therefore a relationship for a can be attained as follows:

$$\frac{F_{TS} C_{th} \sigma_r}{4(\sin\Phi)^2} = \frac{(1-aF)aF}{(1-a)^2} \tag{70}$$

Solving for a, one obtains:

$$a = \frac{2 + Y_1 - \sqrt{4Y_1(1-F) + Y_1^2}}{2(1+FY_1)} \tag{71}$$

where

$$Y_1 = \frac{4F(\sin\Phi)^2}{\sigma_r C_{th} F_{TS}}$$

Analogously, manipulating Eq. (45), making use of Eq. (38), and applying the correction, one obtains:

$$\frac{\rho}{2} C_{tqs} r\, c\, \frac{U_\infty (1-a)\Omega r (1+a')}{\sin\Phi\cos\Phi} dr = \rho r \frac{2\pi}{N_b} dr\, (1-aF) U_\infty\, r^2 2\Omega \mathrm{F} a' = dM_{ox} \tag{72}$$

Therefore a relationship for a' can be attained as follows:

$$\frac{F_{TS} C_{tq} \sigma_r}{4\sin\Phi\cos\Phi} = \frac{(1-aF)a'F}{(1-a)(1+a')} \tag{73}$$

Solving for a', it yields:

$$a' = \frac{1}{\frac{(1-aF)Y_2}{1-a} - 1} \tag{74}$$

where

$$Y_2 = \frac{4F \sin\Phi \cos\Phi}{\sigma_r C_{tq} F_{TS}}$$

Shen et al. (2005) propose a critical value for the induction factor of a_c=1/3, which corresponds to a critical value for the coefficient *CH* (following AeroDyn's treatment) of:

$$CH_{cs} = \frac{4F}{3}\left(1 - \frac{F}{3}\right) \tag{75}$$

Therefore *a* can be calculated as:

$$a = \begin{cases} \dfrac{1 - \sqrt{1 - CH}}{2F}, CH \leq CH_{cs} \\ \dfrac{2 + Y_1 - \sqrt{4Y_1(1 - F) + Y_1^2}}{2(1 + FY_1)}, CH > CH_{cs} \end{cases} \tag{76}$$

The expression of *a'* is unchanged and can be taken from Eq. (74).

8. CONE ANGLE EFFECTS

A utility-scale upwind HAWT is generally coned, i.e. the blade axes are not perpendicular to the rotor shaft, but tilted upwind (negative cone angle) to further prevent possible tower strike due to blade deflections. Additionally, the rotor shaft may be tilted with respect to the horizontal plane (X_{FF0},Y_{FF0}) (see Figure 5).

If a positive cone angle is employed, the goal is to take advantage of centrifugal stiffening, or inertia induced bending moment which tends to relieve the flapwise, thrust-induced bending. A downwind HAWT may also be coned away from the tower.

In order to account for the cone angle Θ, the horizontal component of the freestream (or local wind velocity) can be decomposed along the blade axis and along the normal to that axis. The normal component acts like U_∞ of the previous sections. The component along the blade generates secondary and three-dimensional effects on the boundary layer.

AeroDyn first calculates the wind velocity in an inertial reference frame (FF0), then adjusts the wind velocity for the presence of the tower (see Section 10). It then calculates the components along and normal to the 0-pitch local y axis (Y_{FFb}) (tangent to the rotational circle described by the local element) (see ***AD_CalculateLoads*** (***Aerodyn***), and Appendix B). These components are then treated as 'along' and 'normal' to the rotational plane, i.e. the coning effect is disregarded. The component of the velocity normal to the rotor does not seem to be calculated accurately in ***AD_CalculateLoads*** (***Aerodyn***).

In particular if coning and/or tilt exist, the ***AD_CalculateLoads***'s variables *VTTotal* , *VNWind* , *VNElement* are not the actual tangential and normal total and body velocities for the reasons explained above (see also Appendix B).

In order to account for the cone angle, the local velocity needs to be decomposed appropriately along and normal to the local rotational plane, which also needs to account for tilt.

Additionally, the actual air velocities need to be considered as the vector sum (total velocity) of the wind velocity and body velocities (due to translations, rotations and deflections altogether).

If the airfoil definition is kept on planes normal to the pitch axis, there will be some parts of the airfoil (namely the suction side for a negative cone angle) that would see slightly higher air speeds than others, since they will be located at a higher effective radial distance from the rotational axis. Neglecting this minor effect, the freestream velocity $\underline{U}_\infty$ may be decomposed along the normal to the pitch axis, and the local relative air velocity can be expressed as:

$$U^2 = U_\infty^2(1-a)^2(\cos\Theta)^2 + (1+a')^2\,(\Omega r\cos\Theta)^2 = \frac{U_\infty^2(1-a)^2(\cos\Theta)^2}{(\sin\Phi)^2}$$
$$= \frac{(1+a')^2\,(\Omega r\cos\Theta)^2}{(\cos\Phi)^2} = \frac{(1+a')\Omega r(1-a)U_\infty(\cos\Theta)^2}{\sin\Phi\cos\Phi} \qquad (77)$$

Eq. (40) changes as follows: on the MT side of the equation, the radial distance r (dr)(still measured along the blade z-axis) becomes $r\cos\Theta(dr\cos\Theta)$; Eq. (77) (2nd equality) replaces U^2 in the BEM side of the

equation; additionally the factor cos Θ needs to be inserted on the same side of the equation to account for the thrust component along the axis of rotation. Carrying out the algebra yields a new expression for the induction factor *a*:

$$a = \frac{1}{1 + \frac{4(\sin\Phi)^2}{\sigma_r C_{th} \cos\Theta}} \tag{78}$$

Analogously, the factor CH in AeroDyn, in the module ***Aerosubs*** and routine ***AXIND*** (see Appendix C), i.e. Eq. (42) can be replaced by the following expression:

$$CH = \frac{U^2 C_{th}}{U_\infty^2 \cos\Theta}\sigma_r \tag{79}$$

Its solution, calculated as Eq. (43), remains unaltered.

For the moment of momentum equations: Eq. (45) needs to be modified on the MT side of the equation to account for the radial distance from the rotational axis, so r (dr)(still measured along the blade z-axis) becomes r cos Θ(dr cos Θ); on the BEM side, the arm r becomes r cos Θ; the last equality in Eq. (77) may then be used to substitute for U^2. Eq. (46) then becomes :

$$a' = \frac{1}{\frac{4\sin\Phi\cos\Phi\cos\Theta}{\sigma_r C_{tq}} - 1} \tag{80}$$

So the equations for a and a' for a coning angle Θ can be easily obtained from the unconed ones (Eq.s (41), (46), (54), (60), and (61), as well as Shen et al's (2005) extension Eq.s (71) and (74), (76)), replacing C_{th} with $C_{th}\cos\Theta$, and C_{tq} with $C_{tq}/\cos\Theta$.

If the wake-rotation induced pressure-loss is included, Eq. (53) (or better Eq. (62) accounting for tip and hub loss), by carrying out similar substitutions in its derivation as done above, becomes:

$$a = \frac{K}{K+1}$$

with (81)

$$K = \frac{\sigma_r}{4F(\sin\Phi)^2}\left[C_{th}\cos\Theta - \frac{\sigma_r\, C_{tq}^2}{4F(\sin\Phi)^2}\right]$$

Note that in Eq. (81) the cone angle appears to solely affect the coefficient C_{th}.

Another aspect to consider is that the 2D definition of the blade elements, i.e. the airfoil stations, are likely defined along sections normal to the blade axis. However, the effective airfoil shape is that obtained through a cross-section on a plane normal to the local rotational plane. As a result, the camber, twist, and thickness (and potentially the chord, if the blade is tapered and twisted) of the effective airfoil would be

altered from the originals. Consequently, the aerodynamic coefficients used in the 2D BEM should be modified accordingly.

An additional effect of the cone angle is that the component of the total velocity along the blade span affects the boundary-layer dynamics and therefore the airfoil aerodynamics of the individual blade elements. This aspect needs to be considered together with centrifugal and Coriolis effects during the treatment of 3D augmentation effects and delayed stall. It would add or subtract to inertial effects on the boundary layer depending on the blade azimuthal position.

The effects of coning may be significant only for the larger utility-scale wind turbines and should be analyzed in detail.

The tilt angle affects the whole rotor plane; the freestream velocity component along the normal to the rotor plane can then be easily calculated (see also Figure 5). Furthermore, the component along the rotor plane causes three-dimensional effects, similar to those due to coning. However, in the case of tilt, a change of sign occurs between the effects on the upper semi-circle and on the lower-semicircle described by the local blade element, in contrast to the coning situation where the sign remains constant (i.e., against centrifugal stall delay with negative coning). Nevertheless, the tilt angle has profound implications on the skewness of the wake and the associated induction, thus it needs to be accounted for together with yaw and off-plane aerodynamics (see Section 9).

9. YAW AND TILT ANGLE AND THEIR EFFECTS ON SKEWED WAKE

The aerodynamics of a yawed (and/or tilted) wind turbine is extremely complex and subject to considerable uncertainty. Several flow features complicate the situation:

- Skewed component of wind velocity acting towards and away from the blade tip depending on the rotational semi-cycle.
- Cyclic change in AOA experienced by the blade as it alternatively advances into and retreats from the incoming flow.
- A complex wake structure giving rise to major modification of the distribution of inflow velocities at the rotor disk.

Unsteady effects and radial flow are capable of significantly modifying airfoil characteristics from those of 2D tabular data. The standard BEMT is highly challenged in this situation.

The work of Glauert (1926) (see also Burton et al. (2001)) was based on the autogyro inflow aerodynamics, and it starts from the basic idea of correcting the actuator-disk average value of the induction factor a using a Fourier series in the azimuth angle Ψ_{HR} (measured from the halfway position between upwind and downwind side of the rotor):

$$a_{skw}(r,\Psi_{HR}) = \overline{a}\left[1+\sum_{n=1}^{\infty} K_{ns}(\gamma,r/R)\sin\Psi_{HR} + K_{nc}(\gamma,r/R)\cos\Psi_{HR}\right] \tag{82}$$

Glauert (1926) truncated the series to only the first sine term, which increases the induction values on the downwind side of the rotor and decreases it on the upwind side. Other researchers proposed various formulas for the correction (e.g.: Coleman et al. (1945), Meyer Drees (1949), Pitt and Peters (1981)).

The following formula is attributed to Pitt and Peters (1981) and Coleman et al. (1945) for the derivation of the term K_{1s}:

$$a_{skw} = a\left[1+\frac{r}{R}\frac{15\pi}{32}\sin\Psi_{HR}\tan(\chi/2)\right] \tag{83}$$

In AeroDyn, the wind velocity is decomposed into in-plane (*Vinplane*) and normal to rotor plane (*VROTORX*) accounting for both yaw and tilt angle; an angle of attack *ANGFLW* (α_D) is calculated between the wind velocity vector and the rotor plane; an additional angle ∂ is calculated between the *Vinplane* vector and the vertical reference line in the rotor plane (see ***DiskVel*** (***AeroSubs***), and Appendix C).

AeroDyn corrects the induction factor as in Eq. (84):

$$a_{skw} = a\left[1+\frac{r}{R}\frac{15\pi}{32}\sqrt{\frac{1-\sin\alpha_D}{1+\sin\alpha_D}}\left(\sin\partial\sin\Psi+\cos\partial\cos\Psi\right)\right] \tag{84}$$

It follows (loosely) Pitt and Peters (1981) and Coleman et al. (1945), with the term in parentheses representing the actual cosine of the azimuth angle measured from the most downwind position of the rotor, after accounting for tilt and yaw. Note that this is equivalent to the $\sin\Psi_{HR}$ in the original work of Galuert (1926), where the convention for the azimuth in AeroDyn is such that the angle is measured from the vertical (down) position of the blade.

In the original work of Pitt and Peters (1981), the correction term included a $\tan(\chi/2)$ term, which is set to 1 following Hansen (1992), where χ is the wake skew angle, i.e. the angle formed by the wake axis and the normal to the rotor.

Furthermore, the helicopter aerodynamics models that gave origin to formulations such as Eq. (83) were meant to be applied to the entire rotor disk, and as a-posteriori corrections to the overall disk-average induction factor. AeroDyn's approach, based on the infinitesimal element is quite different from the original.

The effects of off-axis flow are challenging to represent in a parsimonious model such as the extended BEMT in AeroDyn. It seems, however, (see also Chaney et al. (2001)), that the application of a formulation similar to Eq. (83), and to an elemental volume as opposed to the whole rotor disk, brings enough fidelity for the model to retain this option.

Further notes on AeroDyn:

- The reference frames should be verified against what is actually implemented in AeroDyn, and included in the theory manual.
- The air velocity should be calculated as combined effect of wind + body motion, where the correct kinematics is developed for all terms. (e.g.: ***DiskVel*** (***AeroSubs***) computes *VROTORY* from the wind component with a contribution of *YAWVEL* calculated in ***AD_CalculateLoads*** (***Aerodyn***) as partial contribution of body kinematic terms; see also Appendix B and Appendix C)

More research and more validation against experimental data are needed to confirm this approach however. This is beyond the scope of this contract, but the NWTC/NREL staff is encouraged to promote this effort.

10. TOWER EFFECTS

The presence of the tower affects the field everywhere, being the equations of motion (Eq.s (1), (4), (10)) of elliptical type. Therefore the effects on the flow can be seen upwind (a.k.a. dam (or blockage) effects) as well as downwind (a.k.a. wake (or shadow) effects) of the tower.

The flow field, however, is affected by the tower as much as, if not more, by the rotor blades. This effect is not modeled in AeroDyn. Consequently, the tower would affect a field already modified by the presence and actions of the rotor. These effects are not linear and not independent, and cannot arbitrarily be superimposed. Additionally, not only the mean flow field, but also the turbulent field is significantly affected by the presence of the tower and rotor. At a first level of approximation, however, and for large rotor-diameter-to-tower-diameter ratios, the tower effect is that of a bluff body affecting the surrounding mean flow and the wind velocities as seen by the rotor. The effect on the vertical component of the flow may also be neglected for a tall tower.

AeroDyn utilizes a model based on Bak et al. (2001) and Powles (1983), and it assumes a fixed tower (i.e. undeflected by either structural or aerodynamic loading).

The tower wake model proposed by Powles (1983) is:

$$u_{wk} = \frac{C_{dt}}{\sqrt{d}} \cos\left(\frac{\pi}{2}\frac{y}{\sqrt{d}}\right) \tag{85}$$

where C_{dt} is the 2D drag coefficient for the tower section, y is the normalized lateral distance under consideration from the wake axis, and $d = \sqrt{x^2 + y^2}$ is the normalized distance of the same blade element from the tower centerline. The normalization is based on the tower section radius.

There are two models available in AeroDyn, the old and the new tower shadow model.

In the old model, C_{dt} is given as a user input (*TWRSHAD*), d and y are normalized by a distance given by the user (*T_Shad_Refpt*) (usually taken as yaw-axis to hub center distance), and y is normalized by a wake halfwidth (*SHADHWID*) given by the user and considered applied at the *T_Shad_Refpt* distance. Additionally, if the blade element under examination is above the hub-height, y is calculated as the radial distance from the wake axis imagined passing through the tower top: i.e., the wake departing from the tower top is assumed three dimensional and with a semicircular cross-section of radius equal to $\sqrt{d}$ (see also Figure 10).

Note that in AeroDyn, the distances y and d are calculated solely based on the FF0 reference frame (as the input comes externally from the *Blade*(*IElement*,*IBlade*) marker (**AllAeroMarkers** (***SharedTypes***), see Appendix F), which then assumes a mean wind velocity along X_{FF0}. This may or may not be the accurate wind direction, especially in yawed configurations, where the rotor and its wake influence may be skewing the wake axis direction. The freestream wind velocity components in the horizontal are then reduced by a u_{wk} fraction:

$$\underline{U}_{\infty h} = \underline{U}_{\infty h}\,(1 - u_{wk}) \tag{86}$$

No vertical component adjustment is performed.

In the new model, the user provides an additional input file where cross-sectional diameters and C_{dt} values are given at various tower stations along the z coordinate (possibly as a function of the Reynolds number). Eq. (85) in its original form (Powles (1983)) is used for the downwind wake/shadow effect, with the extra correction at the top of the tower as done in the older model (see Figure 10).

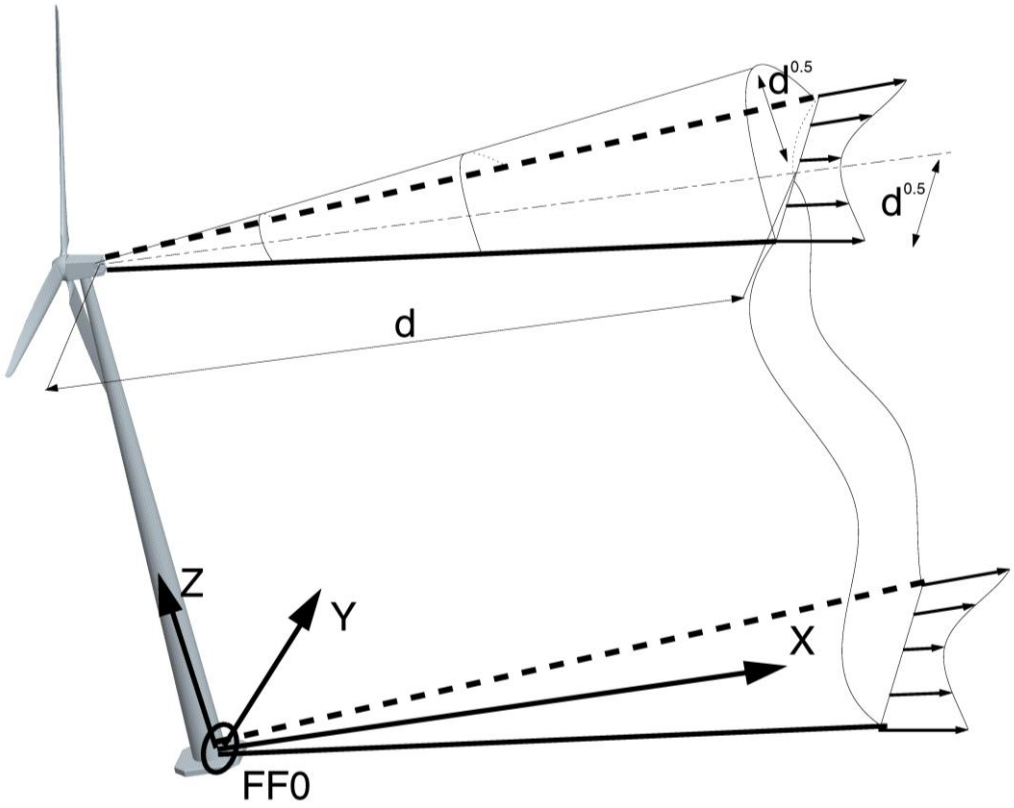

Figure 10. Tower wake schematic. See text for details.

Additionally, the new model accounts for the dam effect upwind of the tower:

$$u_w = 1 - \frac{(x + TwrC)^2 - y^2}{[(x + TwrC)^2 + y^2]^2} + \frac{C_{dt}}{2\pi}\frac{x + TwrC}{(x + TwrC)^2 + y^2}$$
$$v_w = -2\frac{(x + TwrC)y}{[(x + TwrC)^2 + y^2]^2} + \frac{C_{dt}}{2\pi}\frac{y}{(x + TwrC)^2 + y^2} \quad (87)$$

where u_w and v_w are multiplicative factors to correct for the wind velocity components in the horizontal plane; x and y are the blade element coordinates along the wind reference frame normalized by the tower radius; and *TwrC* is a constant, usually set equal to 0.1 in Bak et al.'s (2001) model.

Note that Eq. (87) implies a reference frame aligned with the mean wind. In AeroDyn, that should be FF0, yet the program transforms the blade element position coordinates into the local wind direction, performs the calculations in Eq. (87), applies the correction to the magnitude of the horizontal wind velocity, and then transforms the results back to FF0. This is inconsistent with the treatment of the tower-shadow correction, where FF0 is used for all of the calculations.

The general formula for correction is:

$$\underline{U}_{\infty h} = \underline{U}_{\infty h} \begin{pmatrix} u_w \\ v_w \end{pmatrix} \tag{88}$$

where the mean wind velocity reference frame is assumed for both $\underline{U}_{\infty h}$ and $\begin{pmatrix} u_w \\ v_w \end{pmatrix}$.

In order to account for end effects at the top of the tower, if the blade element position under consideration is above the tower top, the coordinate y in Eq. (87) is transformed into the radial distance from the axis X_{FF0}, similarly to what is done for the wake portion of the correction.

These models are semi-empirical and based on the potential flow solution around a cylinder and tend to account for the mean flow field, but turbulence or unsteadiness in the flow are ignored as are possible 3D effects.

11. ROTATIONAL AUGMENTATION EFFECTS

The theory in the foregoing makes use of lookup tables for the airfoil aerodynamics. Unsteady aerodynamics can be accounted for with a LBM type of model, but even that method requires basic 2D airfoil tables of static C_l and C_d.

The effects of rotation, however, tend to yield larger power and thrust on the wind turbine rotors than those predicted with simple 2D BEM data. In the literature several models have been proposed to account for increased lift or delay of stall to larger AOAs (see Lindenburg (2004) for a brief review) due to rotational effects.

Most of the models propose a correction (κ_{Cl}, κ_{Cd}) to the non-rotating lift coefficient, and a few also include a correction to the drag coefficient:

$$C_{l3D} = C_l + \kappa_{Cl}$$
$$C_{d3D} = C_d + \kappa_{Cd} \tag{89}$$

The theoretical basis is that pockets of fluid (inner boundary layer, separation bubble, turbulent separated volume at the TE) are subject to an apparent force in the rotating reference system, which causes them to accelerate outboard along the span. This radial velocity has a direct effect on the spanwise pressure distribution, but also an indirect effect, due to Coriolis acceleration, on the chordwise distribution. The correction factor is thus expected to depend on the (c/r) (chord-to-radius) ratio.

As a result of these effects, the boundary layer is thinner and more stable than would be in absence of rotation, and LE separation bubbles and stall are suppressed or delayed. Therefore, there is a need for tables where the LE stall is suppressed (Lindenburg (2004)).

In terms of effects on drag, the literature has shown some conflicting results, with some studies showing a decrease and others an increase in drag coefficients. The uncertainty is in part due to the increase of the aerodynamic coefficients witnessed near the root and the decrease near the tip, which make deductions based on shaft torque measurements difficult to interpret. Furthermore, integration of pressure-tap measurements in the tangential (~chordwise) direction is in general of low accuracy, and also quite sensitive to small errors in AOA data.

AeroDyn uses a pre-processor program (***FoilCheck*** or the more recent ***AirFoilPrep.xls*** version) to manipulate 2D static data for rotational effects as well as to extend lookup table data to large AOAs (Viterna and Janetzke's (1982) method) usually not available from experimental data of aeronautical type. AirFoilPrep.xls uses the correction for the lift coefficient based on Du and Selig (1998):

$$\kappa_{Cl} = \frac{1}{C_{l\alpha}}\left[\frac{1.6(c/r)}{0.1267}\frac{\kappa_a - (c/r)^{\frac{\kappa_c R}{\Delta r}}}{\kappa_b + (c/r)^{\frac{\kappa_c R}{\Delta r}}} - 1\right]$$
$$\kappa_{Cd} = \frac{1}{C_{l\alpha}}\left[\frac{1.6(c/r)}{0.1267}\frac{\kappa_a - (c/r)^{\frac{\kappa_c R}{2\Delta r}}}{\kappa_b + (c/r)^{\frac{\kappa_c R}{2\Delta r}}} - 1\right] \tag{90}$$

with κ_a, κ_b, $\kappa_c$empricial constants (usually all =1), and where the actual correction is as follows:

$$C_{l3D} = \kappa_{Cl}[C_{l\alpha}[\alpha - \alpha_0] - C_l] + C_l \tag{91}$$

where $C_{l\alpha}$ is the 2D slope of the C_l-α curve, and α_0 the 0-lift AOA. The drag coefficient is modified following Eggers et al. (2003):

$$C_{d3D} = C_d + \kappa_{Cl}\,[C_{l\alpha}[\alpha - \alpha_0] - C_{l\alpha}]\,\frac{\sin(\alpha) - 0.12\cos(\alpha)}{\cos(\alpha) + 0.12\sin(\alpha)} \tag{92}$$

Other models are also relatively easy to implement, such as the 'centrifugal pumping' model (Lindenburg (2004)) which accounts for the extent of the TE separated region also following Schlichting's (1979) separated flow model (see also Section 12.2), or the Corrigan and Schillings (1994) model evaluated by Tangler and Selig (1997).

Almost all of the stall-delay models are based on the assumption of continuous flow over the span, and therefore end-effects are rarely captured. Additionally, it has to be expected that the resulting pressure gradient will have a strong dependence on the airfoil shape, especially for thick airfoils, given the dependence on the separation point. For this reason, most models need multiple tunable constants.

A recent comparison of multiple models to experimental data (Guntur et al. (2011)) has not confirmed any of them as preferable tools to predict stall delay and rotational effects. CFD has shown much more promising results, though it is computationally significantly more expensive.

Besides effects related to inertia, the in-plane component of the velocity (due to yaw errors or tilt angle) or the spanwise component of the velocity in case of the coning angle as mentioned in Sections 8-9 produce additional modifications of the boundary layer. While coning would produce an additive effect (positively or negatively depending on the cone angle sign) onto the stall delay phenomena, yaw and tilt have cyclical influence on the radial and Coriolis flow as the blade rotates around the rotor plane.

More research is needed to provide accurate predictions of rotational effects on wind turbines including effects on moment coefficients; that is beyond the scope of this study, but it is worth mentioning that at least the current pre-processor could be relatively easily made part of the AeroDyn's initialization subroutine. That would eventually lead to faster model validation of current and future models.

12. UNSTEADY AERODYNAMICS AND DYNAMIC STALL

Dynamic stall is a well-known phenomenon that can affect wind turbine performance and loading especially during yawed operations, and that can result in large unsteady stresses on the structure.

Dynamic stall manifests as a delay in the onset of flow separation to higher angles of attack that would otherwise occur under static (steady) conditions, followed by an abrupt flow separation from the leading edge (LE) of the airfoil (Leishman (2011)). The LE separation is the fundamental characteristic of the dynamic stall of an airfoil; in contrast, quasi-steady stall would start from the airfoil trailing edge (TE).

Figure 11 and Figure 12 summarize the conventionally assumed five stages of the dynamic stall:

1. Onset of flow reversal
2. Flow separation and vorticity accumulation at the LE
3. Shedding of the vortex and convection along the suction surface of the airfoil (lift increases)
4. Lift stall: vortex is shed in the wake and lift abrupt drop-off
5. Reattachment of the flow at angles considerably lower than static stall angles (hysteresis)

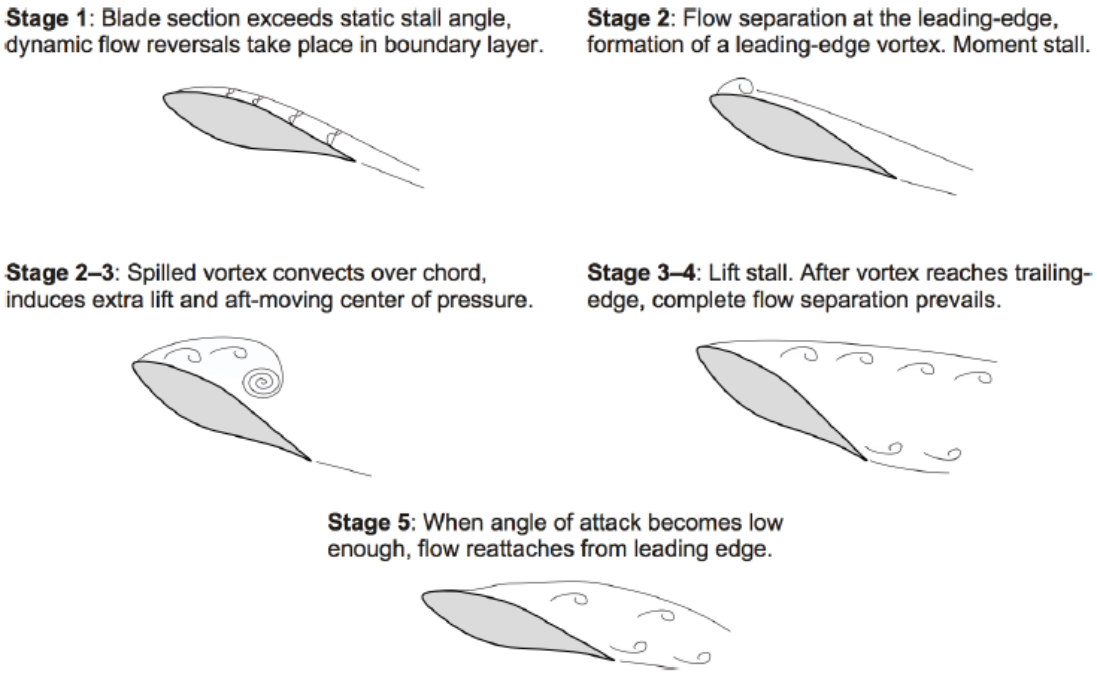

Figure 11. Conventional stages of dynamic stall phenomenon (from Leishman (2006)).

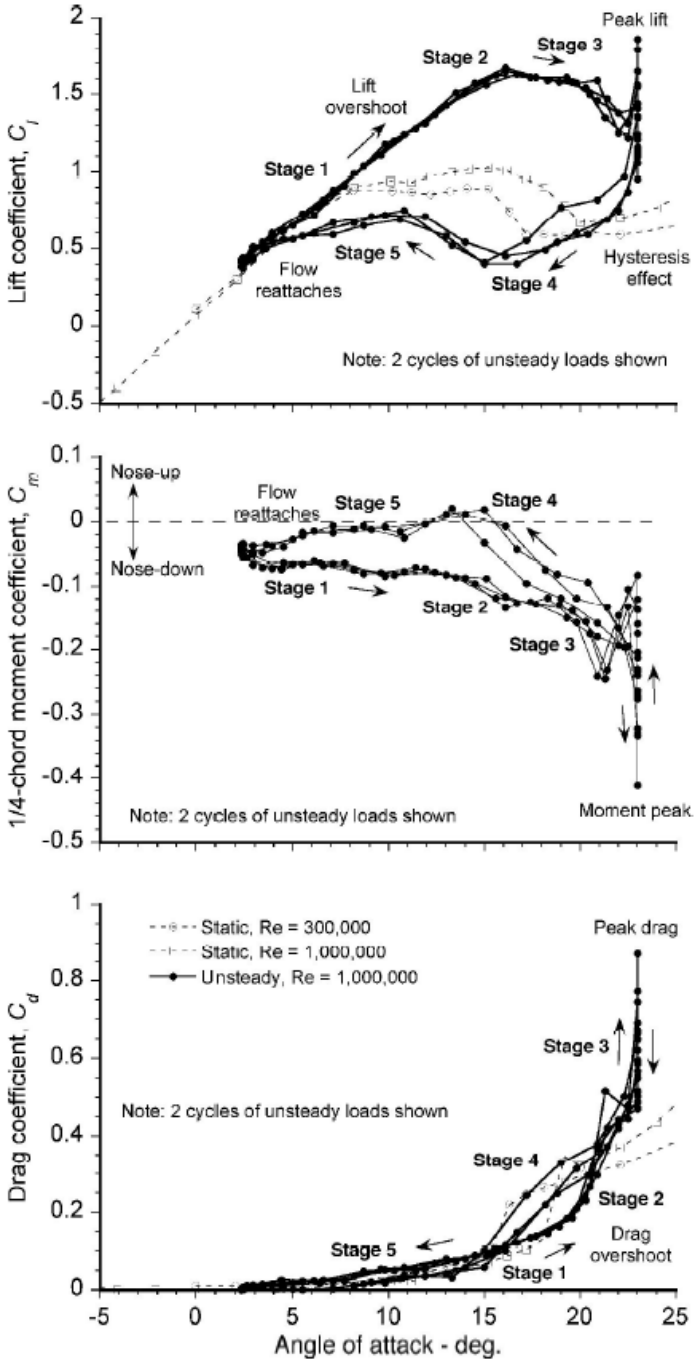

Figure 12. C_l, C_d, and C_m as functions of AOA during dynamic stall. Conventional stages of dynamic stall are also shown (from Leishman (2006)).

Various models have been proposed in the literature, but AeroDyn uses the Leishman-Beddoes indicial treatment (LBM) (Beddoes (1983-1984); Leishman and Beddoes (1989)). A review of the model is also given by Leishman (2011). This model (like most) was originally developed for helicopters, but has been successfully applied to wind turbines (see Pierce (1996) and Gupta and Leishman (2006)).

In order to represent the various unsteady phenomena, the LBM uses multiple first-order dynamic sub-systems together with an indicial treatment and semi-empirical sub-models derived from experiments on

unsteady airfoil aerodynamics. The LBM output provides a representation of the unsteady lift and pitching moment produced on airfoils undergoing time-varying motion into dynamic stall.

In particular, the LBM models a number of unsteady aerodynamics conditions, namely: attached flow conditions and TE separation before stall; delays and lags associated with the unsteady onset of dynamic stall and accompanying boundary layer development; advection of the LE vortex, shedding in the wake, and suppression of TE separation in favor of LE separation.

Currently, yawed flow conditions as well as Coriolis and centrifugal inertial effects, which lead to three-dimensional flow effects, are not included in the model, which is mainly a 2D approximation of the phenomenon.

AeroDyn uses the LBM as an a-posteriori correction to the airfoil aerodynamic coefficients C_l and C_d, after completing the calculation of the induction factors utilizing the static airfoil data. Yet, the LBM should be included in the iterative calculation of the induction factors providing the values of the aerodynamic coefficients in all situations, i.e. during attached and separated boundary layer flow. From a theoretical stand-point, the time scale associated with dynamic stall is proportional to the $c/U \approx c/(\Omega R)$ ratio; on the other hand, the time scale associated with dynamic inflow effects, and wake induction, is proportional to the D/U_∞. For a utility-scale wind turbine, the two time-scales correspond to: tenths of a second vs. tens of seconds respectively, i.e. a difference of two orders of magnitude. Therefore, while it is true that the wake cannot adapt to the rapidly changing conditions under unsteady aerodynamics, it seems more appropriate that the wake be driven by the results of the BEM under unsteady conditions rather than vice versa.

The primary subsystems in the LBM are:

1. Unsteady Attached Flow Solution via Indicial Treatment (potential flow)
2. Trailing Edge Flow Separation
3. Dynamic Stall and Vorticity Advection

The following sections discuss the equations of the LBM in detail, and the main references used are: Leishman (2006; 2011).

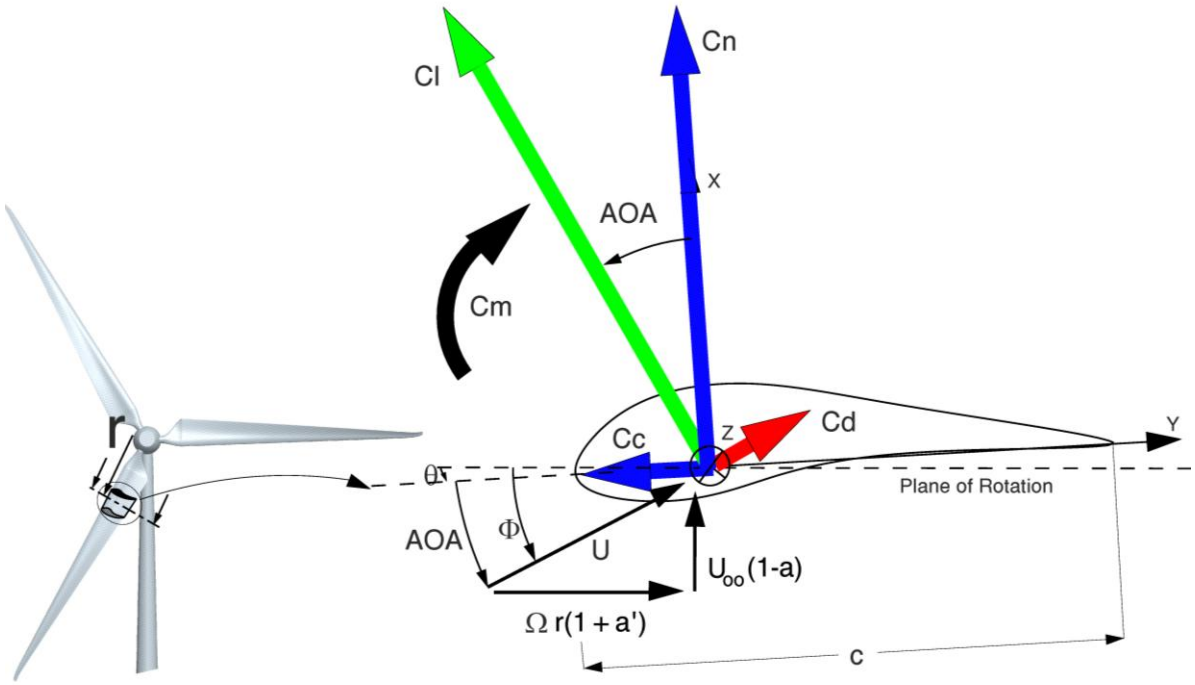

Figure 13. Main definitions of the BE forces (denoted by their normalized coefficients) utilized in the unsteady aerodynamics treatment.

The LBM calculates the C_n, C_c, C_m, which are the normal-to-chord force, chordwise force, and ¼-chord moment coefficient respectively (see Figure 13). The relationships between C_n, C_c and C_l, C_d are given by Eq. (93):

$$C_l = C_n \cos(\alpha) + C_c \sin(\alpha)$$
$$C_d = C_n \sin(\alpha) - C_c \cos(\alpha) + C_{d0} \tag{93}$$

From these relationships, C_n and C_c can be calculated via the known static C_l and C_d as functions of α (i.e. the AOA) or look-up tables.

12.1 Unsteady Attached Flow and Its Indicial Treatment

The advantage of the indicial treatment is that a response to an arbitrary forcing can be obtained through superposition of response-functions to a step variation in AOA, in pitch rate, or in heave motion. The superposition is carried out via the so-called Duhamel Integral (see also Leishman (2006)). The Duhamel Integral for the generic response $F_R(t)$ to a generic disturbance $\varepsilon(t)$ reads as follows:

$$F_R(t) = \varepsilon(0)\phi(t, M) + \int_0^t \frac{d\varepsilon}{d\sigma_t}(\sigma_t)\ \phi(t - \sigma_t, M) d\sigma_t$$

or (94)

$$F_R(s) = \varepsilon(0)\phi(s, M) + \int_0^s \frac{d\varepsilon}{d\sigma_s}(\sigma_s)\, \phi(s - \sigma_t, M) d\sigma_t$$

where s is a non-dimensional distance proportional to time t defined below; $\phi(t-\sigma_t, M) = \frac{\partial F_R}{\partial \varepsilon}\Big|_{\varepsilon=\varepsilon(0)}$ is the indicial response function, of arguments time and Mach number.

The indicial functions are idealized into two components: the first component of the response is related to the non-circulatory loading (piston theory and acoustic wave theory); the second originates from the development of circulation about the airfoil. The non-circulatory part depends on the instantaneous airfoil motion, but also on the time history of the prior motion.

It can be shown that the circulatory response may be calculated via the 'lumped approach', where the effects of step changes in AOA, pitch rate, heave motion, etc., are combined into an effective angle of attack at the ¾-chord station.

The indicial functions ($C_{n_{\alpha,q}}$) for the normal force coefficient in response to a step change in AOA and pitch-rate can be written in general form as follows:

$$C_{n_{\alpha,q}}(s,M) = C_{n_\alpha}(s,M) + C_{n_q}(s,M) = C_{n\alpha}(s,M)\alpha + C_{nq}(s,M)q$$

$$C_{n\alpha}(s,M) = \frac{4}{M}\phi_\alpha^{nc}(s,M) + \frac{C_{l\alpha}}{\beta_M}\phi_\alpha^{c}(s,M) \tag{95}$$

$$C_{nq}(s,M) = \frac{1}{M}\phi_q^{nc}(s,M) + \frac{C_{l\alpha}}{2\beta_M}\phi_q^{c}(s,M)$$

where ϕ_α^{nc} through ϕ_q^c are the indicial response functions for the normal force coefficient, with superscripts indicating circulatory (c) and non-circulatory (nc) components, and subscripts indicating the forcing being a step change in AOA (α) or non-dimensional pitching-rate q; M is the Mach number; s is the distance traveled by the airfoil in semi-chords; β_M is the Prandlt-Glauert compressibility correction factor ($\sqrt{1-M^2}$); $C_{l\alpha}$ is the slope of the C_l vs. α curve.

The non-dimensional pitching-rate is defined as in Eq. (96):

$$q = \dot{\alpha}c/U \tag{96}$$

where c is the local chord.

The non-dimensional travel distance is:

$$s = \frac{2}{c}\int_0^t U(t)dt$$

or in differential/discretized form: (97)

$$\Delta s = \frac{2}{c}U(t)\Delta t$$

The circulatory and non-circulatory components of the indicial responses w.r.t. a variation in AOA and pitching rate can be approximated as follows (see also Leishman and Beddoes (1989); Johansen (1999)):

$$\phi_\alpha^c(s,M) = \phi_q^c(s,M) = 1 - A_1 \exp(-b_1\,\beta_M^2\,s) - A_2 \exp(-b_2\,\beta_M^2\,s)$$

$$\phi_\alpha^{nc}(s,M) = \exp\left(-\frac{s}{T'_\alpha}\right) \tag{98}$$

$$\phi_q^{nc}(s,M) = \exp\left(-\frac{s}{T'_q}\right)$$

where T'_α and T'_q are time constants dependent on the Mach number.

By making use of exact results for short times (0 ≤ s ≤ 2M/(M+1)) (Lomax (1952)), it can be shown that (Leishman (2011)):

$$T_\alpha(M) = \frac{c}{2U}T'_\alpha = \frac{c}{2Ma_s}T'_\alpha = \frac{c}{2Ma_s}\frac{2M}{(1-M) + \frac{C_{l\alpha}}{2}M^2\beta_M(A_1b_1 + A_2b_2)} = k_\alpha(M)T_I$$

with

$$k_\alpha(M) = \left[(1-M) + \frac{C_{l\alpha}}{2}M^2\beta_M(A_1b_1 + A_2b_2)\right]^{-1} = \left[(1-M) + \frac{C_{l\alpha}}{2}M^2\beta_M 0.413\right]^{-1} \tag{99}$$

$$T_I = \frac{c}{a_s}$$

where the following values, based on experimental results, have been used for the coefficients: $A_1 = 0.3$; $A_2 = 0.7$; $b_1 = 0.14$; $b_2 = 0.53$;.

Also based on airfoil measurements in unsteady flow, Leishman (2011) proposes to use 0.75 T_α in place of T_α to account for three-dimensional effects not included in piston theory.

In AeroDyn's ***ATTACH*** routine (***AeroSubs***, see Appendix C), $k_\alpha(M)$ is calculated assuming $C_{l\alpha} = 2\pi$; this may be corrected to account for the actual $C_{l\alpha}$ value of the airfoil. Additionally, β_M is squared and that appears to be an error, though the literature seems to offer both versions. More investigation is required to clear this point.

For what stated earlier, it can be demonstrated that by means of the Duhamel Integral of the indicial functions, the circulatory response could be attained assuming the static $C_{n\alpha}$ and an effective angle of incidence (AOI) at the ¾-chord:

$$C_{n_{\alpha,q}}^c(s,M) = C_{n\alpha}\alpha_E(s,M) = C_n^c(s,M) \tag{100}$$

where α_E refers to the effective AOI at ¾-chord due to all the contributions (pitching rate, heave, step change in AOA, gust velocities, etc. see Figure 14).

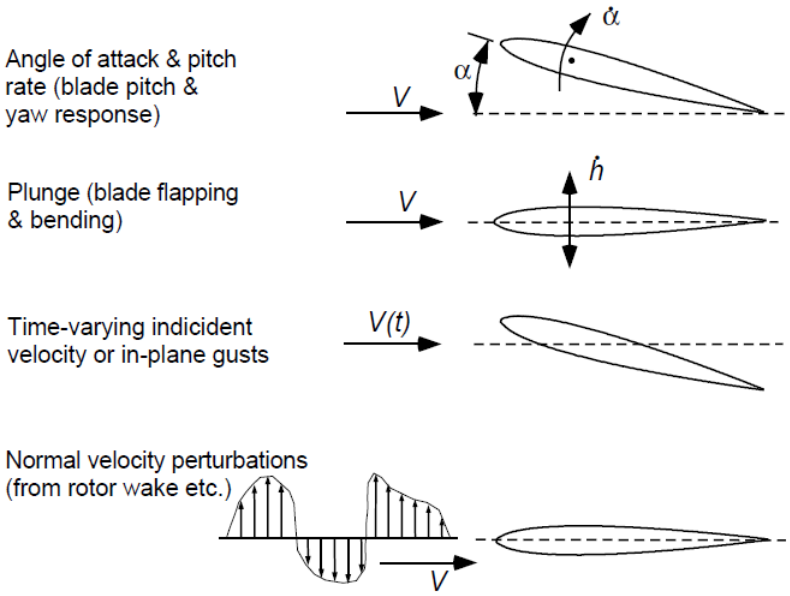

Figure 14. Decomposition of flow field into constituent elements of net aerodynamic forcing (from Lesihman (2002)).

Discretizing in time (or distance s), it can be proved (Leishman (2011)) that α_E at the *t-th* time step, due solely to AOA and pitching motions is given by:

$$\alpha_{E,t}(s,M) = (\alpha_t - \alpha_0) - X1_t(\Delta s) - X2_t(\Delta s) \tag{101}$$

where the subscript t denotes the current time step, and the deficiency functions are expressed as

$$\begin{aligned} X1_t &= X1_{t-1}\exp(-b_1\beta_M^2\,\Delta s) + A_1\Delta\alpha_t\ \exp\left(-b_1\beta_M^2\frac{\Delta s}{2}\right) \\ X2_t &= X2_{t-1}\exp(-b_2\beta_M^2\,\Delta s) + A_2\Delta\alpha_t\ \exp(-b_2\beta_M^2\,\Delta s/2) \end{aligned} \tag{102}$$

In AeroDyn's ***ATTACH*** (***AeroSubs***, see Appendix C), the expressions in Eq.s (101)-(102) are called *ANE*, *XN*, and *YN*, respectively.

Note that α, the AOA, is modified (*ANE*) in AeroDyn to account for absolute values of the AOA greater than π/2; it seems more appropriate that that correction be performed in ***BEDDOES***, (***AeroSubs***, see Appendix C) rather than ***ATTACH***, and that the resulting angle be called α_m (*AM*) and not α_E to avoid confusion on the AOA vs AOA$|_{3/4c}$.

For the non-circulatory part of $C_n(s)$, the lumped approach cannot be applied. Therefore, the contributions from a step change in AOA and a step-change in pitching rate need to be kept separate:

$$C_n^{nc}(s,M) = C_{n_\alpha}^{nc}(s,M) + C_{n_q}^{nc}(s,M) \tag{103}$$

However, invoking superposition and by means of the Duhamel Integral, the non-circulatory component $C_{n_\alpha}^{nc}(s,M)$ at the t-th time-step can be written as:

$$C_{n_\alpha}^{nc}(s,M) = \frac{4\,T_\alpha(M)}{M}\left(K_{\alpha_t} - K'_{\alpha_t}\right)$$

with (104)

$$K_{\alpha_t} = \frac{\alpha_t - \alpha_{t-1}}{\Delta t}$$

The deficiency function K'_α for the non-circulatory portion $C_{n_\alpha}^{nc}$ is given by:

$$K'_{\alpha_t} = K'_{\alpha_{t-1}} \exp\left(-\frac{\Delta t}{T_\alpha(M)}\right) + \left(K_{\alpha_t} - K_{\alpha_{t-1}}\right) \exp\left(-\frac{\Delta t}{2\,T_\alpha(M)}\right) \quad (105)$$

AeroDyn's ***ATTACH*** (***AeroSubs***) calculates K_α(*ADOT* (***Bedoes*** (***AeroMods***), see Appendix C and Appendix D) through a process that limits its potential spikes: if the variable normalized by the ratio of *U*/*c* is above a threshold of 3%, then it is set at 10% of the difference between the actual value and the threshold. It is not clear how this 'saturation limiting process' was derived.

Analogously, the non-circulatory component $C_{n_q}^{nc}$ at the *t*-th time-step can also be written as:

$$C_{n_q}^{nc}(s,M) = -\frac{T_q(M)}{M}\left(K_{q_t} - K'_{q_t}\right)$$

with (106)

$$K_{q_t} = \frac{q_t - q_{t-1}}{\Delta t}$$

The time-constant for the non-circulatory pitching-rate contribution to $C_n(s)$ (analogously to Eq. (99)) is:

$$T_q(M) = 0.75\frac{c}{2U}T'_q = 0.75k_q(M)T_I$$

with (107)

$$k_q(M) = [(1-M) + C_{l\alpha}M^2\beta_M(A_1b_1 + A_2b_2)]^{-1} = [(1-M) + C_{l\alpha}M^2\beta_M 0.413]^{-1}$$

Note that a factor of 0.75 has been applied in a similar fashion to what was done for $T_\alpha(M)$.

The deficiency function K'_q for the non-circulatory portion $C_{n_q}^{nc}$ is given by:

$$K'_{q_t} = K'_{q_{t-1}} \exp\left(-\frac{\Delta t}{T_q(M)}\right) + \left(K_{q_t} - K_{q_{t-1}}\right) \exp\left(-\frac{\Delta t}{2\,T_q(M)}\right) \quad (108)$$

AeroDyn's ***ATTACH*** (***AeroSubs***) sets $k_q(M)$ in Eq. (107) with a power of 2 for β_M; furthermore, $C_{l\alpha}$ is set at 2π. Also, the same routine assumes $T_q(M) = T_\alpha(M)$, i.e. $k_q(M) = k_\alpha(M)$, which should be corrected. All these discrepancies should be revised.

Note also that while calculating the sum in Eq. (103), AeroDyn's ***ATTACH*** (***AeroSubs***) makes sure $C_n^{nc}(s)$ is within [-1;1].

Finally, after calculating all of the contributions, the overall normal force coefficient, $C_n^{pot}(s)$, for the attached flow (potential) conditions can be calculated as in Eq. (109):

$$C_n^{pot}(s,M) = C_n^{nc}(s,M) + C_n^c(s,M) = C_{n_\alpha}^{nc}(s,M) + C_{n_q}^{nc}(s,M) + C_n^c(s,M) \tag{109}$$

The chord force coefficient derives from the normal coefficient as in Eq. (110) (Leishman (2011)):

$$C_c^{pot}(s,M) = C_n^{pot}(s,M)\tan(\alpha_E + \alpha_0) \tag{110}$$

Note that the 0-lift AOA needs to be re-introduced into α_E in order to account for AOA and not AOI.

AeroDyn's ***ATTACH*** (***AeroSubs***) approximates $\tan(\alpha_E + \alpha_0) \approx (\alpha_E + \alpha_0)$, which is usually legitimate for small AOAs associated with attached flow (errors <1% for AOA<15°).

12.1.1 Pitching Moment Model

Following what was done in Section 12.1, the indicial functions for the moment coefficient $C_{m_{\alpha,q}}$ about the ¼-chord in response to a step change in AOA and pitch-rate can be written in general form as in Eq. (111):

$$C_{m_{\alpha,q}}(s,M) = C_{m_\alpha}(s,M) + C_{m_q}(s,M) = C_{m\alpha}(s,M)\alpha + C_{mq}(s,M)q$$

$$C_{m\alpha}(s,M) = \frac{-1}{M}\phi_{m,\alpha}^{nc}(s,M) - \frac{C_{l\alpha}}{\beta_M}\phi_\alpha^c(s,M)[\hat{x}_{AC} - .25] \tag{111}$$

$$C_{mq}(s,M) = \frac{-7}{12M}\phi_{m,q}^{nc}(s,M) - \frac{C_{l\alpha}}{16\beta_M}\phi_{m,q}^c(s,M)$$

where $\phi_{m,\alpha}^{nc}$ through $\phi_{m,q}^c$ are the indicial response functions for the moment coefficient; $\hat{x}_{AC}$ is the distance of the aerodynamic center from the LE as a fraction of the chord length.

The circulatory and non-circulatory components of the moment indicial responses w.r.t. a variation in AOA and pitching rate can be approximated as follows (Leishman and Beddoes (1989); Johansen (1999)):

$$\phi_{m,q}^c(s,M) = 1 - A_5\exp(-b_5\,\beta_M^2\,s)$$

$$\phi_{m,\alpha}^{nc}(s,M) = A_3\exp\left(-\frac{s}{b_3T'_{m,\alpha}}\right) + A_4\exp\left(-\frac{s}{b_4T'_{m,\alpha}}\right) \tag{112}$$

$$\phi_{m,q}^{nc}(s,M) = \exp\left(-\frac{s}{T'_{m,q}}\right)$$

where A_3-A_5 and b_3-b_5 are other constants of the model; $T'_{m,\alpha}$ and $T'_{m,q}$ are the analogous of T'_α and T'_q, respectively, and are time constants dependent on the Mach number.

The non-circulatory part of $C_{m_{\alpha,q}}(s,M)$ also writes (Leishman and Beddoes (1986); Johansen (1999):

$$C_{m_\alpha}^{nc}(s,M) = -\frac{1}{4}C_{n_\alpha}^{nc}(s,M)$$

$$C_{m_q}^{nc}(s,M) = \frac{-7}{12M}\phi_{m,q}^{nc}(s,M) = \frac{-7}{12M}\frac{T_{m,q}}{4}\left[K_q - K_q''\right] \tag{113}$$

where $T_{m,q}$ is the analogous of T_q. Those results are again outcome of a superposition integral.

The first equality in Eq. (113) implies: $\phi_{m,\alpha}^{nc}(s,M) = \phi_{\alpha}^{nc}(s,M)$.

The deficiency function K_q'' for the $C_{m,q}^{nc}$ term is given by:

$$K_{q_t}'' = K_{q_{t-1}}'' \exp\left(-\frac{\Delta t}{T_{m,q}(M)}\right) + \left(K_{q_t} - K_{q_{t-1}}\right) \exp\left(-\frac{\Delta t}{2\,T_{m,q}(M)}\right) \tag{114}$$

Minnema (1998) transforms the second equality in Eq. (113) into the following:

$$C_{m_q}^{nc}(s,M) = \frac{-7}{12M}\phi_{m,q}^{nc}(s,M) = -\frac{C_{n_q}^{nc}(s,M)}{4} - \frac{[k_\alpha(M)]^2 T_I}{3M}\left[K_q - K_q''\right] \tag{115}$$

AeroDyn's ***ATTACH*** (***AeroSubs***) uses Eq. (115), and it also makes the approximation $T_{m,q}(M) = k_\alpha(M) * T_\alpha(M)$. This should be verified.

No circulatory contribution to $C_{m_{\alpha,q}}(s,M)$ is calculated by AeroDyn's ***ATTACH*** (***AeroSubs***), however $C_{m_\alpha}^{c}(s,M)$ gets re-introduced in AeroDyn's ***SEPAR*** (***AeroSubs***) (see Appendix C).

The circulatory part of the $C_{m_{\alpha,q}}(s,M)$ can be written (Johansen (1999)) as:

$$\begin{aligned} C_{m_{\alpha,q}}^{c}(s,M) &= C_{m0} + C_{m_\alpha}^{c}(s,M) + C_{m_q}^{c}(s,M) \\ C_{m_\alpha}^{c}(s,M) &= [x_{AC} - .25]C_{n_\alpha}^{c}(s,M) \\ C_{m_q}^{c}(s,M) &= -\frac{C_{l\alpha}}{16\beta_M}\left(q_m - K_q'''\right)\frac{c}{U} \end{aligned} \tag{116}$$

where C_{m0} is the 0-lift aerodynamic moment and K_q''' is given by Eq. (117) for the t-th time step:

$$K_{q_t}''' = K_{q_{t-1}}''' \exp(-b_5\beta_M^2\,\Delta s) + A_5\Delta q_t \exp\left(-b_5\beta_M^2\frac{\Delta s}{2}\right) \tag{117}$$

The total $C_{m_{\alpha,q}}(s,M)$ then writes:

$$\begin{aligned} C_{m_{\alpha,q}}(s,M) &= C_{m_{\alpha,q}}^{c}(s,M) + C_{m_{\alpha,q}}^{nc}(s,M) \\ &= C_{m_0} + C_{m_\alpha}^{c}(s,M) + C_{m_q}^{c}(s,M) + C_{m_\alpha}^{nc}(s,M) + C_{m_q}^{nc}(s,M) \end{aligned} \tag{118}$$

12.1.2 Other Unsteady Aerodynamics Forcing Conditions

As mentioned previously, the lumped approach can be utilized for the circulatory contribution to the normal force response. For all other unsteady airloads, the various contributions from AOA, pitching-rate, heave motion, etc., need to be kept separate. AeroDyn accounts for AOA and pitching-rates, but it

does not include changes in AOA due to disturbances of length-scales comparable to the airfoil chord, as for instance wind gusts.

Classical aerodynamics has provided models for step gusts, or cosine gusts, and the results could be incorporated into AeroDyn. This is beyond the scope of this project, but it is worth mentioning an expression for the normal force response to a gust of speed w_g directed normal to $\underline{U}$:

$$C_{n_g}(s) = \frac{C_{l\alpha}}{U\,\beta_M}\left[w_g - Z_1 - Z_2\right]$$

with

$$Z_{1_t}(s,M) = Z_{1_{t-1}}(s,M)\exp(-g_1\beta_M^2\,\Delta s) + G_1\left[w_{g_t} - w_{g_{t-1}}\right]\exp\left(-g_1\beta_M^2\,\frac{\Delta s}{2}\right)$$

$$Z_{2_t}(s,M) = Z_t(s,M)\exp(-g_2\beta_M^2\,\Delta s) + G_2\left[w_{g_t} - w_{g_{t-1}}\right]\exp\left(-g_2\beta_M^2\,\frac{\Delta s}{2}\right) \quad (119)$$

where the constants $g_1$through G_2 can be found in Bisplinghoff et al. (1955) and Leishman (2011) for instance.

12.2 TRAILING EDGE FLOW SEPARATION

12.2.1 Quasi-Static treatment

Trailing edge progressive boundary layer separation is a fundamental characteristic of thick and leading-edge cambered airfoils, including those used on wind turbines. The base for this subsystem is Kirchoff's theory, which can be expressed as follows (Leishman (2006)):

$$C_n(\alpha,f) = C_{n\alpha}(\alpha - \alpha_{0L})\left(\frac{1+\sqrt{f}}{2}\right)^2$$

$$C_c(\alpha,f) = \eta_e\, C_{n\alpha}\,(\alpha - \alpha_{0L})\sqrt{f}\tan(\alpha) \quad (120)$$

where f is the separation-point distance from the LE as a fraction of the chord; $\eta_e$is the recovery factor (0.85-0.95) for the airfoil, which accounts for viscous effects at limited or no separation, and needs to be introduced to adjust the "potential flow" chord force (C_c) that would be obtained otherwise.

Eq. (120) can, in fact, be interpreted as a modification to the circulatory portion of the normal force coefficient under attached (potential) flow conditions, modifying the term $C_{n\alpha}(\alpha - \alpha_0)$ by the factor $\left(\frac{1+\sqrt{f}}{2}\right)^2$, where $\alpha - \alpha_0$ should be replaced by α_E.

If the airfoil static characteristics are known, Eq. (120) can be rearranged and solved for f. Leishman (2011) suggests the use of best-fit curves obtained from static measurements on airfoils, of the type:

$$f = \begin{cases} 1 - 0.3\exp\left(\frac{\alpha - \alpha_1}{S_1}\right), & if\ \alpha < \alpha_1 \\ 0.04 + 0.66\exp\left(\frac{\alpha_1 - \alpha}{S_2}\right), & if\ \alpha > \alpha_1 \end{cases} \quad (121)$$

where α_1 is the AOA at f=0.7 (a condition corresponding to static stall angle of many airfoils), and S_1 and S_2 are constants that define the abruptness of the static stall.

AeroDyn (in ***BEDINIT*** and ***SEPAR*** (***AeroSubs***), see Appendix C) uses two different lookup tables to calculate two values of f (f and f_c) as functions of the airfoil 2D static characteristics, basically reverting Eq. (120). One lookup table is used for reconstructing C_n, and the other for reconstructing C_c. A mathematical expedient is used to preserve the sign of C_n and C_c when squaring the equation (see Moriarty and Hansen (2004)).

Leishman (2011) argues in favor of the use of a best-fit type of approach, as that helps filter out fluctuations in the measured airloads in the post-stall regime as well as potential errors in the measurements associated with static airfoil tests. AeroDyn's approach, however, seems legitimate and has been proven to be effective at reconstructing airloads on wind turbine airfoils (Moriarty and Hansen (2004)).

AeroDyn does not make use of the recovery factor η_e(see ***BedInit*** (***AeroSubs***), and Appendix C). Note that its effect is linked to the component along the chord of the resultant of the viscous stresses. C_{d0}, instead, is the drag coefficient at 0-lift angle of attack, and may represent both viscous and normal stresses' resultant along the local air velocity direction, and it too needs to be added in reconstructing the drag on the airfoil.

The absence of η_e can be justified by the fact that a separate value of f (obtained from the same static lookup tables) is used for reconstructing C_c, which then implicitly includes η_e, i.e. $f_c = \eta_e^2 f$. Also note, that in the model implementation in order to account for unsteady conditions (see below), f_c'' and f'' are actually used rather than f_c and f, except for the initial time step.

12.2.2 Unsteady Aerodynamics Effects on the TE Separation and Boundary Layer Development

Under unsteady conditions, the TE separation point gets modified on account of temporal effects on airfoil pressure distribution and boundary layer response.

Analogously, the LE separation leading to the actual dynamic-stall is also modified w.r.t. to static conditions. In other words, the static critical pressure gradient at the LE, related to a critical value of the normal force coefficient for instance, needs to be modified to account for the usual lags and delays of unsteady aerodynamics.

A new normal coefficient is then defined starting from the potential-flow normal coefficient as follows:

$$C_n' = C_n^{pot} - D_p \tag{122}$$

where the deficiency function D_p at the t-th time step is given by:

$$D_{p_t} = D_{p_{t-1}} \exp\left(-\frac{\Delta s}{T_p}\right) + \left(C_{n_t}^{pot} - C_{n_{t-1}}^{pot}\right) \exp\left(-\frac{\Delta s}{2\,T_p}\right) \tag{123}$$

and where T_p is a time constant associated with the LE pressure gradient. Note that one result of this lag in normal force coefficient is that the LE separation occurs at higher AOA and C_n than under static conditions.

C_n' will also be used to check whether or not conditions have been met for the onset of LE separation and flow reattachment, i.e. it will be compared to a threshold value C_{n1} (see Section 12.3).

In AeroDyn, T_p is initialized (and fixed) in ***BEDDAT*** (***AeroSubs***) at 1.7 s (see Appendix C), however, this is a parameter that should be customized depending on the type of airfoil used, Mach and Reynolds number (e.g., Leishman (2011); Gupta and Leishman (2006); Pereira (2010)). T_p should be calculated empirically by finding the value that collapses data from unsteady airfoil measurements of LE pressure response vs. C_n' (see Leishman (2011)).

Using the newly attained C_n', the LBM proceeds to calculate a new effective AOA, which would give the same unsteady LE pressure gradient under static conditions, and which can represent the lags associated with the boundary layer evolution:

$$\alpha_f = \frac{C_n'}{C_{n\alpha}} + \alpha_0 \tag{124}$$

This new AOA can then be used to calculate an effective point of separation f' under unsteady conditions, by reverting Eq. (120) and via static airfoil characteristics. Additionally, a lag accounting for unsteady boundary-layer response can be introduced in the effective separation point as follows:

$$f'' = f' - D_f \tag{125}$$

where the deficiency function D_f at the t-th time step is expressed as:

$$D_{f_t} = D_{f_{t-1}} \exp\left(-\frac{\Delta s}{T_f}\right) + (f_t' - f_{t-1}') \exp\left(-\frac{\Delta s}{2\,T_f}\right) \tag{126}$$

T_f is a time constant, again dependent on airfoil shape, Mach and Reynolds numbers (Leishman (2011)). In AeroDyn, T_f is fixed at 3.0 s in ***BEDDAT*** (**AeroSubs**) (see Appendix C); it is then scaled by a 1.5 factor if the AOA is decreasing at the time step under examination (see vortex decay below, and the variable *TFE* in ***SEPAR*** (***AeroSubs***), and Appendix C).

AeroDyn's ***SEPAR*** (***AeroSubs***) calculates two values for both f' and f'', i.e. one for C_n and one for C_c, from Eq.s (124)-(125) and by reverting Eq. (120) using α_f as input to look-up tables, similarly to the static case mentioned previously. AeroDyn's ***SEPAR*** (***AeroSubs***) also first modifies and then assures that the newly calculated α_f (*AFE*) is within [-π;π], analogously to what was done for α in Section 12.1 for large AOAs.

The normal and chordwise force-coefficients are then modified from the values calculated under attached/potential flow for unsteady TE separation as follows:

$$C_n = C_{n\alpha}\alpha_E\left(\frac{1+\sqrt{f''}}{2}\right)^2 + C^{nc}_{n_{\alpha,q}}(s,M) = C^{c}_{n_{\alpha,q}}(s,M)\left(\frac{1+\sqrt{f''}}{2}\right)^2 + C^{nc}_{n_{\alpha,q}}(s,M)$$
$$C_c = \eta_e\, C_{n\alpha}\, \alpha_E(s,M)\sqrt{f''}\, \tan(\alpha_E + \alpha_{0L}) = \eta_e\, C_n^{pot} \tan(\alpha_E + \alpha_0)\sqrt{f''} = \eta_e C_c^{pot}\sqrt{f''} \quad (127)$$

where the $C^{c}_{n_{\alpha,q}}(s,M)$ is the potential-flow circulatory contribution calculated from Eq. (100) (Section 12.1); here it gets multiplied by the separation correction factor following Kirchoff's theory (Eq. (120)). Also note that $\alpha_E(s,M)$ is the effective AOI at the ¾-chord, as discussed in Section 12.1. The C_c's second and third equalities derive from Eq.s (100) and (110).

AeroDyn's ***SEPAR*** (***AeroSubs***) omits the recovery factor in Eq.(127) for the reasons mentioned above.

12.2.3 Pitching Moment Model

Leishman (2011) offers a general form for the normalized (by the chord length) distance of the center of pressure from the airfoil LE, under unsteady, separated conditions:

$$\hat{x}_{cp} = k_0 + k_1(1 - f'') + k_2 \sin(\pi(f'')^{k_3}) \quad (128)$$

where $k_0 = 0.25 - \hat{x}_{AC}$, i.e. the offset of the aerodynamic center from the ¼-chord location; k_1, k_2, and k_3 are constants to be obtained through a best fit of static pitching moment measurements. Analogously to what was done for C_n and C_c, in fact, a value for f''as a function of the AOA can be derived from static C_m data, assuming the pitching moment given by the following:

$$C_m(\alpha, f'') = C_{m_0} + C^{c}_{n_{\alpha,q}}\, \hat{x}_{cp}\, c + C^{c}_{m_q}(s,M) + C^{nc}_{m_\alpha}(s,M) + C^{nc}_{m_q}(s,M) \quad (129)$$

where C_m is the moment coefficient w.r.t. the ¼-chord location; c is the chord length; $C^{c}_{n_{\alpha,q}}$ is calculated as in the first term of the sum in the RHS of Eq. (127); $C^{c}_{m_q}(s,M)$ is calculated by Eq. (116); $C^{nc}_{m_\alpha}(s,M)$ is calculated via the first of Eq. (113); and $C^{nc}_{m_q}(s,M)$ via the second of Eq. (113) or via Eq. (115).

Minnema (1998) states that Eq. (128), and thus Eq. (129), do not work for the range of AOAs of interest to wind turbines; he proposes the following procedure to calculate the C_m subject to TE flow separation effects.

First a new AOA, α'_f, is calculated starting from α_f:

$$\alpha'_f = \alpha_f - D_{\alpha_f} \quad (130)$$

with the deficiency function D_{α_f} at the t-th time step given by:

$$D_{\alpha_{f_t}} = D_{\alpha_{f_{t-1}}} \exp\left(-\frac{\Delta s}{T_f}\right) + \left(\alpha_{f_t} - \alpha_{f_{t-1}}\right) \exp\left(-\frac{\Delta s}{2\, T_f}\right) \quad (131)$$

Note that in Eq. (131) the same T_f time constant (dependent on airfoil shape, Mach and Reynolds numbers) is used as in Eq.(126), being the two deficiency functions part of the same separation physical approximation.

In order to compute the C_m under unsteady and boundary-layer TE separation conditions, the new AOA is then used as input to a lookup table of static C_m values for the airfoil under consideration.

AeroDyn's ***SEPAR*** (***AeroSubs***, see Appendix C) follows Minnema's (1998) approach, and uses the output of the look-up procedure as an effective circulatory contribution to C_m.

12.3 DYNAMIC STALL

The onset of dynamic stall involves LE separation and the formation of a vortex (shear-layer roll up) that travels over the airfoil's suction-side before getting shed into the wake.

As mentioned in Section 12.2.2, a condition needs to be met for the LE separation: $C_n' > C_{n1}$, with C_n' given by Eq. (122). This condition is checked in AeroDyn's ***SEPAR*** (***AeroSubs***) routine (see Appendix C).

A non-dimensional time variable is introduced, τ_V, such that τ_V =0 corresponds to the onset of the LE separation, and $\tau_V = T_{VL}$ to the vortex at the TE just before leaving the airfoil. T_{VL} is another time constant associated with the vortex advection process. AeroDyn's ***SEPAR*** (***AeroSubs***) routine increments τ_V if the condition $C_n' > C_{n1}$ is satisfied.

C_{n1} values may be derived from measurements on airfoils for different Mach and Reynolds numbers, by relating the lift (or normal force) to the LE pressures at the onset of dynamic stall. This, however, may be difficult to obtain; an alternative consists of using static values corresponding to breaks in pitching moments or loss of chordwise force at stall. This condition should correlate well to the maximum C_n under static conditions for low Mach numbers though it may not always (for any airfoil shape) apply (Leishman (2011)).

Due to the camber in the airfoils, a similar condition is applied under negative AOAs: $C_n' < C_{n2}$, where C_{n2} is the analog of C_{n1} for negative stall angles. AeroDyn (***SEPAR*** and ***VORTEX*** (***AeroSubs***)) uses the logical variable *BEDSEP* to track those conditions (.TRUE. means critical conditions met for vortex advection).

The normal force coefficient at the *t*-th time-step, due to the presence of the LE vortex, is written as in Eq. (132), following Leishman (2011):

$$C_{n_t}^v = C_{n_{t-1}}^v \exp\left(-\frac{\Delta s}{T_V}\right) + \left(C_{V_t} - C_{V_{t-1}}\right) \exp\left(-\frac{\Delta s}{2\,T_V}\right) \tag{132}$$

where T_V is a time constant; the term C_V represents the accumulation of new vorticity and associated lift in the LE vortex.

The increment in vortex lift is assumed to be proportional to the difference in circulatory contributions to C_n by the attached and TE-separated flow normal force coefficients as follows:

$$C_{V_r} = C^c_{n_{\alpha,q}}(s,M) - C^c_{n_{\alpha,q}}(s,M)\left(\frac{1+\sqrt{f''}}{2}\right)^2 = C^c_{n_{\alpha,q}}(s,M)\left(1-\left(\frac{1+\sqrt{f''}}{2}\right)^2\right)$$
$$= C_{n\alpha}\alpha_E(s,M)\left(1-\left(\frac{1+\sqrt{f''}}{2}\right)^2\right) \tag{133}$$

The vortex is allowed to accumulate vorticity as long as it is not shed in the wake ($\tau_V \leq T_{VL}$).

Following Pierce (1996), AeroDyn's ***VORTEX*** and ***SEPAR*** (***AeroSubs***) (see Appendix C) include an additional condition based on whether or not the AOA is decreasing (away from stall) at the current time step. In order to reduce the noise associated with the time derivative of the AOA, AeroDyn's ***SEPAR*** uses the difference in C'_n (Eq. (122)) between two successive time steps, $\Delta C'_n$, eventually multiplied by the AOA (*ANE* in ***SEPAR*** (***AeroSubs***)) to account for situations of both positive and negative AOAs. A flag (*SHIFT* (***Beddoes***) in ***SEPAR*** (***AeroSubs***)) is set to identify this condition on the AOA, whereas another flag (*VOR* (***Beddoes***) in ***VORTEX*** (***AeroSubs***)) denotes whether or not the vortex has reached the TE. In case any of those two conditions applies, i.e. either $\tau_V = T_{VL}$ (VOR=.FALSE.) or AOA is decreasing away from stall (SHIFT=.TRUE.) (see ***SEPAR*** and ***VORTEX*** (***AeroSubs***) in Appendix C), Eq. (132) is modified to rewrite as in Eq. (134):

$$C^v_{n_t} = C^v_{n_{t-1}} \exp\left(-2\,\frac{\Delta s}{T_V}\right) \tag{134}$$

where the vorticity decay is accelerated at twice the initial rate and no further vorticity accretion is introduced. Pierce (1996) suggests that the same (accelerated) decay rate be applied if $C'_n < C_{n1}$ ($C'_n > C_{n2}$), but this does not occur in AeroDyn, and should be revised.

The final value for the normal force coefficient is then given by:

$$C_n = C^c_{n_{\alpha,q}}\left(\frac{1+\sqrt{f''}}{2}\right)^2 + C^{nc}_{n_{\alpha,q}} + C^v_n \tag{135}$$

where $C^c_{n_{\alpha,q}}$ and $C^{nc}_{n_{\alpha,q}}$ are given by the attached flow treatment in Section 12.1.

In order to account for the presence of the vortex and the associated pressure distribution at the LE, the chordwise force is calculated (Leishman and Beddoes (1989)) as:

$$C_c = \begin{cases} C_{n\alpha}\,\alpha_E(s,M)\sqrt{f''}\,\sin(\alpha_E+\alpha_0)\,, & C'_n \leq C_{n1} \\ k_1 + C_{n\alpha}\,\alpha_E(s,M)\sqrt{f''}(f'')^{k_2}\,\sin(\alpha_E+\alpha_0)\,, & C'_n > C_{n1} \end{cases} \tag{136}$$

with

$$k_2 = 2(C'_n - C_{n1}) + (f'' - f)$$

where k_1 is a new best-fit constant based on static data of C_c, and the other symbols were introduced in the previous sections.

AeroDyn's ***VORTEX*** and ***SEPAR*** (***AeroSubs***) (See Appendix C) follow the work of Pierce (1989) by defining the total chordwise force as in Eq. (137):

$$C_c = \eta_e C_c^{pot} \sqrt{f''} + C_n^v \tan(\alpha_E(s, M)) \, (1 - \tau_V) \tag{137}$$

where the presence of the vortex gives a contribution similar to that of the circulatory part under attached flow conditions, but including a correction factor based on the location (τ_V) of the vortex. The first term on the RHS of Eq. (137) is the normal force coefficient under unsteady separated conditions (see Eq. (127)). The recovery factor η_e is omitted in AeroDyn for reasons explained previously.

Both T_V and T_{Vl} are time constants dependent on the type of airfoil, Mach and Reynolds number, though the dependence on the Mach number has been shown to be weak (Leishman (2011)).

AeroDyn's ***VORTEX*** (***AeroSubs***) lets multiple vortices being shed from the LE according to a Strohual's dimensionless frequency of 0.19. To this purpose a new time constant $T_{sh} = \frac{2(1-f'')}{0.19}$ is utilized; if $\tau_V = 1 + T_{sh}/T_{Vl}$, then $\tau_V$is reset to 0 and a new vortex cycle may commence.

12.3.1 Pitching Moment Model

The presence and downstream advection of the concentrated vorticity on the airfoil suction side causes the center of pressure to move aft. Leishman (2011) offers a form for the normalized (by the chord length) aft distance of the center of pressure from the ¼-chord location:

$$\hat{x}_{cp}^v(\tau_V) = \bar{\bar{x}}_{cp} \left(1 - \cos\left(\frac{\pi \tau_V}{T_{Vl}}\right)\right) \tag{138}$$

with $\bar{\bar{x}}_{cp} = 0.2$ for most airfoil. The pitching moment contribution from the vortex added lift is then:

$$C_m^v = -\hat{x}_{cp}^v C_n^v \tag{139}$$

where C_m^v is the moment coefficient w.r.t. the ¼-chord location due to the presence of the LE vortex (sign convention as in Figure 12).

The total pitching moment coefficient (Eq. (129)) then re-writes:

$$C_m = C_{m_0} + C_{n_{\alpha,q}}^c \, \hat{x}_{cp} \, c + C_{m_q}^c + C_{m_\alpha}^{nc} + C_{m_q}^{nc} + C_m^v \tag{140}$$

If one uses Minnema's (1998) approach as mentioned in Section 12.2.3, the total C_m is then given by:

$$C_m = C_m^c + C_{m_\alpha}^{nc} + C_{m_q}^{nc} + C_m^v \tag{141}$$

where C_m^c is the output of the look-up procedure described in Section 12.2.3, $C_{m_\alpha}^{nc}$ and $C_{m_q}^{nc}$ are given by Eq.s (113)a and (115) in Section 12.1.1. That is the approach followed by AeroDyn's ***VORTEX*** (***AeroSubs***).

12.4 CONCLUDING NOTES ON THE LEISHMAN-BEDDOES UNSTEADY AERODYNAMIC MODEL AS IMPLEMENTED IN AERODYN

The LBM is a relatively arduous model to implement, given the complex physics it tries to represent and the interactions between the sub-systems (see Section 12).

Various interpretations and modifications to the original Leishman and Beddoes (1989) have been used in AeroDyn. Some have been substantiated by dedicated Master's Theses, yet it is not clear how extendable the validations of the various modifications might be. Leishman (2011) argues that AeroDyn has taken certain liberties in the selection of the various constants and omissions of various correction factors, strategies for time constant modifications, and the like. A few items are worth emphasizing in this report:

1. The recovery factor η_e has been omitted from the calculations of the chordwise force coefficients in AeroDyn. This seems plausible since the reconstruction of C_c follows the calculation of a dedicated f (or better f'') from static airfoil data.
2. The vortex decay is not modified (accelerated) if the critical shedding condition for the LE vortex is not met. This may be revised.
3. The moment coefficient treatment is substantially different from the originally proposed LBM model. In particular the circulatory responses to changes in AOA and pitching rate are ignored, and the only circulatory contribution is given by a modified treatment of the TE separated-flow conditions and the vortex lift contribution in terms of displaced center of pressure. The TE-separated flow model uses again a table lookup of static values as a function of a modified AOA (α'_f, see Section 12.2.2) and that may at least account for the 0-lift contribution C_{m0}.
4. The time constants related to the pitching rate deficiency functions are set equal to those related to step changes in AOA: $T_q(M) = T_\alpha(M)$ (see Section 12.1). This should be revised.
5. The Prandtl-Glauert factor β_M is squared in the definitions of the time constants T_q andT_α; that appears to be an error, though its effect is minimal at subsonic speeds. More investigation is required to clear this point.
6. The time constants T_f, T_V are not modified following the same criteria as in the original model (see also Leishman (2011) for a review on the strategies for time constant modifications).
7. The total chordwise force treatment is also quite different from the original LBM. The adopted model follows the work of Pierce (1996) (see Section 12.3).

13. GENERALIZED DYNAMIC WAKE THEORY

The Generalized Dynamic Wake Theory (GDW or GDWT) is based on the Peters-He model (Peters et al. (1989)) and it has been implemented in AeroDyn following the work of Suzuki (2000).

The GDW is a dynamic inflow model, i.e. a model that attempts at predicting skewed wake and time lag effects due to transient loading (and inflow conditions) of the rotor. Historically, in rotorcraft aerodynamics, inflow has been denoting induced flow, or induced velocity (aU_∞), thus the GDW intends to account for transient effects on induced velocity. Since vorticity distribution in the wake (primarily the result of tip and TE vorticity shed by the rotor blades) is responsible for the induced velocity, the name GDW finds its justification in that it tries to assess effects on the induced velocity at the rotor due to time varying vorticity in the wake.

In this Section, the main equations leading to the implementation of the GDW are repeated for completeness, however more details on the derivation can be found in Suzuki (2000), Moriarty and Hansen (2004), Peters et al. (1989), Peters and He (1991).

It is worth outlining the sign convention and notation used in the original model, following the reference frame in Figure 6.

The advance ratio μ and the non-dimensional velocity normal to the rotor λ_f (or $-\lambda_w$ in wind turbine sense) are defined as follows:

$$\begin{aligned} \mu &= \frac{U_\infty \sin(\chi_0)}{\Omega R} = \frac{U_H}{\Omega R} \\ -\lambda_f = \lambda_w &= \frac{U_\infty \cos(\chi_0)}{\Omega R} = \frac{V_H}{\Omega R} \end{aligned} \tag{142}$$

They are to be considered average values across the rotor-disc of the normalized, relative air velocity. The corresponding component of the spatially-averaged induction velocity, normal to the rotor disc, is indicated with λ_m, and assumed positive (just as for λ_f) if directed as Z_{FFHR}. In Figure 6, it is then $\lambda_f < 0$, or equivalently $\lambda_w > 0$; furthermore, in that 'wind-turbine state', $\lambda_m > 0$, i.e. it is directed upwind as it should.

This sign convention is to be preferred to the current one used in AeroDyn, where $\lambda_f > 0$ and $\lambda_m < 0$, since the rotor does not change rotational direction nor does it flip its orientation going across different wake states (see also Peters (2011)). It is recommended that the figures and nomenclature used for the GDW treatment in the AeroDyn's Theory Manual (Moriarty and Hansen (2004)) be replaced by those in this report, in particular Figure 12 of the manual could be replaced by Figure 6.

Note, also, that a relation exists between λ_m and the spatially-averaged induction factor $\bar{a}$:

$$\frac{\bar{a}\, V_H}{\Omega R} = \lambda_m \tag{143}$$

V_H(as well as U_H) should include the body motion contributions (see also Section 5.2).

The spatially-averaged, instantaneous resultant-velocity (total velocity accounting for induction) at the rotor disc ($\underline{V_{TOT}}$) has magnitude expressed by:

$$V_{TOT} = \sqrt{\mu^2 + \left(\lambda_f + \lambda_m\right)^2} \tag{144}$$

The wake-skew angle χ (see also Figure 6 and Section 2) is defined as the smaller angle between $\underline{V_{TOT}}$ and the Z_{FFHR} axis, whereas the wake skew parameter X_W is given by:

$$X_W = \tan\left(\frac{\chi}{2}\right) = \frac{\mu}{\left(\left|\lambda_f + \lambda_m\right| + V_{TOT}\right)} \tag{145}$$

The second equality in Eq. (145) can be proven by utilizing the following equations:

$$\begin{aligned} \frac{\mu}{\left|\lambda_f + \lambda_m\right|} &= \tan(\chi) = \frac{2\tan\left(\frac{\chi}{2}\right)}{1 - \left[\tan\left(\frac{\chi}{2}\right)\right]^2} \\ \tan\left(\frac{\chi}{2}\right) &= \frac{1 - \cos(\chi)}{1 + \cos(\chi)} = \frac{V_{TOT}[1 - \cos(\chi)]}{V_{TOT} + \left|\lambda_f + \lambda_m\right|} \end{aligned} \tag{146}$$

The mass-flow parameter (V_M) is defined as in Eq. (147):

$$V_M = \frac{\partial(V_{TOT}\lambda_m)}{\partial\lambda_m} = V_{TOT} + \frac{\left(\lambda_f + \lambda_m\right)\lambda_m}{V_{TOT}} \tag{147}$$

V_M does not have a 'physical' velocity meaning, but it will be useful for other equations below.

The GDW stems from a solution to a linearized Eulerian formulation of the equations of motion, under the following hypotheses:

- Incompressible flow (div($\underline{v}$)=0)
- Inviscid fluid
- $\underline{v} = \underline{U_\infty} + \underline{u}$, where $\underline{u}$ is the induced velocity vector field
- $|\underline{u}| \ll |\underline{U_\infty}|$ .AND. $\left|\frac{\partial\,\underline{u}}{\partial t}\right| \ll \left|\frac{\partial \underline{U_\infty}}{\partial t}\right|$, linearizable
- $\underline{U_\infty}$ is a uniform field
- x, y, z reference frame as in Figure 6

The momentum equation can thus be written as follows (removing higher order terms):

$$\frac{\partial \underline{u}}{\partial t} + \underline{U_\infty} \cdot \vec{\nabla}\underline{u} = -\vec{\nabla}p \tag{148}$$

Taking the divergence of Eq. (148), the momentum equation reduces to a Laplace equation for the pressure field:

$$\nabla^2 p = 0 \tag{149}$$

The original formulation of the model (see for instance Peters et al. (1989)) was given in non-dimensional terms following the normalization below for time, displacement, velocities and pressure:

$$\hat{t} = \Omega t$$

$$\hat{x}_i = \frac{x_i}{R}$$

$$\hat{u}_i = \frac{u_i}{\Omega R} \tag{150}$$

$$\hat{U}_\infty = \frac{U_\infty}{\Omega R}$$

$$\phi_W = \frac{p}{\rho(\Omega R)^2}$$

Eq. (149) thus becomes:

$$\nabla^2 \phi_W = 0 \tag{151}$$

with boundary conditions given by the aerodynamic loading at the rotor blades, thus by the requirement that the rotor thrust be equal to the difference in the pressure integrals on either sides of the rotor plane, and by the requirement that the pressure in the distance field be equal to ambient pressure p_∞ ($\phi_{W\infty}$).

The momentum equation (Eq. (148)) becomes:

$$\frac{\partial \underline{\hat{u}}}{\partial \hat{t}} + \underline{\hat{U}}_\infty \cdot \hat{\nabla} \underline{\hat{u}} = -\hat{\nabla} \phi_W$$

where

$$\hat{\nabla} = \begin{Bmatrix} \frac{\partial}{\partial \hat{x}} \\ \frac{\partial}{\partial \hat{y}} \\ \frac{\partial}{\partial \hat{z}} \end{Bmatrix} \tag{152}$$

By separating Eq. (152)(a) into two contributions, assuming $\phi_W = \phi_W^A + \phi_W^V$, i.e. an acceleration part and a spatial advection part, one may write:

$$\frac{\partial \underline{\hat{u}}}{\partial \hat{t}} = \breve{\underline{u}} = -\hat{\nabla} \phi_W^A$$

$$\underline{\hat{U}}_\infty \cdot \hat{\nabla} \underline{\hat{u}} = -\hat{U}_\infty \underline{\hat{\xi}} \cdot \hat{\nabla} \underline{\hat{u}} = -\hat{U}_\infty \frac{\partial \underline{\hat{u}}}{\partial \hat{\xi}} = -\hat{\nabla} \phi_W^V \tag{153}$$

or, for *i*=1..3:

$$-\hat{U}_\infty \frac{\partial \hat{u}_i}{\partial \hat{\xi}} = -\frac{\partial \phi_W^V}{\partial \hat{x}_i}$$

where $\underline{\breve{u}}$ is the non-dimensional time-derivative of $\underline{\hat{u}}$; $\underline{\hat{\xi}}$ is a unit vector aligned with $\underline{U}_\infty$, but pointing in the opposite direction, and $\hat{\xi}$ the associated coordinate (equal to 0 at the rotor-disc);

From the last of Eq.s (153), considering the third component of the induced velocity, i.e. the assumed normal to the rotor-disc from Figure 6, one can write:

$$\begin{aligned} \breve{u}_3 &= -\frac{\partial}{\partial \hat{z}}\phi_W^A = [E]\phi_W^A \\ \hat{u}_3 &= \frac{1}{\hat{U}_\infty}\int_0^\infty \frac{\partial \phi_W^V}{\partial \hat{x}_3}\partial\xi = [L]\phi_W^V \end{aligned} \tag{154}$$

where $[E]$ and $[L]$ are linear operators assumed invertible, with $[M] = [E]^{-1}$.

Therefore, the following expressions can be obtained:

$$\begin{aligned} [M]\,\breve{u}_3 &= \phi_W^A \\ [L]^{-1}\hat{u}_3 &= \phi_W^V \end{aligned} \tag{155}$$

thus

$$\phi_W = \phi_W^A + \phi_W^V = [M]\,\breve{u}_3 + [L]^{-1}\hat{u}_3$$

Eq. (155) is the general form of the GDWT governing equation (see also Suzuki (2000) and Moriarty and Hansen (2004) for more details).

Kinner (1937) developed a solution for Eq. (151) which would allow for a discontinuity at the rotor plane, and thus a finite thrust developing at the rotor disc. The solution was cast in an ellipsoidal coordinate system $(O; \upsilon, \eta, \Psi_{HR})$ form:

$$\phi_W(\upsilon, \eta, \Psi_{HR}, \hat{t}) = \sum_{m=0}^{\infty} \sum_{n=m+1,m+3,\ldots}^{\infty} P_n^m(\upsilon) Q_n^m(j\eta)[C_n^m(\hat{t})\cos(m\Psi_{HR}) + D_n^m(\hat{t})\sin(m\Psi_{HR})] \tag{156}$$

where P_n^m, Q_n^m are Legendre functions of the first and second kind respectively; C_n^m and D_n^m are time-dependent coefficients of the Fourier expansion. The index m refers to the harmonic expansion mode in azimuth; the n index refers to the radial expansion mode.

At $\eta = 0$, i.e. at the disc surface, the solution is discontinuous, and the differential pressure can be calculated as (Peters et al. (1989)):

$$\phi_{WD}(v,\Psi_{HR},\hat{t}) = \sum_{m=0}^{\infty}\sum_{n=m+1,m+3,\ldots}^{\infty} \hat{P}_n^m(v)[\tau_n^{mc}(\hat{t})\cos(m\Psi_{HR}) + \tau_n^{ms}(\hat{t})\sin(m\Psi_{HR})]$$

with

$$\hat{P}_n^m(v) = (-1)^m \frac{P_n^m(v)}{\rho_n^m}$$

$$\rho_n^m = \sqrt{\frac{1}{2n+1}\frac{(n+m)!}{(n-m)!}} \tag{157}$$

$$\tau_n^{mc} = (-1)^{m+1} 2 Q_n^m(j0)\rho_n^m C_n^m$$

$$\tau_n^{ms} = (-1)^{m+1} 2 Q_n^m(j0)\,\rho_n^m D_n^m$$

The induced velocity component normal to the plane of the rotor can also be expressed in a Legendre/Fourier series, with indices k and l playing the same role as m and n in the previous pressure expansions:

$$\hat{u}_3(\hat{r}(v),\psi,\hat{t}) = \sum_{k=0}^{\infty}\sum_{l=k+1,k+3,\ldots}^{\infty} \varphi_l^k(v)\left[\alpha_l^k(\hat{t})\cos(k\Psi_{HR}) + \beta_l^k(\hat{t})\sin(k\Psi_{HR})\right] \tag{158}$$

where $\alpha_l^k(\hat{t})$ and $\beta_l^k(\hat{t})$ are the model states; the sign convention for $\hat{u}_3$ is the same as for λ_m; the non-dimensional radial coordinate is given by:

$$\hat{r}(v) = \sqrt{1-v^2}$$

and the expressions for the radial shape functions, $\varphi_l^k(v)$, are as in the following:

$$\varphi_l^k(v) = \varphi_l^k(\hat{r}(v)) = \sqrt{(2l+1)H_l^k}\sum_{q=k,k+2,\ldots}^{\infty} \hat{r}^q \frac{(-1)^{\frac{q-k}{2}}(q+l)!!}{(q-k)!!\,(q+k)!!\,(l-q-1)!!}$$

with

$$H_l^k = \frac{(l+k-1)!!\,(l-k-1)!!}{(l+k)!!\,(l-k)!!} \tag{159}$$

$$n!! = \begin{cases} n(n-2)(n-4)\ldots 3\cdot 1 \text{ if } n = \text{odd} \\ n(n-2)(n-4)\ldots 4\cdot 2 \text{ if } n = \text{even} \\ 1 \text{ if } n = 0 \end{cases}$$

Because of the way $\hat{u}_3$ (and analogously ϕ_{WD}) is defined, the only indices that are used in φ_l^k ($\hat{P}_n^m$, τ_n^{mc}, τ_n^{ms}) are of the kind: [k (or m)=0; l (or n) =1,3,5,7,..]; [k (or m)=1; l (or n) =2,4,6,8,…]; etc..

By substituting Eq. (158) and Eq. (157) into Eq. (155) and manipulating the algebra, one can obtain relationships relating $\alpha_l^k(\hat{t})$ and $\beta_l^k(\hat{t})$ to the $\tau_n^{mc}$and τ_n^{ms} pressure coefficients, i.e. the core equations of the GDW method:

$$[M^c]\{\breve{\alpha}_l^k\} + [L^c]^{-1}\{\alpha_l^k\} = \left\{\frac{\tau_n^{mc}}{2}\right\}$$
$$[M^s]\{\breve{\beta}_l^k\} + [L^s]^{-1}\{\beta_l^k\} = \left\{\frac{\tau_n^{ms}}{2}\right\} \tag{160}$$

where the curly braces indicate arrays.

The above equations are decoupled on the LHS, i.e. the operator matrix $[M]$ (also called apparent-mass matrix) is diagonal and with terms for cosine factors decoupled (sequential) from those of sine factors; $[M^c]$ and $[M^s]$ are substantiallty the same matrix, except for the first row in $[M^c]$ which has terms for m=0:

$$[M] = \begin{bmatrix} \ddots & & \\ & \frac{2}{\pi}H_n^m & \\ & & \ddots \end{bmatrix} \tag{161}$$

where the definition of H_n^m is given in Eq. (159). Suzuki (2000) argues that a time-lag coefficient could be applied to Eq. (161) to account for a different time scale between helicopter and wind turbine wakes. While some indications seem to confirm that argument, more experimental data is needed for a more definitive conclusion.

The $[L]$ operators are functions of the skew angle χ and can be put in the form:

$$[L^c]^{-1} = [V^c][\tilde{L}^c]^{-1}$$
$$[L^s]^{-1} = [V^s][\tilde{L}^s]^{-1} \tag{162}$$

with the following expressions for the matrices $[\tilde{L}^c]$ and $[\tilde{L}^s]$:

$$[\tilde{L}_{ln}^{0m}]^c = (X_w)^m\,[\Gamma_{ln}^{0m}]$$
$$\left[\tilde{L}_{ln}^{km}\right]^c = \left((X_w)^{|m-k|} + (-1)^b (X_w)^{|m+k|}\right)\left[\Gamma_{ln}^{km}\right]$$
$$\left[\tilde{L}_{ln}^{km}\right]^s = \left((X_w)^{|m-k|} - (-1)^b (X_w)^{|m+k|}\right)\left[\Gamma_{ln}^{km}\right] \tag{163}$$

with

$$b = \min(k, m)$$

and where:

$$\Gamma_{ln}^{km} = \begin{cases} \dfrac{(-1)^{\frac{n+l-2k}{2}}}{\sqrt{H_n^m H_l^k}} \dfrac{2\sqrt{(2n+1)(2l+1)}}{(l+n)(l+n+2)[(l+n)^2-1]}, & \text{if } k+m = \text{even} \\ \dfrac{\pi}{2\sqrt{H_n^m H_l^k}} \dfrac{\text{sign}(k-m)}{\sqrt{(2l+1)(2n+1)}}, & \text{if } k+m = \text{odd and } |l-n| = 1 \\ 0, & \text{if } k+m = \text{odd and } |l-n| \neq 1 \end{cases} \tag{164}$$

And finally the flow parameter matrix:

$$[V^c] = \begin{bmatrix} \ddots & & \\ & V_n^m & \\ & & \ddots \end{bmatrix} \text{ with } \quad m = 0,1,2,\ldots$$

$$[V^s] = [V^c] \quad \text{with } m = 1,2,\ldots \tag{165}$$

with

$$V_n^m = \begin{cases} V_{TOT} & \text{for } (m,n) = (0,1) \\ V_M & \text{for } (m,n) \neq (0,1) \end{cases}$$

Note that some confusion arises on this point in the AeroDyn's Theory Manual (Moriarty and Hansen (2004)).

The theory also brings forth an approximation for the $\lambda_m$induced velocity (see Peters and He (1991)):

$$\lambda_m = \frac{2}{\sqrt{3}}\{1 \quad 0 \quad \cdots \quad 0\}[\tilde{L}^c]^{-1}\{\alpha_l^k\} \approx \sqrt{3}\alpha_1^0 \tag{166}$$

The boundary conditions for the model in Eq. (160) are given by the blade aerodynamic loading; therefore a link must be attained between the pressure coefficients τ_n^{mc}, τ_n^{ms} and the blade loading via BEM (see also Figure 15).

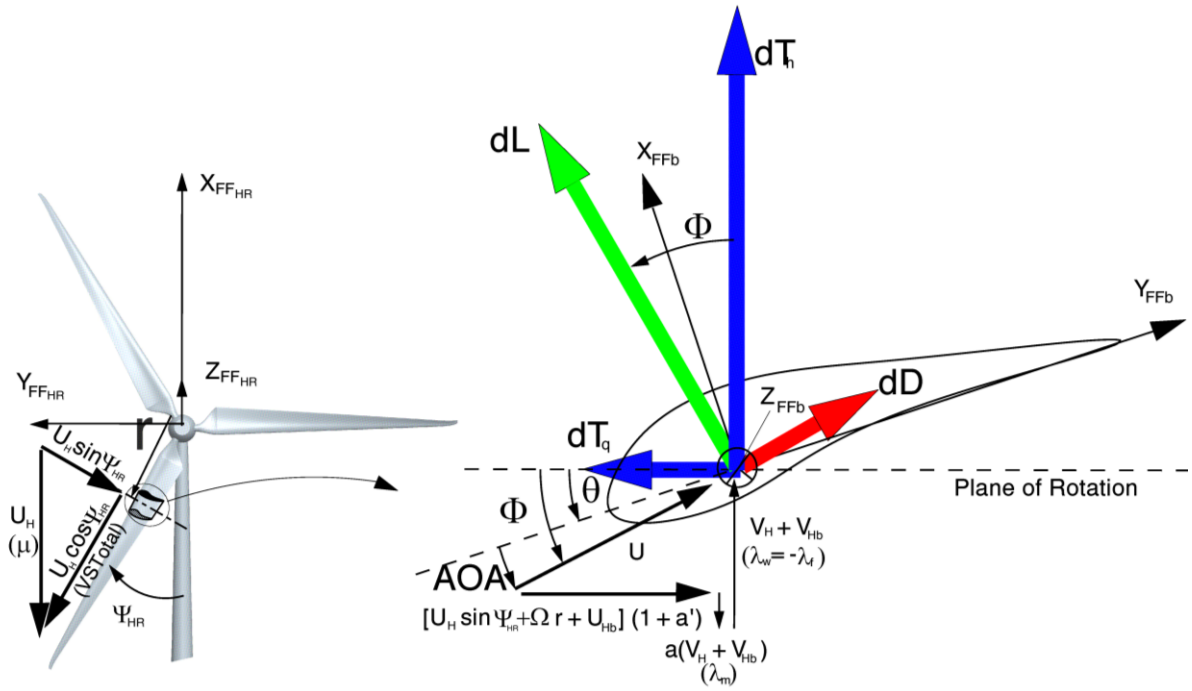

Figure 15. Induction in the rotorcraft reference system and BEM.

Let the normalized thrust coefficients for the generic blade b and blade element e be expressed as:

$$C_{th_{b,e}} = \frac{L_{b,e}}{\rho S(\Omega R)^2} = \frac{L_{b,e}}{\rho \pi \Omega^2 \mathrm{R}^4} \tag{167}$$

where $L_{b,e}$ is the elemental lift, and the contribution from drag is ignored. The pressure coefficients τ_n^{mc}, τ_n^{ms} can be seen as normalized total thrust multiplied by the radial shape function $\varphi_n^m(\hat{r}_e)$ and the generic azimuthal mode shape (Suzuki (2000)):

$$\tau_n^{0c} = \frac{1}{2\pi\rho\Omega^2 \mathrm{R}^4} \sum_{b=1}^{N_b} \left[\sum_{e=1}^{N_e} L_{e,b} \varphi_n^0(\hat{r}_e) \right]$$

$$\tau_n^{mc} = \frac{1}{\pi\rho\Omega^2 \mathrm{R}^4} \sum_{b=1}^{N_b} \left[\sum_{e=1}^{N_e} L_{e,b} \varphi_n^m(\hat{r}_e) \right] \cos(m\Psi) \tag{168}$$

$$\tau_n^{ms} = \frac{1}{\pi\rho\Omega^2 \mathrm{R}^4} \sum_{b=1}^{N_b} \left[\sum_{e=1}^{N_e} L_{e,b} \varphi_n^m(\hat{r}_e) \right] \sin(m\Psi)$$

In practice, the number of modes along the radial and azimuthal directions need to be finite. One could think of including enough modes to capture the so-called mP (m per revolution) terms; for instance, for a three bladed turbine, at least 0P through 3P terms are expected to be significant. Peters and He (1991) (see also Moriarty and Hansen (2004)) suggest to select modes based on the highest requested power of $\hat{r}$ in the radial shape function $\varphi_l^k(\hat{r})$. It can be shown that a simple relationship can be devised to calculate the number of states given the power of $\hat{r}$ and the maximum number of azimuth harmonics as in Table 1:

Highest Power of $\hat{r}$	Harmonic Number m									**Number of States**
	0	1	2	3	4	5	6	7	8	
0	1									**1**
1	1	1								**3**
2	2	1	1							**6**
3	2	2	1	1						**10**
4	3	2	2	1	1					**15**
5	3	3	2	2	1	1				**21**
6	4	3	3	2	2	1	1			**28**
7	4	4	3	3	2	2	1	1		**36**
8	5	4	4	3	3	2	2	1	1	**45**

Table 1. Number of Shape functions per Harmonic. Note that for m>0 the number of states doubles (due to both cosine and sine terms).

For instance, for a maximum radial polynomial degree of $\hat{r}^4$, and maximum number of harmonics equal to 3, there are 3 states for m=0, and 2*(2+2+1) states for m=1-3; i.e. 13 states in total. If all of the available harmonics are used for that polynomial degree, one would need to solve for 15 states.

AeroDyn assumes by default (***DynInflow*** (***AeroMods***) see Appendix D) 3 harmonics and 10 states: 2 states for m=0 (α_1^0 and α_3^0); 4 states for m=1 (α_2^1 and β_2^1; α_4^1 and β_4^1); 2 states for m=2 (α_3^2 and β_3^2); and 2 states for m=3 (α_4^3 and β_4^3). That corresponds to a maximum power of $\hat{r}^3$, and up to 3P terms (three harmonics). The radial shape functions, or better the factors multiplying the polynomial argument raised to the powers of $\hat{r}$ can thus be calculated a-priori as a function of the (m,n) indices (see ***PHIS*** and ***XPHI*** (***AeroSubs***), Appendix C).

13.1 AeroDyn's Current Implementation of the GDW

AeroDyn starts the GDW at the initial time step (0-th time step) by calculating the states with the assumption that:

$$\{\breve{\alpha}_l^k\} = \{\breve{\beta}_l^k\} = \{0\} \tag{169}$$

Thus Eq.(160) can be re-arranged to solve for the states:

$$\begin{aligned} \{\alpha_l^k\} &= [L^c]\left\{\frac{\tau_n^{mc}}{2}\right\} \\ \{\beta_l^k\} &= [L^s]\left\{\frac{\tau_n^{ms}}{2}\right\} \end{aligned} \tag{170}$$

If the assumptions in Eq. (169) were not used, the time derivative at the 0-th time-step could be expressed in discretized form:

$$\begin{aligned} \{\breve{\alpha}_l^k\} &= \frac{\{\alpha_l^k\}}{\Delta\hat{t}} \\ \{\breve{\beta}_l^k\} &= \{\beta_l^k\}/\Delta\hat{t} \end{aligned} \tag{171}$$

where the states at $\hat{t}$=0 are assumed nil. Therefore Eq. (170) could be replaced by:

$$\begin{aligned} \{\alpha_l^k\} &= \left[\frac{[M^c]}{\Delta\hat{t}} + [L^c]^{-1}\right]^{-1}\left\{\frac{\tau_n^{mc}}{2}\right\} \\ \{\beta_l^k\} &= \left[\frac{[M^s]}{\Delta\hat{t}} + [L^s]^{-1}\right]^{-1}\left\{\frac{\tau_n^{ms}}{2}\right\} \end{aligned} \tag{172}$$

AeroDyn in the subroutine ***InfInit*** (***AeroSubs***) (see Appendix C) calculates (following the definitions given in the foregoing) the (constant) matrix $[M]^{-1}$, Γ_{ln}^{km}, and the flow parameters μ, λ_f, though with a different sign convention. It also computes λ_m from the spatially averaged a (calculated via BEMT at the 0-th time-step) from Eq. (143), though no body motion contribution is considered; it is unclear why V_{TOT}, V_M, and X_w are then determined without the newly calculated λ_m. Before utilizing Eq. (170), ***InfInit*** calculates the $[\tilde{L}^c]$ and $[\tilde{L}^s]$ (and thus the terms H_n^m). Later on, those matrices are inverted.

In order to use Eq. (170) above and get the states at the 0-th time-step, $\tau_n^{mc}$and τ_n^{ms}need to be computed. ***InfInit*** uses Eq. (168), (see also ***GetPhiLq*** and ***GetRM*** (***AeroSubs***) in Appendix C), but where the $L_{e,b}$ is replaced by the magnitude of the total force acting on the blade element (i.e., including the effects of both lift and drag). Peters (2011) argues that only the lift contribution should be considered in Eq. (168), and that the resulting induced flow should be considered directed along the lift vector (i.e. that lift and induced velocity are normal to the vortex sheet). The blade element lift (and drag) comes from the BEM approach (eventually including unsteady aerodynamics and dynamic stall treatment).

Once the states are known, the BE AOA and forces can be calculated for the new time iteration. In particular, AeroDyn's ***VindInf*** (***AeroSubs***) (see Appendix C) first uses Eq. (158), (though with a different sign convention), which gives the local (normalized) induced velocity, normal to the rotor plane; then, re-introduces the tip-speed and 'normalization factor' *VNW* (local wind velocity component normal to the rotor plane) to obtain the axial induction factor a. It seems more correct, however, to assume *VNTotal* in place of *VNW* as discussed in Section 5.2. ***VindInf*** determines the tangential induction factor a' from Eq. (48), though Eq. (46) may be preferred for reasons explained in Section 5. The subroutine ***ElemFrc*** (***AeroSubs***) then calls either ***CLCD*** or ***BEDDOES*** (***AeroSubs***) (see Appendix A.2 and C) to calculate the BEM lift and drag from the known local wind (and body) velocity components and induction factors. They are used in Eq. (168) to calculate τ_n^{mc} and τ_n^{ms} at the next time iteration.

At each of the following time steps, AeroDyn performs similar calculations via ***InfDist*** (***AeroSubs***) (see Appendix C), updating μ, λ_f, V_{TOT}, V_M, X_w, $[\tilde{L}^c]$, $[\tilde{L}^s]$, τ_n^{mc}, and τ_n^{ms}. Note that the tip-speed (used as normalization factor) is updated at each time step as well. That however has some repercussions on the calculations themselves, since the numerical time-derivatives are not correctly calculated if the RPM changes from time-step to time-step (see Section 13.3.5).

InfDist further calculates the RHS of Eq. (173), which is equivalent to Eq. (160) rearranged:

$$\begin{aligned}\{\check{\alpha}_l^k\} &= [M^c]^{-1}\left[-[L^c]^{-1}\{\alpha_l^k\} + \left\{\frac{\tau_n^{mc}}{2}\right\}\right] \\ \{\check{\beta}_l^k\} &= [M^s]^{-1}\left[-[L^s]^{-1}\{\beta_l^k\} + \left\{\frac{\tau_n^{ms}}{2}\right\}\right]\end{aligned} \tag{173}$$

Eq. (173) is then solved via an Adams/Bashforth predictor/corrector method. Finally a new value for λ_m is computed using Eq. (165), which will participate in the calculations of the flow parameters at the next time step.

13.2 Tip-loss and Off-Axis Flow Considerations

Because of the way it is constructed, the GDW theory is suited to predict (once coupled with BEM aerodynamics) airloads also in off-axis situations, such as tilt and yaw error situations. The pressure and induced velocity distributions (see Eq.s (157) and (158)) can, in fact, account for a highly variable 'inflow field' in the plane of the rotor, and given the time description, also highly temporally varying. It has been shown that the GDW, as currently implemented in AeroDyn, provides much better blade load estimates

than BEMT under yawed operation (Suzuki (2000)), with the added advantage of capturing up to 3P fluctuations reasonably well.

The normal BEMT is based on the concept of an actuator disc, and as such it needs to account for tip-loss effects via ad-hoc corrections (see Section 6). The GDW, on the other hand, is developed on the assumption that the discontinuous pressure field due to the presence of a finite number of blades, of finite length, can be described by an expansion in radial shape functions (Legendre) and azimuthal Fourier harmonic modes. It can, in fact, be proven (Peters (2011)) that the GDW would converge to the Prandtl's tip-loss solution as more harmonics are added to the model, though full convergence requires a large number of them (m must be greater than twice the number of blades).

13.3 Improvements to the Current State of the GDW Implementation

13.3.1 Vortex-Ring State and Alleviation of Method Instabilities

It has been reported (see also Suzuki (2000)) that the GDW is unstable (it does not reach convergence) under high TSR operation. At sufficiently large TSRs, the rotor starts acting more like a propeller (propeller state) than a wind turbine (windmill state). Currently AeroDyn reverts to the BEMT if wind speeds are less than 6 m/s to avoid instabilities.

It has been argued that instabilities occur in the transition between wake states, and precisely at the occurrence of the so-called vortex-ring state, when the induction factor approaches zero and the effect of the rotor on the flow (in the MT) would approach nil. Yet the bound vorticity is still shed in the wake of the turbine, and it eventually organizes itself in an unstable and unsteady vortex ring which causes the airflow and the blade loading to be unstable as well.

Peters (2011) proposes a relatively simple strategy to account for the vortex-ring state in the GDW treatment.

First, a low-pass filter (with a time constant of $\frac{32}{15\pi V_M}$, which is common to all wake parameters following Peters and He (2006)) is applied to the incoming flow velocity components, i.e. λ_f and μ in the FF$_{HR}$ reference frame, or equivalently to the *VRotorX*, *VrotorY*, *VrotorZ* (i.e., components in FF$_{HR}$ when $\Psi_0 = 0$) per AeroDyn's ***DiskVel*** routine (also ***InfInif*** and ***InfDist***) (***AeroSubs***) called by ***AD_CalculateLoads*** (***Aerodyn***) (see Appendix A, B, C and D).

The extra equations to implement in the GDW time-integration are the following:

$$\frac{dV_{id}}{d\hat{t}} = \frac{15\pi}{32} V_M [V_i - V_{id}] \quad i = 1..3 \tag{174}$$

where V_i are the normalized (by ΩR) components in FF$_{HR}$ ($\Psi_0 = 0$) of the relative air-velocity (including body motion's contributions), and the V_{id} are the equivalent, low-pass filtered ones. These three additional states of the model could be replaced by two different ones, if the base FF$_{HR}$ system is used, where the low-pass filtered λ_{fd} and μ_d are calculated as:

$$\frac{d\lambda_{fd}}{d\hat{t}} = \frac{15\pi}{32} V_M[\lambda_f - \lambda_{fd}]$$
$$\frac{d\mu_d}{d\hat{t}} = \frac{15\pi}{32} V_M[\mu - \mu_d] \tag{175}$$

These variables need to be calculated before the other flow parameters (see below).

Secondly, the resultant total velocity and the mass-flow parameter (Eq.s (144) and (147)) are replaced by the following expressions:

$$V_{TOT} = \sqrt{\mu^2 + (\lambda_f + \lambda_m)^2 + \Delta_{VR}}$$

with

$$\Delta_{VR} = f_{VR}(\sigma_{VR})\, g_{VR}(\rho_{VR}) v_0^2$$
$$v_0^2 = |\lambda_m V_{TOT}| = \left|\frac{\tau_1^{0c}}{\sqrt{3}}\right|$$
$$\sigma_{VR} = \left|\frac{\mu}{v_0}\right|$$
$$\rho_{VR} = \left|\frac{\lambda_f + \lambda_m}{v_0}\right| \tag{176}$$
$$f_{VR}(\sigma_{VR}) = \begin{cases} 1 - 2\sigma_{VR}^2 & \text{for } \sigma_{VR} < 0.707 \\ 0 & \text{for } \sigma_{VR} \geq 0.707 \end{cases}$$
$$g_{VR}(\rho_{VR}) = \begin{cases} \frac{1}{(2+\rho_{VR})^2} - \rho_{VR}^2 + (1+\rho_{VR})[0.109 + 0.217(\rho_{VR} - 0.15)^2] & \text{for } -1 < \rho_{VR} < 0.6378 \\ 0 & \text{for } \rho_{VR} \leq -1 \text{or } \rho_{VR} \geq 0.6378 \end{cases}$$

And for the mass-flow parameter:

$$V_M = \frac{\partial(V_{TOT}\lambda_m)}{\partial\lambda_m} = \frac{V_{TOT}[\mu^2 + (\lambda_f + \lambda_m)(\lambda_f + 2\lambda_m) + \Delta_{VR}] + v_0^3 f_{VR}(\sigma_{VR}) \frac{g'_{VR}(\rho_{VR})}{2}}{\left[\mu^2 + (\lambda_f + \lambda_m)^2 + \frac{\Delta_{VR}}{2}\right] + \frac{v_0^2}{4}[\rho_{VR} f_{VR}(\sigma_{VR}) g'_{VR}(\rho_{VR}) + \sigma_{VR} f'_{VR}(\sigma_{VR}) g_{VR}(\rho_{VR})]} \tag{177}$$

with

$$f'_{VR}(\sigma_{VR}) = -4\sigma_{VR} \quad \text{for } \sigma_{VR} < 0.707$$
$$g'_{VR}(\rho_{VR}) = \frac{-2}{(2+\rho_{VR})^3} + 0.049 - 1.696\rho_{VR} + 0.651\rho_{VR}^2 \quad \text{for } -1 < \rho_{VR} < 0.6378$$

In Eq.s (176)-(177), the other flow parameters are low-pass filtered, i.e. calculated starting from low-pass filtered quantities derived from Eq. (174) (or (175)).

These new parameters are used in the remainder of the GDW procedure, in particular Eq.s (145), (163), (165), (166), (170) (or (172)), and (173).

13.3.2 Swirl and Tangential Induction Factor

AeroDyn calculates a tangential induction factor from the axial one via Eq. (48), as explained in Section 13. It can be shown, however, that the GDW should provide a total induction, which can then be subdivided into in-plane (tangential) and out-of-plane (normal or axial) components. The presence of swirl (wake rotation), however, carries along other consequences on the implementation of the GDW model as described below.

If the GDW model is driven solely by the circulatory lift of the blade element (Eq. (168)), then the calculated induced velocity (Eq. (158)) is to be intended normal to the resultant flow (i.e., including induction), which is the Goldstein's (1929) assumption. Following the schematic in Figure 16, one could write the following relationship:

$$\tan\Phi = \frac{VNTotal - \frac{u_3}{\cos\Phi}}{VTTotal} \tag{178}$$

where *VNTotal* and *VTTotal* were introduced in Section 5.2, and represent the contribution of both wind and body (rigid and elastic) motions to the normal and tangential relative air-velocity, and u_3 is the induced velocity, normal to the resultant velocity $\underline{U}$. In this section, for the sake of easier nomenclature, the dimensional quantity are used, but the exact same conclusions can be derived by adopting normalized quantities (e.g., $\hat{u}_3$, $\widehat{VNTotal}$, $\widehat{VTTotal}$, $\hat{U}$).

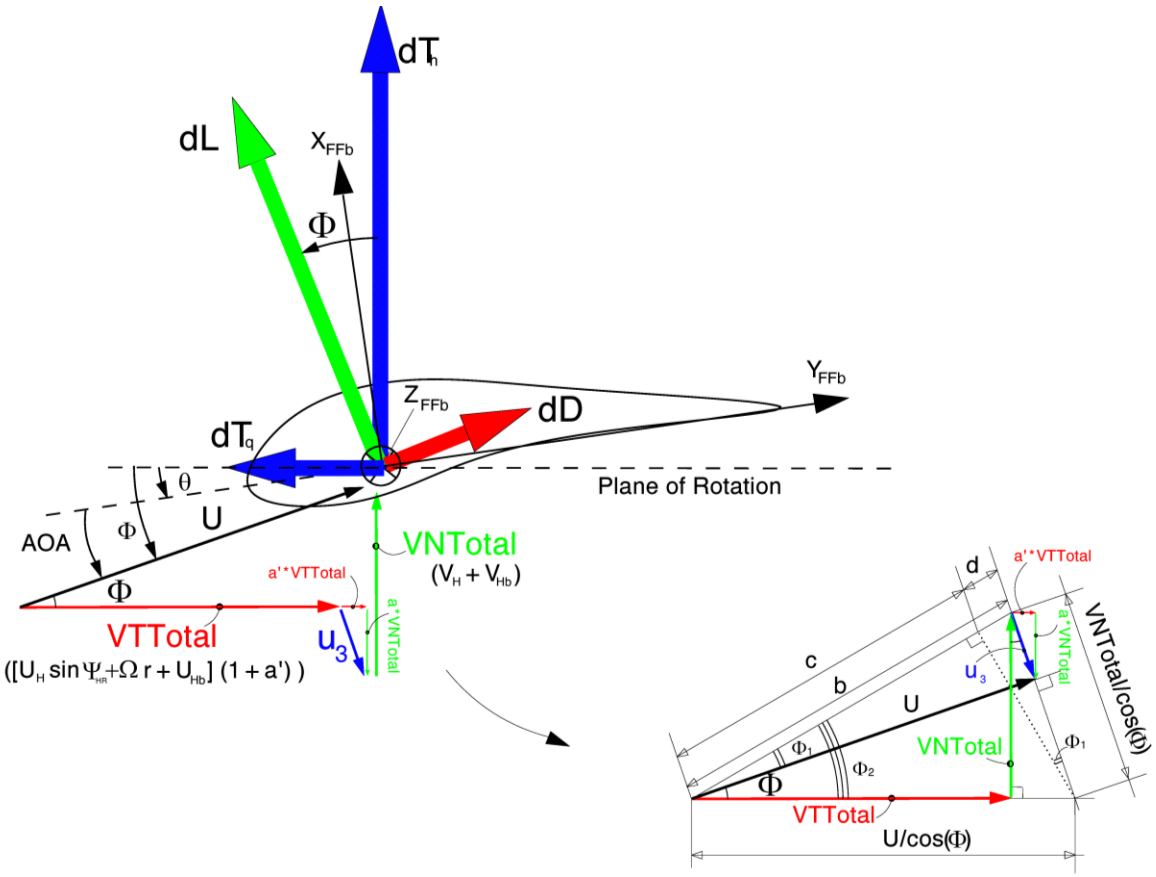

Figure 16. Geometrical construction of air-relative velocity and GDW Goldstein's hypothesis.

The following expression from the law of cosines can also be derived:

$$VTTotal^2 + U^2 - 2\,U * VTTotal * \cos\Phi = VNTotal^2 + u_3^2 - 2\,u_3 * VNTotal * \cos\Phi$$

with (179)

$$U^2 = VTTotal^2 + VNTotal^2 - u_3^2$$

Eq. (179) leads to an expression for cos Φ:

$$\cos\Phi = \frac{VTTotal^2 - u_3^2}{U * VTTotal - u_3 * VNTotal} \tag{180}$$

Using Eq. (180) and Eq. (178), an expression for sin Φ is readily derived as well:

$$\sin\Phi = \frac{VNTotal * \cos\Phi - u_3}{VTTotal} = \frac{VTTotal * VNTotal - U * u_3}{U * VTTotal - u_3 * VNTotal} \tag{181}$$

Peters (2011) proposes the following construction to derive the expressions of sine and cosine of the inflow angle (symbols from Figure 16):

$$b = c + d = \frac{U}{\cos\Phi}\cos\Phi_2 + \frac{VNTotal}{\cos\Phi}\sin\Phi_1 = \frac{U}{\cos\Phi}\frac{VTTotal}{b} + \frac{VNTotal}{\cos\Phi}\frac{u_3}{b}$$
$$b^2 = VTTotal^2 + VNTotal^2 \tag{182}$$

which leads (once combined with Eq. (178)) to:

$$\cos\Phi = \frac{U * VTTotal + u_3 * VNTotal}{VTTotal^2 + VNTotal^2}$$
$$\sin\Phi = \frac{U * VNTotal - u_3 * VTTotal}{VTTotal^2 + VNTotal^2} \tag{183}$$

The inflow angle can then be calculated making use of Eq. (184) and either Eq. (183) or the pair (180)-(181):

$$\Phi = \tan^{-1}\frac{\sin\Phi}{\cos\Phi} \tag{184}$$

From the Goldstein's (1929) hypothesis, and the construction in the foregoing, the induction factors are obtained in one straight shot from the calculation of u_3, which comes from the GDW procedure:

$$a = \frac{u_3\cos\Phi}{VNTotal}$$
$$a' = \frac{u_3\sin\Phi}{VTTotal} \tag{185}$$

The GDW model, however, was not derived with a rotating wake field. In order to account for the extra kinetic energy of the swirl, the mass-matrix [M] needs to be modified as in:

$$[M] = \begin{bmatrix} \ddots & & \\ & \sqrt{\frac{2}{\pi}H_n^m} & \\ & & \ddots \end{bmatrix} \left[[I] + m\,\frac{\kappa^2\lambda_{fd}^2}{N_b^2(1+1.5\,\mu_d^2)}\left[[I] - [A_n^m]^2\right]^{-m} \right] \begin{bmatrix} \ddots & & \\ & \sqrt{\frac{2}{\pi}H_n^m} & \\ & & \ddots \end{bmatrix} \tag{186}$$

with

$$\kappa = 2.2$$

and

$$[A_n^m] = [L_{ln}^{mm}]|_{x_w=0}$$

Note that the $[A_n^m]$ matrix is calculated from a version of the $[\tilde{L}_{ln}^{km}]$ (see Eq. (163)) setting k=m and the skew angle equal to 0 (assuming 0^0=1).

It is worth emphasizing that [M] is no longer a diagonal matrix and that the same filtering as discussed in Section 13.3.1 is considered for the calculations of the flow parameters (i.e., λ_{fd} and μ_d replace λ_f and μ, respectively).

13.3.3 Improved Tip-Loss Model

Peters (2011) states that a partial tip-correction could be implemented to render the lift at the tip exactly equal to zero even with a limited number m of harmonics. The idea is to add an inflow mode to the summation in Eq. (158) such that the AOI goes to 0 at the tip, with the tip-loss mode vanishing as the number of harmonics increases.

That condition forces $\Phi = \theta + \alpha_0$ at the tip; therefore, the induced velocity at the tip can be easily shown to read in that case as (following the schematic in Figure 16):

$$u_{3T} = VNTotal\cos(\theta_T + \alpha_{0T}) - VTTotal\sin(\theta_T + \alpha_{0T}) \tag{187}$$

where the subscript T denotes conditions at the blade tip. Note (again) that the symbols above denote dimensional quantities, but the same conclusions apply for normalized ones (e.g., $\hat{u}_{3T}$, $\widehat{VNTotal}$, $\widehat{VTTotal}$).

One can then make the following modification to Eq. (158):

$$\hat{u}_3(\hat{r}(v),\psi,\hat{t}) = \hat{u}_3(\hat{r}(v),\psi,\hat{t}) + [\hat{u}_{3T} - \hat{u}_3(\hat{r}(v),\psi,\hat{t})]^{F_{TP}}$$

with

$$F_{TP} = \frac{2}{\pi}\cos^{-1}\left[exp\left(-\frac{(m_{max}+1)N_b\left(1-\frac{r}{R}\right)}{\frac{2|\lambda_{fd}|}{\sqrt{1+1.5\,\mu_d^2}}}\right)\right] \tag{188}$$

where m_{max} is the maximum harmonic number used in the GDW implementation, and the usual flow parameters need to be considered as low-pass filtered to alleviate instability problems and vortex-ring transitions.

13.3.4 Wake Curvature and Yaw Rate

In the foregoing, it has been suggested to consider a total air velocity as relative to the lifting bodies, i.e. including the contributions from both rigid and elastic motions of the turbine structure. The presence of a large-scale body motion, as for instance due to a finite yaw rate, has other ramifications, and in particular on the wake development and associated induction. Some recent literature papers (e.g., Zhao et al. (2004)) discuss the theory behind the wake distortion and its effects following a rotor maneuver (yawing), which is beyond the scope of the current study. One of the main results, however, is given by Eq. (189), which gives an equivalent skew parameter accounting for the curvature of the wake, in other words the yaw-rate effect is readdressed as an effect of a wake skew angle:

$$X_{Weq} = X_W + K_{Re}\left[\kappa_{cw}\frac{32}{15\pi}(1-1.5X_W^2) + \kappa_s\frac{5}{2}\mu X_W\right]$$

with

$$1 \le K_{Re} \le 2 \tag{189}$$

and

$$\kappa_{cw} = \frac{1}{\Omega V_M}\frac{d\chi}{dt}$$

where κ_{cw} is the wake curvature due to wind turbine yaw-rate, and κ_s is a term that applies to a helicopter rotor rotating about the wind direction axis, which can be ignored (=0) for wind turbines.

Peters (2011) offers a simple formulation to try and implement Eq.(189). The author suggests modifying the wake skew parameter as in Eq. (190):

$$X_{Weq} = X_W + \frac{2K_{Re}(X_W - X_{Wd})(1 - 1.5X_{Wd}^2)}{(1 + X_{Wd})^2}$$
$$\frac{dX_{Wd}}{d\hat{t}} = \frac{15\pi}{16} V_M [X_W - X_{Wd}] \tag{190}$$

where X_{Wd} is the low-pass filtered value of X_W. That result implies that the wake curvature can be written as:

$$\kappa_c = \frac{15\pi}{16} \frac{(X_W - X_{Wd})}{(1 + X_{Wd})^2} \tag{191}$$

The formulas above account for both yaw-rate and wind direction change effects, since both are present in the computation of the velocities (instantaneous and filtered) that go into X_W and X_{Wd}.

The GDW can then proceed as illustrated in Section 13, with the newly calculated X_{Weq} in place of X_W in the computation of the *[L]* matrices (see Eq.(163)).

13.3.5 Dimensional Form of the GDW To Account for Variable RPM

As mentioned in Section 13.1, AeroDyn's current implementation of the GDW may lead to erroneous results if the RPM (Ω) is not constant, as the normalization factor used in the equations would change at each time-step. First, the Adams-Bashforth method of integration of Eq. (160) implies a constant time-step, and the variation of RPM undermines that hypothesis. Second, the states themselves would be normalized by different factors at different time steps, and thus the actual numerical result of the integration is questionable.

If the instantaneous Ω is replaced by a fixed nominal value, say the rated Ω at rated wind-speed, no further modification is required for the model to perform as expected.

Alternatively, the equations of the GDW can be recast in a dimensional form, where $\alpha_l^k(\hat{t})$ and $\beta_l^k(\hat{t})$ are to be considered dimensional (i.e., with units of m/s, and with $\hat{t}$ becoming t (sec)) and $\hat{u}_3$ in Eq. (158) becomes simply u_3. The non-dimensional versions (used in the previous sections) are then obtained from $\alpha_l^k(\hat{t})/(\Omega R)$ and $\beta_l^k(\hat{t})/(\Omega R)$, keeping the same symbols for sake of brevity, but with different meaning.

The instantaneous flow parameters, λ_f, and μ are to be considered dimensional, and therefore they take the values of $-V_H$ and U_H, respectively; Eq. (192) hence replaces Eq. (142).

$$\mu = U_\infty \sin(\chi_0) = U_H$$
$$-\lambda_f = \lambda_w = U_\infty \cos(\chi_0) = V_H \tag{192}$$

This is necessary because Eq. (175) may be used to low-pass filter them, and also for constructing the dimensional V_{TOT} and V_M, via either the pair Eq. (144) and (147), or the extended versions for vortex-ring transitions Eq.s (176) and (177). Eq.s (165) still gives the matrix V_n^m, but its elements are now dimensional.

The spatially-averaged induced velocity, λ_m, becomes dimensional, straight from Eq. (166), and the relationship in Eq. (143) is replaced by:

$$\bar{a}\, V_H = \lambda_m \tag{193}$$

Note that Eq. (145) does not change, and therefore the matrices $[\tilde{L}^c]$ and $[\tilde{L}^s]$ (Eq.s (163)) do not change.

Eq. (168) is replaced by Eq. (194):

$$\tau_n^{0c} = \frac{1}{2\pi\rho \mathrm{R}^2}\sum_{b=1}^{N_b}\left[\sum_{e=1}^{N_e} L_{e,b}\varphi_n^0(\hat{r}_e)\right]$$

$$\tau_n^{mc} = \frac{1}{\pi\rho \mathrm{R}^2}\sum_{b=1}^{N_b}\left[\sum_{e=1}^{N_e} L_{e,b}\varphi_n^m(\hat{r}_e)\right]\cos(m\Psi) \tag{194}$$

$$\tau_n^{ms} = \frac{1}{\pi\rho \mathrm{R}^2}\sum_{b=1}^{N_b}\left[\sum_{e=1}^{N_e} L_{e,b}\varphi_n^m(\hat{r}_e)\right]\sin(m\Psi)$$

With these changes and the new (dimensional) meaning of the symbols, the basic formulation of Eq. (160) re-writes:

$$\begin{aligned}
[M^c]\left\{\frac{d}{d\Omega t}\alpha_l^k\right\}\frac{1}{\Omega R} + [L^c]^{-1}\{\alpha_l^k\}\frac{1}{(\Omega R)^2} &= \left\{\frac{\tau_n^{mc}}{2}\right\}\frac{1}{(\Omega R)^2} \\
[M^s]\left\{\frac{d}{d\Omega t}\beta_l^k\right\}\frac{1}{\Omega R} + [L^s]^{-1}\{\beta_l^k\}\frac{1}{(\Omega R)^2} &= \left\{\frac{\tau_n^{ms}}{2}\right\}\frac{1}{(\Omega R)^2}
\end{aligned} \tag{195}$$

where again α_l^k, β_l^k, τ_n^{ms} are dimensional (with units: m/s, m/s, and m²/s² respectively).

Simplifying Eq. (195), one obtains the fully-dimensional version of the GDWT, which could be implemented in AeroDyn:

$$\begin{aligned}
R[M^c]\{\dot{\alpha}_l^k\} + [L^c]^{-1}\{\alpha_l^k\} &= \left\{\frac{\tau_n^{mc}}{2}\right\} \\
R[M^s]\{\dot{\beta}_l^k\} + [L^s]^{-1}\{\beta_l^k\} &= \left\{\frac{\tau_n^{ms}}{2}\right\}
\end{aligned} \tag{196}$$

where the 'dot' superscript represents the dimensional time-derivative.

Note that most of the other driving Equations stay the same as shown in Sections 13, and 13.3.1-13.3.4, as long as the matrix $[M]$ is replaced by $R \cdot [M]$, and assuming the new (dimensional) meaning of the symbols as explained. The only exceptions are Eq.s (174),(175), and (190)(b), which are replaced by Eq.s (197),(198), and (199), respectively.

$$\frac{dV_{id}}{dt} = \frac{15\pi}{32R}V_M[V_i - V_{id}] \quad i = 1..3 \tag{197}$$

$$\begin{aligned}
\frac{d\lambda_{fd}}{dt} &= \frac{15\pi}{32R}V_M[\lambda_f - \lambda_{fd}] \\
\frac{d\mu_d}{dt} &= \frac{15\pi}{32R}V_M[\mu - \mu_d]
\end{aligned} \tag{198}$$

$$\frac{dX_{Wd}}{dt} = \frac{15\pi}{16R} V_M [X_W - X_{Wd}] \tag{199}$$

Here, to reiterate, V_{id}, V_i, λ_{fd}, λ_f, μ_d, μ, and V_M are dimensional versions of those in Section 13.3.1. Eq.s (197)-(199) are readily proven by rewriting Eq. (174), (175), and (190)(b) with $V_{id}/(\Omega R)$, $V_i/(\Omega R)$, $\lambda_{fd}/(\Omega R)$, $\lambda_f/(\Omega R)$, $\mu_d/(\Omega R)$, $\mu/(\Omega R)$, and $V_M/(\Omega R)$ replacing the old V_{id}, V_i, λ_{fd}, λ_f, μ_d, μ, and V_M respectively, with the new meaning of the symbols.

PART II: SUGGESTED ALGORITHM ORGANIZATION

14. HIGH-LEVEL FLOWCHART FOR AERODYN

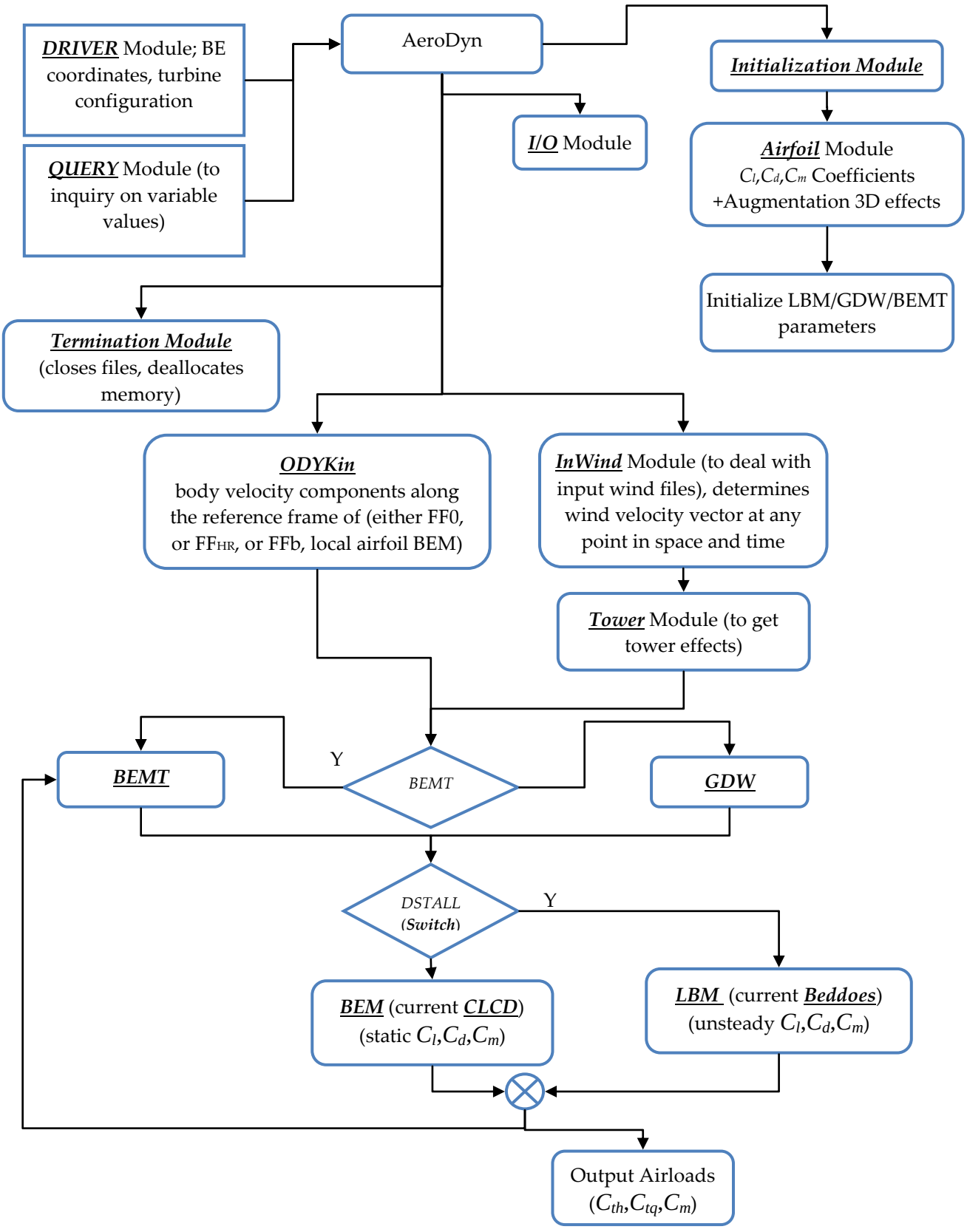

15. ALGORITHM OUTLINE FOR THE BEMT METHOD

In the foregoing, the suggested procedure to perform the BEMT calculations is described.

REQUIRED INPUTS:

- Blade element coordinates in FF0 under deflected conditions (accounting for tilt and coning as well);
- Tower deflected configuration;
- The wind velocity vector at the blade element coordinates;
- The blade element body velocity vector;
- LBM time constants and initialized variables (0-th time step)
- 2D airfoil coefficients (in case augmented for rotational effects)

OUTPUTS:

- Blade element loads (C_{th}, C_{tq}, C_m);
- Induction factors, VN, VT, AOA, Φ, (optional)

The procedure is to be performed on each BE of each blade for the *t*-th time step.

STEPS (SEE ALSO SECTION 15.1)

1. An external driving routine would call AeroDyn's module passing rotor and tower geometrical information (Markers as in ***SharedTypes***, see Appendix F).
2. AeroDyn proceeds to compute the wind velocity at the BE coordinates: any of the current modules (***HHWind*** through ***UserWind***, see Appendices I-M) triggered by ***WindInf_GetVelocity*** (***InflowWind*** see Appendic G) may be used.
3. Calculate the relevant wind direction and the associated wind reference system at the tower level of interest, i.e. the one that would affect the BE under examination. Note: currently this is done with the 'new-tower-model' (See Section 10), however it may be improved in the future to account for the actual meandering of the wake based on some low-pass filter, as the wake will not respond instantaneously to a change in wind direction.
4. Calculate the effect of the tower (based on its deflected configuration). For this step: Eq.s (85)-(88), see also notes in Section 10, in particular the calculations of the wake and dam effects need to be calculated for the wind reference frame pertinent to the tower section of interest.
5. Combine the resulting wind and body velocities accounting for all terms (rigid motions and body deflections)
6. Decompose total velocity along the local (deflected) plane of rotation and normal to it (see Section 5.2): *VNTotal*, *VTTotal*
7. Initial guess on a and a' based on previous time-step values, or =0 if 0-th time step. Set j=0, iteration counter
8. Calculate $VNTotalInd = a * VNTotal$; $VTTotalInd = a' * VTTotal$; $U = \sqrt{VNTotalInd^2 + VTTotalInd^2}$ as resultant relative air-velocity with induction

9. Calculate inflow angle ϕ and AOA from simple geometry (see also Figure 8 and Eq.s (38) where U_∞ needs to be replaced by *VNTotal* and Ωr by *VTTotal*. Note that the coning angle effect (Eq. (77)) would be accounted for with this procedure based on basic geometry markers (see step 1).
10. *j*=*j*+1: Start *j*-th Iteration:
    a. Calculate C_l, C_d, C_m either statically (table look-ups) or via LBM (Eq. (135), (137), (141) and (93) ; see also Section 12 and subroutine ***BEDDOES*** (***AeroSubs***) in Appendix C). Note that AeroDyn's current BEDDOES procedure could be easily transferred into the iteration process, after correcting some of the inconsistencies noted in Section 12.
    b. Calculate BE loads: C_{tq}, C_{th}, C_m: Eq.s (39) where, however, the exact geometry should be considered with blade element reference frame in the deflected configuration (coned and tilted as well), and the components along and normal-to the local rotational plane are considered for C_{tq}, C_{th}. (See also Section 8).
    c. Calculate Tip/Hub losses: Eq.s (57)-(59) or alternatively (64) for tip loss following Shen et al. (2005), in which case the induction factor calculation should follow their method too.
    d. Calculate BEMT a and a' : Use either one of the following options depending on what is deemed more efficient and on instability issues:
        i. Eq. (60) and Eq. (61)
        ii. Eq.s (62) and Eq. (61) accounting for wake-rotation induced pressure-drop
        iii. Either i or ii with Eq. (61) replaced by Maniaci's (2011) method, i.e. Eq.s (54)-(56)
        iv. Eq. (71) and Eq. (74) following Shen et al. (2005) tip correction, eventually modified analogously to Maniaci's (2011) method
        v. Note that if this procedure is followed, the effect of the cone angle would be automatically included, else modifications as in Section 8 need to be implemented
    e. Extend to other turbine states:
        i. IF using Shen et al.'s (2005) method .AND. $CH>CH_{cs}$ (Eq. (75)) THEN:
            1. As in 10.d.iii with Eq. (71) replaced by Eq. (76)
        ii. ELSEIF $CH>0.96/F$ (using other methods) THEN: either one of the following alternatives
            1. As in 10.d.i and Eq. (60) replaced by either Eq. (66) or Eq. (67)b
            2. As in 10.d.ii and Eq. (62) replaced by either Eq. (66) or Eq. (67)b
    f. Correct for OFF-AXIS (YAW/TILT): Eq. (84) or similar Pitt & Peters (1980), Coleman et al. (1945) correction
    g. IF $|a_j - a_{j-1}|$>TOLERANCE .AND. $|a'_j - a'_{j-1}|$>TOLERANCE THEN GOTO 9
    h. ELSE:
        i. Output aerodynamic loads on the rotor BE at that instant of the simulation.

15.1 HIGH-LEVEL FLOW-CHART FOR THE BEMT TYPICAL TIME-STEP PROCESS

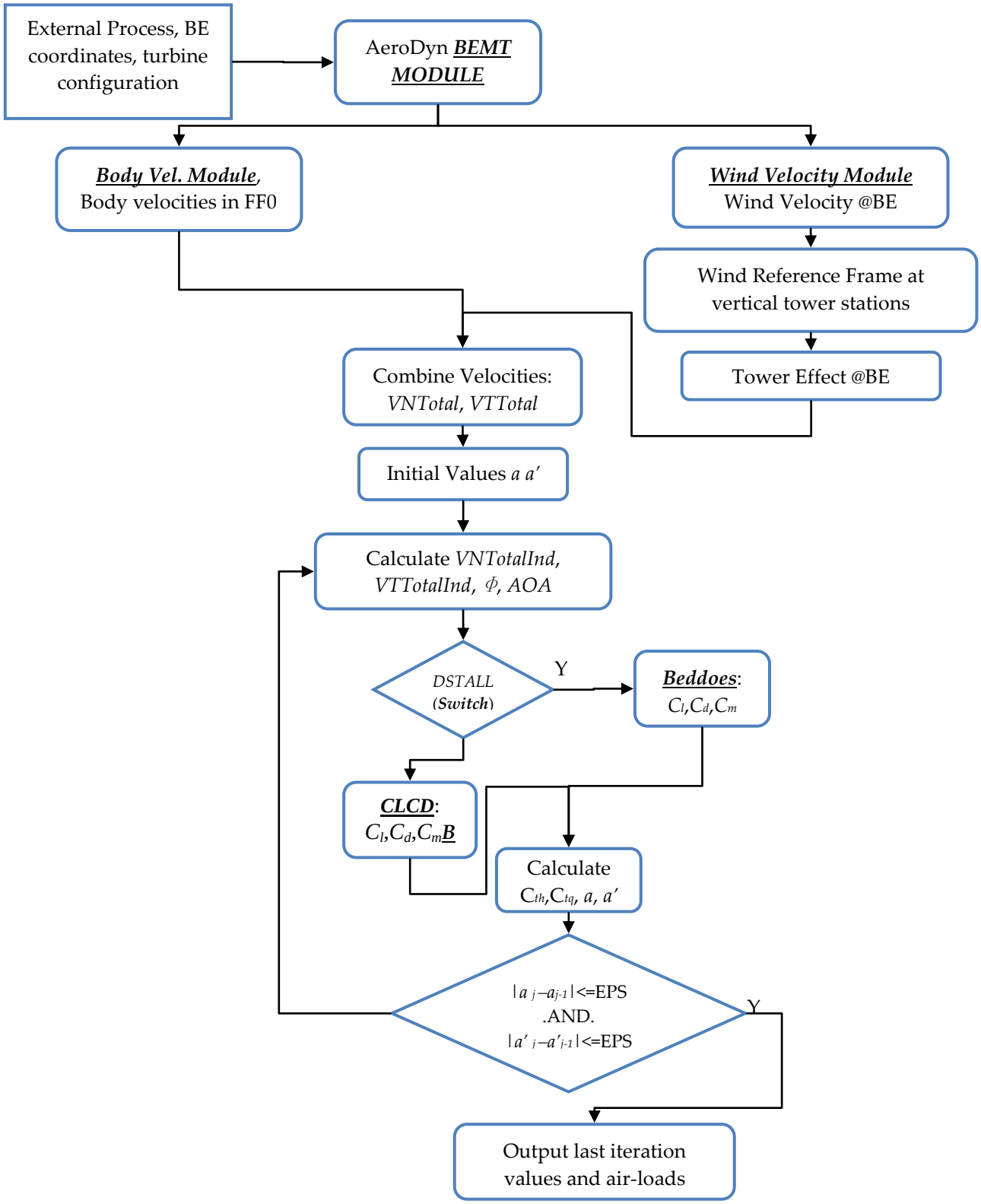

16. ALGORITHM OUTLINE FOR THE GDW METHOD

The suggested procedure to implement the GDW calculations is described below.

REQUIRED INPUTS:

- Number of harmonic modes (m_{max}+1) and radial modes to retain (n_{max})
- LBM time constants and initialized variables (0-th time step)
- 2D airfoil coefficients (in case augmented for rotational effects)
- At each time step:
  - blade element coordinates in FF0 under deflected conditions (accounting for tilt and coning as well);
  - tower deflected configuration;
  - the wind velocity vector at the blade element coordinates (including tower effects);
  - the blade-element 'body-velocity' vector;
  - the spatially (across the rotor plane) averaged wind velocity vector including body motion effects and tower effects

OUTPUTS:

- Blade element loads (C_{th}, C_{tq}, C_m);
- Induction factors, VN, VT, AOA, Φ, (optional)

STEPS (SEE ALSO SECTION 13)

1. An external driving routine would call AeroDyn's GDW module passing rotor and tower geometrical information (Markers as in ***SharedTypes***, see Appendix F) at each time step.
2. Initialization, 0-th time step:
   a. Calculate the radial shape function constant terms (Eq. (159)) as a function of the indices m=0.. m_{max}, and n=1..n_{max}. Also the values for the partition Γ_{ln}^{km} (see Eq. (164))
   b. BEMT calculates induction factors (a, a'), and spatially averaged $\bar{a}$ and BE lift
   c. Initialize states $\{\alpha_l^k\}$, $\{\beta_l^k\}$:
      i. Calculate instantaneous flow parameters: χ_0, λ_f(<0 for the sign convention assumed, unless the yaw error is greater than 90°), μ, and λ_m in the FF_{HR} reference frame (dimensional versions for unsteady RPM) Eq.s (192)-(193), from $V_H$and U_H (see also Figure 6), which need to include body motion contributions (tower effects on wind field as well).
      ii. Calculate τ_n^{mc} and τ_n^{ms} from Eq. (194), with BE lift from BEMT;
      iii. Calculate flow parameters: V_M, V_{TOT} from either Eq.s (144) and (147), or from (176) and (177) to account for vortex-ring state transitions
      iv. Calculate flow parameter X_W via Eq. (145)
      v. Calculate $[L^c]$ and $[L^s]$ via Eq.s (162)-(163)
      vi. Calculate $R \cdot [M]$ via Eq. (186) (only if second option selected below (2.c.vii))
      vii. Calculate $\{\alpha_l^k\}$, $\{\beta_l^k\}$, from Eq. (170) or Eq. (172) using $R \cdot [M]$ in place of $[M]$
   d. Initialize low-pass filtered quantities (including three additional states V_{id} $(i = 1..3)$:

i. $V_{id} = V_i (i = 1..3)$ (i.e., equal to the components in FF$_{HR}$ ($\Psi_0 = 0$) of the relative air-velocity (including body motion's contributions), and the V_{id} are the equivalent, low-pass filtered ones (all dimensional for unsteady RPM)).

ii. $\lambda_{fd} = \lambda_f, \mu_d = \mu, X_{Wd} = X_W$

iii. Initialize $X_{Weq} = X_W$

e. Calculate induced velocity $u_3\left(\hat{r}(v), \psi, t|_{0-th\ timestep}\right)$ from Eq. (158) and its correction for Tip-Loss Eq.s (187)-(188) (all in their dimensional forms (symbols' new meaning as explained in Section 13.3.5 for unsteady RPM)

f. Calculate <u>new</u> λ_m via Eq. (166) to be used at the next time step

g. For all the blades/BEs:

i. Calculate *VTTotal*, *VNTotal*, and U for the BE under investigation (body motions and tower effects included)

ii. Calculate inflow angle Φ via Eq.s (183)-(184)

iii. Calculate <u>new</u> inductions factors a and a' via Eq. (185) (whose terms are dimensional accounting for unsteady RPM)

iv. Calculate <u>new</u> BE forces to be used at the next time step; they are based on BE *VTTotal*, *VNTotal* , a and a' (see also Section 15 steps 10.a and 10.b):

1. Calculate C_l, C_d, C_m either statically (table look-ups) or via LBM (Eq. (135), (137), (141) and (93); see also Section 12 and subroutine ***<u>BEDDOES</u>*** (***AeroSubs***) in Appendix C). Note that AeroDyn's current BEDDOES procedure could be easily transferred into the iteration process, after correcting some of the inconsistencies noted in Section 12.

2. Calculate BE loads: C_{tq}, C_{th}, C_m: Eq.s (39) where, however, the exact geometry should be considered with blade element reference frame in the deflected configuration (coned and tilted as well), and the components along and normal to the local rotational plane are considered for C_{tq}, C_{th}. (See also Section 8).

3. For each new time step:

a. Update rotor-spatially-averaged $V_i (i = 1..3)$

b. Compute instantaneous flow parameters: χ_0, λ_f, μ, X_W in the FF$_{HR}$ reference frame (Eq.s (192) and (145)) from $V_H$and U_H (see also Figure 6), which need to include body motion contributions (tower effects on wind field as well).

c. Calculate τ_n^{mc} and τ_n^{ms} from Eq. (194), BE lift from previous step; (note: it includes τ_1^{0c} for new flow parameters to be calculated below)

d. Calculate low-pass filtered quantities:

i. <u>New</u> V_{id} via Eq. (197) and Adams-Bashforth

ii. <u>New</u> λ_{fd}, μ_d via Eq. (192) using V_{id} in place of V_i

iii. <u>New</u> V_M, V_{TOT} via Eq.s (176) and (177) to account for vortex-ring state transitions, or from Eq.s (144) and (147), using the lagged variables from previous 3.d.ii; (symbols' new meaning as explained in Section 13.3.5 for unsteady RPM)

iv. New X_{Wd} via Eq. (199) and Adams-Bashforth

v. New X_{Weq} via Eq. (190)(a)

e. Calculate $[L^c]$,$[L^s]$ via Eq.s (162)-(163), (165) with X_{Weq} in place of X_W; (matrix V_n^m elements are dimensional (m/s) as explained in Section 13.3.5 for unsteady RPM).

f. Calculate $[L^c]^{-1}$,$[L^s]^{-1}$

g. Calculate new matrix $R \cdot [M]$ via Eq. (186) (the factor R is for dimensional version of GDW and unsteady RPM)

h. Calculate RHS of Eq.s (173) replacing $[M]$ with $R \cdot [M]$

i. Use Adams-Bashforth to solve/integrate Eq.s (173) and compute new values for the states $\{\alpha_l^k\}$, $\{\beta_l^k\}$ (dimensional (m/s) for unsteady RPM)

j. Calculate (normalized) induced velocity $u_3(\hat{r}(v), \psi, t)$ from Eq. (158) and its correction for Tip-Loss Eq.s (187)-(188) (all in their dimensional forms (symbols' new meaning as explained in Section 13.3.5 for unsteady RPM)

k. Calculate new λ_m via Eq. (166) to be used at the next time step

l. For all the blades/BEs:

i. Calculate *VTTotal*, *VNTotal*, and U for the BE under investigation (body motions and tower effects included)

ii. Calculate inflow angle Φ via Eq.s (183)-(184)

iii. Calculate new inductions factors a and a' via Eq. (185) (whose terms are dimensional accounting for unsteady RPM)

iv. Calculate new BE forces to be used at the next time step; they are based on BE *VTTotal*, *VNTotal* , a and a' (see also Section 15 steps 10.a and 10.b):

1. Calculate C_l, C_d, C_m either statically (table look-ups) or via LBM (Eq. (135), (137), (141) and (93); see also Section 12 and subroutine ***BEDDOES*** (***AeroSubs***) in Appendix C). Note that AeroDyn's current BEDDOES procedure could be easily transferred into the iteration process, after correcting some of the inconsistencies noted in Section 12.

2. Calculate BE loads: C_{tq}, C_{th}, C_m: Eq.s (39) where, however, the exact geometry should be considered with blade element reference frame in the deflected configuration (coned and tilted as well), and the components along and normal to the local rotational plane are considered for C_{tq}, C_{th}. (See also Section 8).

v. Output aerodynamic loads on the rotor BEs at that instant of the simulation.

16.1 HIGH-LEVEL FLOW-CHART FOR THE GDW TYPICAL TIME-STEP PROCESS

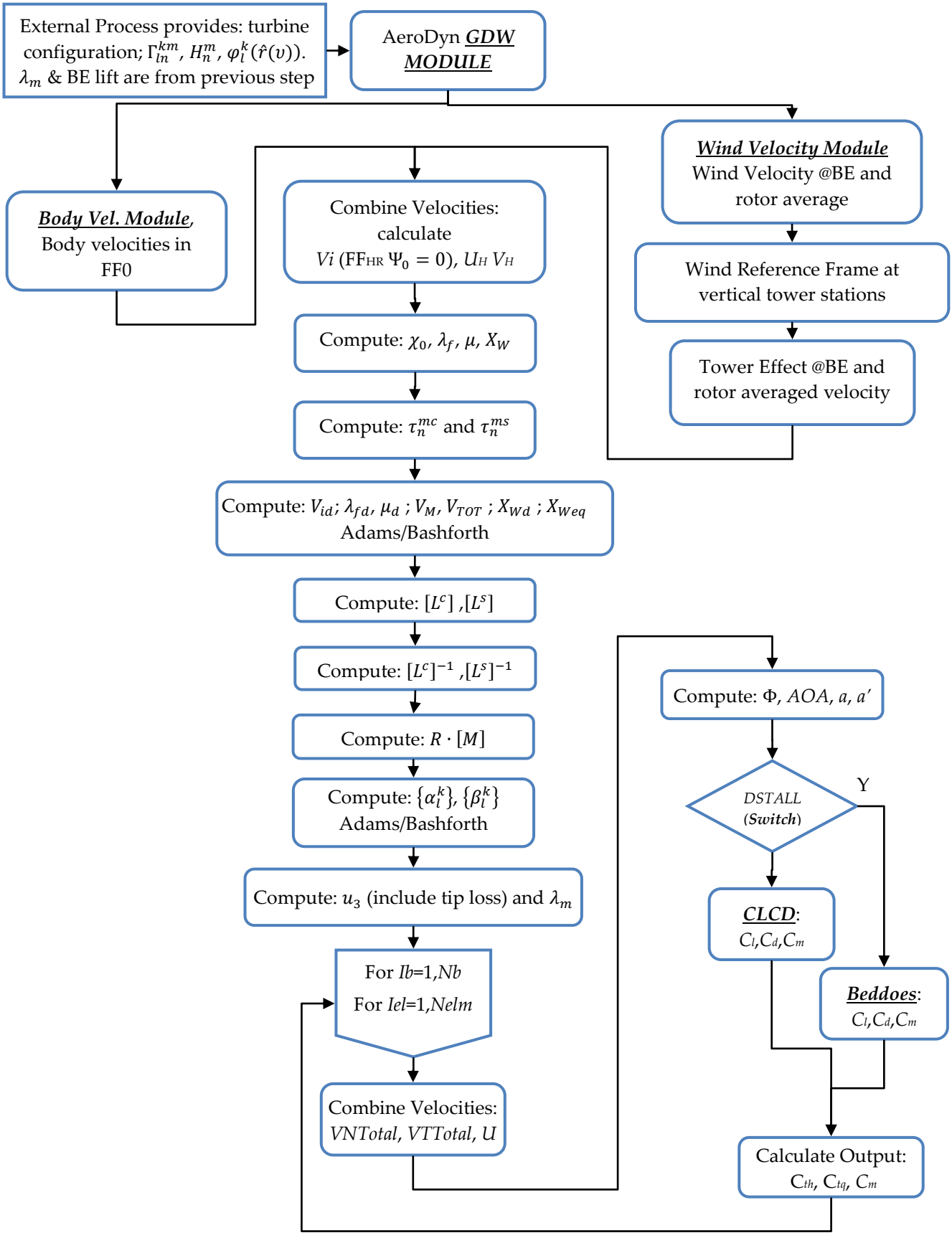

17. CONCLUSIONS AND RECOMMENDATIONS

In this study, the current status of AeroDyn, a program capable of assessing aerodynamic loads on HAWTs (http://wind.nrel.gov/designcodes/simulators/aerodyn/), was critically reviewed.

The first part of the project consisted of a thorough review of the theory behind the various models implemented in the code. A broad examination of the reference frames necessary to develop and interpret those models was also offered together with an exhaustive graphical representation, at times recast to incorporate few modifications deemed necessary to the current AeroDyn's status-quo.

In parallel, all of the routines that make up the code were examined, and their individual algorithms were commented in detail together with the identification of all input and output variables. Various aspects of the algorithms were addressed, which may require improvements, modifications, or a focused re-assessment.

The code is scheduled to undergo a major overhaul based on the current and other parallel studies, with particular attention to modularity. While the current organization already reveals a clear intent to make the various routines modular, it is recommended that the following main modules be implemented in future versions of the program:

1. Initialization Module- to initialize the various variables and sub-modules
2. AIRFOIL Module- to initialize BE aerodynamic coefficient, including 3D augmentation effects
3. Wind Velocity Module- to calculate the wind velocity vector at any point in space
4. Tower Shadow Module- to calculate effects due to tower wake or blockage
5. Body Kinematics Module- to calculate relevant components of the body motion velocities
6. BEM Module- to calculate BE lift and drag coefficients from static or partially modified look-up tables
7. LBM Module- to calculate BE lift and drag coefficients from unsteady aerodynamics via indicial treatment
8. TIP-LOSS Module- to calculate tip and eventually hub losses via MT or GDW
9. BEMT Module- to calculate induction factors via the classic BEM – MT interaction
10. GDW Module- to calculate the induced velocity across the rotor plane in place of the MT
11. I/O Module- to read/write information from/to files
12. Query Module- to return specific variables from an external query (useful for debugging as well as for interfacing with other programs that may request the values of various variables for other purposes)
13. Driver Module- to be able to run/test/validate AeroDyn as a stand-alone program
14. Termination Module- to close all files and deallocate memory

It is also recommended that AeroDyn encompass and supersede WTPerf and similar turbine-performance programs at the NWTC, so to reduce the maintenance overhead, while making the routine capable of being run as a quasi-stand-alone to facilitate validation efforts of the various modules.

AeroDyn has been written in the course of a decade or more and by different programmers and engineers, and as such it contains parts that could be re-written for improved computational efficiency. Nevertheless, except for a few points discussed in this report, the code appears to be rid of any major bug.

Five main issues, however, were noted and discussed in the previous sections.

First, the treatment of the body-relative air velocities. In AeroDyn, the axial induction is calculated on the wind velocity alone, i.e. excluding the contribution from body motions, whereas the tangential induction factor includes that contribution. This seems at least inconsistent, and it is suggested that the velocity participating in all of the calculations be considered as 'body-relative', where both rigid-body and elastic deflection kinematics are vector-summed with the wind velocity.

Second, it seems more appropriate to include the LBM in the iteration process within the BEMT treatment. While time scales of induction and dynamic-stall are two orders of magnitude apart, as discussed in this report, one would expect to have the BEM air-loading portion of the BEMT to drive the shedding of vorticity and wake development, more than vice versa. Since the LBM consists of a number of look-up searches, and other 1D (non-array) calculations, the extra computational burden is not expected to be unacceptable.

Third, the treatment of the GDW may be revised to implement changes in the sign conventions as discussed in this document. In that sense, some of the figures and illustrations of this report could further substitute or complement those in the AeroDyn's Theory Manual.

Fourth, within the GDW, some inconsistencies exist between the original Peters and He (1991) model and the AeroDyn's implementation. In particular, the induced velocity should be considered normal to the resultant velocity (which includes induction) at the generic BE. The subsequent treatment of the tangential induction factor is not in line with what the authors had originally devised. Additionally, the presence of swirl, or wake rotation, brings forth new terms in the apparent-mass matrix that are not accounted for in AeroDyn. It is therefore recommended that the GDW be re-implemented following the algorithm and equations as described in this report (see Section 16).

Fifth, there appears to be a problem with the time integration of the current GDW formulation in case of variable RPM, due to the updating of a normalization factor at each time step. The non-dimensional form of the equations does not lend itself to a direct numerical integration via the Adam-Bashforth scheme, because of changes in the time-step size, and because the states are normalized by different factors at different time-steps. Two alternatives were discussed: one requires minimum modification to the equations, by simply fixing the normalization parameter to a constant value; the other implies changing a few equations in order to have the model in fully dimensional form.

A few more minor issues were found and explained in this report, and briefly mentioned below.

In the treatment of the tower effects, the choice of reference frame is not consistent between blockage (or dam) effects and shadow (or wake) effects. That should be rectified.

The effects of tilt and/or yaw are more complex than what a simple correction to the basic BEMT could achieve. Nevertheless, it has been reported that simplified formulations as that shown in this document

can produce acceptable results. While the formulation discussed herewith is loosely connected to the work of Pitt and Peters (1981) and Coleman et al. (1945), a direct comparison and match of the various terms could not be established. More research is certainly needed in the treatment of BEMT and off-axis situations.

In AeroDyn's LBM implementation, a few potential typos were found and the correct versions of certain formulas were proposed to be consistent with the original Leishman and Beddoes (1989) model. For instance, the expressions of the time-constants for the non-circulatory contributions to the normal force due to a step change in AOA and in pitching rate currently are set to be equal; yet, the original LBM model provides two different formulations, distinct for AOA and pitching rate step disturbances. Correct expressions to be implemented in the future version of AeroDyn were provided. Furthermore, the current pitching moment model under attached (potential) flow conditions does not include any circulatory contribution to the response to pitching rate. Formulas to account for that further contribution were provided. The vortex strength decay-rate under certain criteria (normal force coefficient below threshold value for boundary-layer reattachment) was also shown to be in need of revision. Finally, the treatment of the small AOA was extended to larger AOA (for effects on tan (AOA) values), and the lift slope (2π) was modified to account for the actual airfoil properties.

New extensions to the current capabilities were also explored.

A new tip-loss model was proposed based on recent scientific work in the literature (Shen et al. (2005)).

The extension of the BEMT to other wake states was examined in detail, and various methods to accomplish that were proposed, also attempting to alleviate reported BEMT solution-instability issues.

The effects of a coning angle were also discussed. A rigorous kinematic management of the geometry of the wind turbine and rotor BE can yield to an incorporation of primary effects with minimum impact on the basic equations. An alternative method consists of decomposing the velocities along and normal-to the local rotational plane, though the effective airfoil characteristics would be slightly altered from those associated with the original airfoil defined in a cross-section normal to the blade pitch-axis. Secondary effects add on to the rotational augmentation effects due to boundary-layer spanwise development, and more research is needed in that field.

A brief review of the state-of-the-art in the study of rotational augmentation effects and delayed stall was offered. While the subject is still the focus of current research, it is expected that AeroDyn's new version may implement one or more flavors of a delayed stall model.

A possible expansion of AeroDyn to include changes in AOA due to disturbances of length-scales comparable to the airfoil chord was discussed in the theory review of the LBM model; in particular, a normal force response to a wind gust was proposed.

Following Peters (2011), extensions to the GDW current implementation were illustrated to provide: tip-loss correction enforcement with a limited number of retained harmonics; vortex-ring state transition treatment and alleviation of reported instabilities at low wind speeds; better handling of the induced velocity, and axial/tangential induction factors; inclusion of wake curvature effects due to finite yaw rate.

AeroDyn and the theory behind it are quite complex topics, and they will certainly undergo several more improvement and validation cycles in the future. This study meant to lead the way in that sense, and offered a comprehensive review of the current status while also pushing beyond towards a future revised implementation. A possible organization of the main algorithms was, in fact, provided describing the interactions between the main modules and the relevant physical equations to implement, including extensions to the current capabilities.

In the future, AeroDyn's modules will be further validated with field data, while supplementary modules will expand its current capabilities. On the one hand, for instance, the treatment of yawed and off-axis flow will need to be carefully assessed. The BEMT formulation may need to be overhauled, whereas the GDW procedure may require further refinements in terms of wind turbine characteristic time scales. Suzuki (2000) argues that a lag constant may be required in the GDW, as the dynamics and induction associated with a wind turbine wake are 'slower' than those of a helicopter wake. While currently there is no conclusive evidence in that regard, this is certainly a topic of investigation for future wind-turbine aerodynamics research.

On the other hand, the implementation of wake-vortex methods will likely bring forth overall higher fidelity, while yielding more accurate results than BEMT or GDW in configurations that undermine the very hypotheses upon which those models rely.

18. REFERENCES

Bak, C.; Aagaard Madsen, H.; Johansen, J. (2001): *Influence from Blade-Tower Interaction on Fatigue Loads and Dynamics (poster); Wind energy for the new millennium.* Proceedings: EWEC'01; Copenhagen (DK), 2-6 Jul 2001. Helm, P.; Zervos, A. (eds.), (WIP Renewable Energies, München 2001) p. 394-397

Beddoes, T.S., (1983): *Representation of Airfoil Behavior*. Vertica, 7 (2), 183-197

Beddoes, T.S., (1984): *Practical Computation of Unsteady Lift*. Vertica, 8 (1), 55-71

Bisplinghoff, R. L., and Ashley, H., and Halfman, R. L., (1996): *Aeroelasticity*, Dover Edition, 860 pp.

Buhl, M. L. Jr., (2005): *A New Empirical Relationship between Thrust Coefficient and Induction Factor for the Turbulent Windmill State*. NREL Technical Report, NREL/TP-500-36834

Burton, T. and Sharpe, D. and Jenkins, N. and Bossanyi, E., (2001): *Wind Energy Handbook*. Wiley & Sons, New York

Chaney, K., Eggers, A.J., Moriarty, P.J., and Holley, W.E., (2001): *Skewed Wake Induction Effects on Thrust Distribution on Small Wind Turbine Rotors*. J. Sol. Energy Eng., 123 (4), 290-295

Coleman, R. P., Heingold, A. M., and Stempin, C.W., (1945): *Evaluation of the Induced-Velocity Field of an Idealized Helicopter Rotor*. NACA ARR No. L5E10

Corrigan, J.J., and Schilling, J.J., (1994): *Empirical Model for Stall Delay Due to Rotation*. Proceedings of the American Helicopter Society Aeromechanics Specialists Conference, San Francisco, CA

Du, Z., and Selig, M.S., (1998): *A 3-D Stall Delay Model for Horizontal Axis Wind Turbine Performance Prediction*. AIAA-98-0021, ASME, Reno, NV, 9-19

Eggers, A.J., and Chaney, K., and Digumarthi, R., (2003): *An Assessment of Approximate Modeling of Aerodynamic Loads on the UAE Rotor*. 41st Aerospace Sciences Meeting and Exhibit, Reno, NV, 6-9 January, 283–292

Eggleston D.M. and Stoddard, F.S. (1987): *Wind Turbine Engineering Design*. Van Nostrand Reinhold, New York

Glauert H., (1926a): *The Analysis of Experimental Results in the Windmill Brake and Vortex Ring States of an Airscrew*. ARCR R&M No. 1026

Glauert H., (1926b): *A General Theory of the Autogyro*. ARCR R&M No. 1111

Glauert H., (1963): *Airplane Propellers,* In *Aerodynamic Theory*. Durant WF (ed.), Dover: New York, 169-360

Goldstein, S., (1929): *On the Vortex Theory of Screw Propellers*. Proceedings of the Royal Soc. of London. Series A, Containing Papers of a Mathematical and Physical Character, 123(792), 440-465

Guntur, S.K., and Bak, C., and Sørensen, N.N., (2011): *Analysis of 3D Stall Models for Wind Turbine Blades Using Data from the MEXICO Experiment*. Wind Energy Research. http://windenergyresearch.org/?p=2361

Gupta, S., Leishman, J. G., (2006): *Dynamic Stall Modelling of the S809 Aerofoil and Comparison with Experiments*. Wind Energy, 9 (6), 521–547

Hansen, A. C., (1992): *Yaw Dynamics of Horizontal Axis Wind Turbines, Final Report*. NREL/TP-442-4822

Hansen, A. C., (1998): *Users Guide to the Wind Turbine Dynamics Computer Programs YawDyn and AeroDyn for ADAMS*. Mech. Eng. Dept., Univ. of Utah

Hansen, M.O.L., (2000): *Aerodynamics of Wind Turbines*. James & James (Science Publishers) Ltd, 144 pages

Harman, C.R., (1994): *PROPX: Definitions, Derivations and Data Flow*. Oregon State University

Hibbs, B. and Radkey, R.L., (1981): *Small Wind Energy Conversion Systems (SWECS) Rotor Performance Model Comparison Study*. NREL Technical Report, Subcontract No. PFN-13470W, Contract No. DE-AC04-76DPO3533

Johansen, J. (1999): *Unsteady Airfoil Flows with Application to Aeroelastic Stability*. Technical Report Risoe-R-1116(EN), Risoe, DK

Kinner, W., (1937): *Theory of Circular Wing*. Ingenieur Archiv, 7, Translation No. 2345, ministry of Aircraft Production, U.K.

Laino, D.J. and Hansen, A.C., (2002): *User's Guide to the Wind Turbine Aerodynamics Computer Software AeroDyn*. Windward Engineering, LC

Leishman, J.G., and Beddoes, T.S., (1986): *A Generalized Model For Airfoil Unsteady Behavior and Dynamic Stall Using the Indicial Method*. Proceedings of the 42nd Annual Forum of the American Helicopter Society, Washington, D.C., 243-266

Leishman, J.G., and Beddoes, T.S., (1989): *A Semi-Empirical Model for Dynamic Stall*. J. of the American Helicopter Soc., (34) 3, 3-17

Leishman, J.G., (2002): *Challenges in Modeling the Unsteady Aerodynamics of Wind Turbines*. 21st ASME Wind Energy Symposium and the 40th AIAA Aerospace Sciences Meeting, Reno, NV

Leishman, J.G., (2006): *Principles of Helicopter Aerodynamics*. Cambridge University Press, 2nd Edition, New York, NY

Leishman, J.G., (2011): *Final report: Assessment of 'Aerodyn' Theory basis including Unsteady Aerodynamics Modules*. NREL Subcontract No. LFC-1-11303-01 under Prime Contract No. DE-AC36-08GO28308

Lindenburg, C., (2004): *Modeling of Rotational Augmentation based on Engineering Considerations and Measurements*. ECN-RX—04-131, European Wind Energy Conference, London, 22-25 November

Lomax, H. and Heaslet, M.A., Fuller, F.B., and Sluder, L., (1952): *Two and Three Dimensional Unsteady Lift Problems in High Speed Flight*. NACA Report 1077

Maniaci, D.C., (2011): *An Investigation of WT_Perf Convergence Issues*. 49th AIAA Aerospace Sciences Meeting including the New Horizons Forum and Aerospace Exposition, 4-7 January, Orlando, Florida

Meyer Drees, J., (1949): *A Theory of Airflow Through Rotors and its Application to Some Helicopter Problems*. J. Helicopter Soc., UK, 3 (2)

Manwell, J.F., McGowan, J.G., and Rogers, A.L., (2002): *Wind Energy Explained: Theory, Design and Application*. John Wiley & Sons, New York

Minnema, J. E. (1998): *Pitching Moment Predictions on Wind Turbines Blades Using the Beddoes-Leishman Model for Unsteady Aerodynamics and Dynamic Stall*. The University of Utah, MS Thesis

Moriarty, P. J. and Hansen, A.C. (2004): *AeroDyn Theory Manual*. NREL/EL-500-36881, NREL

Pereira, R.B.dS., (2010): *Validating the Beddoes-Leishman Dynamic Stall Model in the Horizontal Axis Wind Turbine Environment*. Instituto Superior Técnico, Universidade Técnica de Lisboa, M.S. Thesis

Peters, D.A., and Boyd, D.D., and He, C.J., (1989): *A Finite-State Induced-Flow Model for Rotors in Hover and Forward Flight*. Journal of the American Helicopter Society, 34(4), 5-17

Peters, D.A.,and He, C.J., (1991): *Correlation of Measured Induced Velocities with a Finite-State Wake Model*. Journal of the American Helicopter Society, 36(3), 59-70

Peters, D.A., and He, C.J., (2006): *Modification of Mass-Flow Parameter to Allow Smooth Transition Between Helicopter and Windmill States*. Technical Note, Journal of the American Helicopter Society, 51(3), 275-278

Peters, D. A., (2011): *Fifth Monthly Progress Report*, NREL Subcontract No. LAM-1-11304-01 under Prime Contract No. DE-AC36-08G028308

Pierce, K. G., (1996): *Wind Turbine Load Prediction Using the Beddoes-Leishman Model for Unsteady Aerodynamics and Dynamic Stall*. The University of Utah, MS Thesis

Pierce, K. G., and Hansen, A. C., (1995): *Prediction of Wind Turbine Rotor Loads Using the Beddoes-Leishman Model for Dynamic Stall*. Journal of Solar Energy Engineering, 117, 200–204

Pitt, D. M., and Peters, D. A., (1980): *Theoretical Predictions of Dynamic-Inflow Derivatives*. 6th European Rotorcraft and Powered Lift Aircraft Forum, Bristol, England

Powles, S.R.J., (1983): *The Effects of Tower Shadow on the Dynamics of a HAWT*. Wind Engineering, 7 (1), 26-42

Prandtl L., (1927): *Vier Abhandlungen zur Hydrodynamik und Aerodynamik, Göttinger Nachr*. Göttingen, 88-92. (See also textbooks and Burton et al. (2001) and Manwell et al. (2002))

Pratumnopharat, P. and Leung, P.S. (2011): *Validation of Various Windmill Brake State Models Used by Blade Element Momentum Calculation*. Renewable Energy, in press

Schepers, J.G. and Snel, H. (1995): *Joint Investigation of Dynamic Inflow Effects and Implementation of an Engineering Method*. ECN Report: ECN-C-94-107. ECN, Petten, Holland

Schlichting, H., (1979): *Boundary Layer Theory*. McGraw-Hill, New York

Shey, H.M., (1973): *Div, Grad, Curl, and All That: an Informal Text on Vector Calculus*. W.W. Norton & Company, NY

Shen, W. Z., (2005): *Tip Loss Corrections for Wind Turbine Computations*. Wind Energy, 8, 457-475

Shen, W. Z., (2009): *Computational Aerodynamics and Aeroacoustics for Wind Turbines*. Technical University of Denmark, Section of Fluid Mechanics, PhD Thesis

Snel, H., and Schepers, J.G., (1995): *Joint Investigation of Dynamic Inflow Effects and Implementation of an Engineering Method*. ECN-C-94-107, Petten: Energy Research Centre of the Netherlands, April

Suzuki, A., (2000): *Application of Dynamic Inflow Theory to Wind Turbine Rotors*. The University of Utah, PhD Dissertation

Tangler, J.L, and Selig, M.S., (1997): *An Evaluation of an Empirical Model for Stall Delay due to Rotation for HAWTS*. AWEA WindPower Conference, June 15-18

Viterna, L.A., and Janetzke, D.C. (1982): *Theoretical and Experimental Power from Large Horizontal-Axis Wind Turbines*. NASA Technical Report, NASA TM-82944, Washington, DC

Xu, G., and Sankar, L. N., (2002): *Development of Engineering Aerodynamics Models Using a Viscous Flow Methodology on the NREL Phase VI Rotor*. Wind Energy, 5, 171-183

Zhao, J., and Prasad, J. V. R., and Peters, D. A., (2004): *Rotor Dynamic Wake Distortion Model for Helicopter Maneuvering Flight*. Journal of the American Helicopter Society, 49(4), 414–424

PART III: APPENDICES